Flavored S_3 Non-Minimal Left-Right Symmetric Model

F. Gonzalez-Canales[1,*] and Juan Carlos Gómez-Izquierdo[2,3,†]

[1] *Fac. de Cs. de la Electrónica, Benemérita Universidad Autónoma de Puebla, Apdo. Postal 542, Puebla, Pue. 72000, México.*

[2] *Instituto Politécnico Nacional, CECyT No.16, Carretera Pachuca-Actopan Kilómetro 1+500, Distrito de Educación, Salud, Ciencia, Tecnología e Innovación, San Agustín Tlaxiaca, Hidalgo, C.P. 42162, México.*

[3] *Instituto Politécnico Nacional, UPIIH, Carretera Pachuca-Actopan Kilómetro 1+500, Distrito de Educación, Salud, Ciencia, Tecnología e Innovación, San Agustín Tlaxiaca, Hidalgo, C.P. 42162, México.*

(Dated: **October 26, 2026)**

arXiv:2610.31770v1 [hep-ph] 22 Oct 2026

In this work we investigate fermion masses and flavor mixings in a non-minimal left-right symmetric model endowed with the non-Abelian discrete symmetry S_3. The scalar sector contains three Higgs bidoublets, while one left-handed and one right-handed triplet generate Majorana neutrino masses. Assigning the first two fermion families to an S_3 doublet and the third family to a singlet, together with a specific alignment of the bidoublet vacuum expectation values, leads to a common and analytically tractable structure for the fermion mass matrices. We study both the pseudomanifest and manifest left-right realizations, in which the fermion mass matrices are complex symmetric and Hermitian, respectively, and derive analytical expressions for the left- and right-handed CKM and PMNS mixing matrices. A numerical likelihood test shows that the model successfully reproduces the observed quark and lepton mixing patterns for both normal and inverted neutrino mass orderings at the level of oscillation data. Remarkably, the manifest scenario emerges as a more restrictive realization of the pseudomanifest one, with the main distinction residing in their CP-phase structure. We further explore the phenomenological consequences for the neutrinoless double-beta decay, the muon anomalous magnetic moment, and the lepton-flavor-violating decay $\mu \to e\gamma$. The right-handed contribution exhibits the characteristic dependence on the heavy-neutrino and W_R mass scales, while flavor corrections are found to be subleading over most of the allowed parameter space. These results show that an S_3 flavor symmetry can simultaneously organize fermion mixing and lead to distinctive low-energy signatures within left-right symmetric theories.

I. INTRODUCTION

The discovery of the Higgs boson in 2012 [1, 2] represented a major triumph for the Standard Model (SM) of elementary particles, which is currently the most successful theory describing the interactions among fundamental particles. Nevertheless, several important questions remain unanswered, such as the origin of neutrino masses[3–5], the flavor puzzle [6–8], and the nature of dark matter [9].

In this context, the Minimal Left-Right Symmetric Model (MLRSM) [10–14] provides an appealing framework that addresses several shortcomings of the SM. For instance, it offers a natural explanation for parity violation at low energies, which is closely related to the origin of neutrino masses [15]. Consequently, the seesaw mechanism [14, 16–21] emerges naturally, providing an elegant explanation for the smallness of neutrino masses. Furthermore, within the MLRSM, the SM hypercharge (Y) acquires a physical interpretation in terms of baryon and lepton number difference ($B - L$). These features make the MLRSM an attractive candidate for physics beyond the SM.

Over the years, the MLRSM has attracted considerable attention, since many physical processes have been proposed to search for characteristic signatures that could be observed at the LHC [22–32]. In addition, the right-handed CKM matrix, which is the counterpart of the left-handed CKM matrix [33, 34], has been extensively studied due to its direct impact on the physics of the W_R boson, neutrinoless double beta decay [35–38], and the theoretical constraints arising from K- and B-meson physics [39, 40]. On the other hand, in the lepton sector, the right-handed PMNS matrix contributes to the anomalous magnetic moment of the muon as well as to lepton-number-violating processes [41]. These

* felix.gonzalezc@correo.buap.mx

† cizquierdo@ipn.mx

studies provide additional motivation to further explore this theoretical framework from different phenomenological perspectives.

Nonetheless, due to the gauge structure of the MLRSM, the Yukawa sector contains a large number of free couplings, which represents an important drawback of the model. Although the imposition of parity symmetry partially alleviates this issue, it is still desirable to understand the fermion mixing patterns from the perspective of flavor symmetries [42–47].[1] For this reason, the study of fermion mixings in this class of models has attracted comparatively limited attention [52–59]. Closely related flavored non-minimal left-right symmetric models were previously studied in Refs. [54, 56], where the flavor structure was based on the enlarged discrete symmetry $S_3 \otimes Z_2 \otimes Z_2^e$. Those constructions employed three Higgs bidoublets together with three left-handed and three right-handed triplets, and the leptonic mixing pattern was analyzed through a soft breaking of the $\mu \leftrightarrow \tau$ symmetry. The present work differs from that realization in several essential aspects. Here, the flavor sector is governed solely by S_3, the first two fermion families transform as a doublet while the third family transforms as $\mathbf{1}_S$, and only one left-handed and one right-handed Higgs triplet are retained. This reduced field content leads to a different Majorana sector and to a common analytical structure for the quark, charged-lepton, and Dirac-neutrino mass matrices. Beyond these structural differences, the present analysis develops the left- and right-handed flavor sectors simultaneously in both the pseudomanifest and manifest left-right realizations. We derive explicit analytical expressions for the corresponding CKM [33, 34] and PMNS [60, 61] mixing matrices and show that the manifest realization can be understood as a more restrictive limit of the pseudomanifest one, mainly through its reduced CP-phase structure. The numerical analysis is updated using current quark and neutrino data and accommodates both normal and inverted neutrino mass orderings at the level of oscillation data. Furthermore, in contrast with Ref. [56], the analysis is extended beyond fermion masses and mixings to the phenomenology of neutrinoless double-beta decay, the muon anomalous magnetic moment, and the lepton-flavor-violating decay $\mu \to e\gamma$, including the constraints imposed by the current MEG II limit. These differences motivate a renewed analysis of the flavor structure, with particular emphasis on obtaining a unified description of the markedly different CKM and PMNS mixing patterns, which play a crucial role in several relevant physical processes.

To this end, in this work we focus on the well-studied non-Abelian group S_3 (see, for instance, the references therein [42–47]), which constitutes an attractive candidate for describing fermion mixing patterns, within the framework of the left-right symmetric theory. In order to consistently implement the flavor symmetry, the scalar sector must also be extended, requiring the introduction of three Higgs bidoublets. To preserve a minimal matter content in the Majorana sector, one left-handed and one right-handed Higgs triplet are introduced to generate the corresponding neutrino masses. With these ingredients, all fermion fields are treated on the same footing under the flavor symmetry, with the three families assigned to the irreducible representations $\mathbf{2} \oplus \mathbf{1}_S$. In this way, a unified treatment of fermion masses is achieved. At high energies, parity symmetry is imposed in the model, although it is spontaneously broken at lower energies. In addition, we adopt a specific alignment of the Higgs-bidoublet vacuum expectation values as a phenomenological working assumption. This alignment, specified explicitly below, selects a symmetric direction in the S_3-doublet scalar sector and considerably reduces the number of independent entries in the fermion mass matrices. Its dynamical realization would require a dedicated analysis of the complete scalar potential, which is not attempted in the present work. Together, these assumptions determine the flavor structure analyzed below. We then study both the pseudomanifest and manifest left-right realizations, in which the fermion mass matrices are complex symmetric and Hermitian, respectively, and derive analytical expressions for the left- and right-handed CKM and PMNS mixing matrices. A numerical likelihood test shows that the model successfully reproduces the observed quark and lepton mixing patterns for both normal and inverted neutrino mass orderings. In the literature, these mass orderings are also commonly referred to as the normal and inverted hierarchies, NH and IH, respectively [56]. Remarkably, the manifest scenario emerges as a more restrictive realization of the pseudomanifest one, with the main distinction residing in their CP-phase structure. We further explore the phenomenological consequences for the neutrinoless double beta decay, the muon anomalous magnetic moment, and the lepton-flavor-violating decay $\mu \to e\gamma$. The right-handed contribution exhibits the characteristic dependence on the heavy-neutrino and W_R mass scales, while flavor corrections are found to be subleading over most of the allowed parameter space. These results show that an S_3 flavor symmetry can simultaneously organize fermion mixing and lead to distinctive low-energy signatures that can be tested in current and future experiments within left-right symmetric theories.

The paper is organized as follows. In Section II, we provide a brief review of the Minimal Left-Right Symmetric Model. In Section III, we introduce the flavored model and explicitly diagonalize the quark and lepton mass matrices in order to construct the CKM and PMNS mixing matrices, whose parameters are determined through a numerical χ^2 analysis. After obtaining a successful fit for the lepton sector, in Section IV we study the implications of the model for neutrinoless double beta decay, the muon anomalous magnetic moment $(g-2)$, and the lepton-flavor-violating process $\mu \to e\gamma$. Finally, our conclusions are presented in Section V.

---

[1] Remarkably, left-right symmetric models have recently been studied within the framework of modular symmetries [48–51].

II. MINIMAL LEFT-RIGHT SYMMETRIC MODEL: A BRIEF REVIEW

The Minimal Left-Right Symmetric Model (MLRSM) [10–14] is based on the gauge symmetry $\mathbf{SU(3)}_c \otimes \mathbf{SU(2)}_L \otimes \mathbf{SU(2)}_R \otimes \mathbf{U(1)}_{B-L}$. The parity symmetry, $\mathcal{P}$, is assumed to be an exact symmetry at high energies and is spontaneously broken at the scale associated with $SU(2)_R$ breaking, above the electroweak scale. This is consistent with the absence of right-handed weak currents at low energies. As is well known, right-handed neutrinos (RHNs) are naturally incorporated into the matter content of the model, as shown in Table I. Then, the gauge-invariant Yukawa

Matter	$\mathbf{SU(3)}_C$	$\mathbf{SU(2)}_L$	$\mathbf{SU(2)}_R$	$\mathbf{U(1)}_{B-L}$
$Q_{(L,R)} = \begin{pmatrix} u \\ d \end{pmatrix}_{(L,R)}$	**3**	**(2, 1)**	**(1, 2)**	$\frac{1}{3}$
$(L,R) = \begin{pmatrix} \nu \\ \ell \end{pmatrix}_{(L,R)}$	**1**	**(2, 1)**	**(1, 2)**	-1
$\Delta_{(L,R)} = \begin{pmatrix} \frac{\delta^+}{2} & \delta^{++} \\ \delta^0 & -\frac{\delta^+}{2} \end{pmatrix}$	**1**	**(3, 1)**	**(1, 3)**	2
$\Phi = \begin{pmatrix} \phi^0 & \phi'^+ \\ \phi^- & \phi'^0 \end{pmatrix}$	**1**	**2**	**2**	0

TABLE I. Matter content in the MLRSM

interaction is given by

$$-\mathcal{L}_Y = \bar{Q}_L \left[y^q \Phi + \tilde{y}^q \tilde{\Phi} \right] Q_R + \bar{L} \left[y^\ell \Phi + \tilde{y}^\ell \tilde{\Phi} \right] R + y^L \bar{L} \Delta_L L^c + y^R \bar{R}^c \Delta_R R + h.c. \tag{1}$$

with $\tilde{\Phi} = -i\sigma_2 \Phi^* i\sigma_2$ and the charged current is explicitly written as

$$\mathcal{L}_{CC} = \frac{g_L}{\sqrt{2}} \left[\bar{Q}_L \gamma_\mu W_L^\mu Q_L + \bar{L} \gamma_\mu W_L^\mu L \right] + \frac{g_R}{\sqrt{2}} \left[\bar{Q}_R \gamma_\mu W_R^\mu Q_R + \bar{R} \gamma_\mu W_R^\mu R \right] + h.c. \tag{2}$$

For simplicity, the family indices have been suppressed in the above expressions.

On the other hand, we emphasize that parity symmetry is assumed in the above Lagrangian. Consequently, the following transformations are required: $\Psi_L \leftrightarrow \Psi_R$ for the fermion fields, and $\Phi \leftrightarrow \Phi^\dagger$ together with $\Delta_L \leftrightarrow \Delta_R^\dagger$ for the scalar fields. As a result, the Yukawa sector is considerably simplified, leading to the relations $y = y^\dagger$, $\tilde{y} = \tilde{y}^\dagger$, and $y^R = y^L$. Likewise, parity symmetry implies the equality of the gauge couplings, namely $g_L = g_R$. A complete analysis of the most general scalar potential invariant under the gauge symmetry, parity, and the S_3 flavor symmetry is beyond the scope of the present work, whose main purpose is to investigate the fermion-mass and flavor-mixing sectors. We therefore do not attempt to derive the vacuum configuration from the minimization conditions of the full scalar potential. Instead, we assume that the scalar potential admits a phenomenologically viable stationary configuration characterized by the usual left-right hierarchy $v_R \gg |k_i|, |k'_i| \gg v_L, \quad i = 1, 2, 3$, together with the bidoublet alignment specified below. The present analysis should therefore be understood as a study of the flavor consequences of this vacuum configuration, rather than as a proof that it corresponds to the global minimum of the complete scalar potential. Questions concerning vacuum stability, possible competing minima, and the physical scalar spectrum are left for a dedicated study.

Within this assumption, parity symmetry is broken at the scale at which the right-handed Higgs triplet Δ_R acquires its vacuum expectation value (VEV). At this stage, the right-handed neutrinos acquire Majorana masses. Electroweak symmetry breaking subsequently occurs when the Higgs bidoublets develop their corresponding VEVs, generating the Dirac fermion masses. Explicitly,

$$\langle \Delta_{(L,R)} \rangle = \begin{pmatrix} 0 & 0 \\ v_{(L,R)} & 0 \end{pmatrix}, \quad \langle \Phi \rangle = \begin{pmatrix} k & 0 \\ 0 & k' \end{pmatrix}, \quad \langle \tilde{\Phi} \rangle = \begin{pmatrix} k'^* & 0 \\ 0 & k^* \end{pmatrix}. \tag{3}$$

Once the scalar fields acquire their VEVs, the corresponding fermion mass terms take the form

$$-\mathcal{L}_Y = \bar{q}_L \mathbf{M}_q q_R + \bar{e}_L \mathbf{M}_e e_R + \frac{1}{2} \begin{pmatrix} \bar{\nu}_L & \bar{\nu}_R^c \end{pmatrix} \overbrace{\begin{pmatrix} \mathbf{M}_L & \mathbf{M}_D \\ \mathbf{M}_D^T & \mathbf{M}_R \end{pmatrix}}^{\mathcal{M}_\nu} \begin{pmatrix} \nu_L^c \\ \nu_R \end{pmatrix} + h.c. \tag{4}$$

where $\mathbf{M}_q$ $(q = u, d)$ and $\mathbf{M}_e$ denote the quark and charged-lepton mass matrices, respectively. In addition, $\mathbf{M}_{(L,R)} = y^{(L,R)} v_{(L,R)}$ and $\mathbf{M}_D = y^\ell k + \tilde{y}^\ell k'^*$ denote the Majorana and Dirac neutrino mass matrices, respectively. The full neutrino mass matrix $\mathcal{M}_\nu$ is diagonalized by a 6×6 unitary matrix $\mathcal{V}$ such that

$$\mathcal{V}^T \mathcal{M}_\nu \mathcal{V} = \begin{pmatrix} \hat{\mathbf{M}}_\nu & \mathbf{0} \\ \mathbf{0} & \hat{\mathbf{M}}_R \end{pmatrix}. \tag{5}$$

In the seesaw limit, the unitary matrix $\mathcal{V}$ can be written as

$$\mathcal{V} = \begin{pmatrix} \mathbf{U} & \mathbf{S} \\ \mathbf{T} & \mathbf{V} \end{pmatrix} \simeq \begin{pmatrix} \mathbf{1} - \frac{1}{2}\theta\theta^\dagger & \theta \\ -\theta^\dagger & \mathbf{1} - \frac{1}{2}\theta^\dagger\theta \end{pmatrix} \begin{pmatrix} \mathbf{U}_{\nu L} & \mathbf{0} \\ \mathbf{0} & \mathbf{U}_{\nu R} \end{pmatrix}, \quad \mathcal{V}\mathcal{V}^\dagger = \mathbf{1} = \mathcal{V}^\dagger\mathcal{V}. \tag{6}$$

where $\hat{\mathbf{M}}_\nu$ and $\hat{\mathbf{M}}_R$ contain the physical light- and heavy-neutrino masses, respectively. In the expression above, terms up to second order in the light-heavy mixing matrix θ have been retained, while higher-order contributions are neglected. Then, $\mathbf{U} \approx \mathbf{U}_{\nu L}$, $\mathbf{S} \approx \theta \mathbf{U}_{\nu R}$, $\mathbf{T} \approx -\theta^\dagger \mathbf{U}_{\nu L}$ and $\mathbf{V} \approx \mathbf{U}_{\nu R}$. Thus, the mass and interaction neutrino eigenstates are related by

$$\begin{pmatrix} \nu_L \\ (\nu_R)^c \end{pmatrix} = \mathcal{V} \begin{pmatrix} \tilde{\nu}_L \\ (\tilde{\nu}_R)^c \end{pmatrix}, \qquad \begin{pmatrix} (\nu_L)^c \\ \nu_R \end{pmatrix} = \mathcal{V}^* \begin{pmatrix} (\tilde{\nu}_L)^c \\ \tilde{\nu}_R \end{pmatrix} \tag{7}$$

As a result, we obtain $\mathbf{U}_{\nu L}^\dagger \mathbf{M}_\nu \mathbf{U}_{\nu L}^* = \hat{\mathbf{M}}_\nu$ and $\mathbf{U}_{\nu R}^\dagger \mathbf{M}_R \mathbf{U}_{\nu R}^* = \hat{\mathbf{M}}_R$ where the effective light-neutrino mass matrix arises from the combined type-I and type-II seesaw contributions and is given by

$$\mathbf{M}_\nu = \mathbf{M}_L - \mathbf{M}_D \mathbf{M}_R^{-1} \mathbf{M}_D^T. \tag{8}$$

Returning to the charged-current Lagrangian, once parity symmetry is imposed, it can be written as

$$\mathcal{L}_{CC} = \frac{g}{\sqrt{2}} \left[\left\{ \bar{d}_L \gamma_\mu u_L + \bar{e}_L \gamma_\mu \nu_L \right\} W_L^{-\mu} + \left\{ \bar{d}_R \gamma_\mu u_R + \bar{e}_R \gamma_\mu \nu_R \right\} W_R^{-\mu} \right] + h.c. \tag{9}$$

where the $W_{1,2}^{\mp\mu}$ mass eigenstates are related to the $W_{L,R}^{\mp\mu}$ interaction ones as

$$\begin{pmatrix} W_L^{\mp\mu} \\ W_R^{\mp\mu} \end{pmatrix} = \begin{pmatrix} \cos\zeta & \sin\zeta \\ -\sin\zeta & \cos\zeta \end{pmatrix} \begin{pmatrix} W_1^{\mp\mu} \\ W_2^{\mp\mu} \end{pmatrix} \tag{10}$$

Finally, using Eqs. (7) and (10), we have

$$\begin{aligned} \mathcal{L}_{CC} \;=\; & \frac{g}{\sqrt{2}} \left[\bar{d}_L \gamma_\mu u_L + \bar{e}_L \gamma_\mu \left(\mathbf{U} \tilde{\nu}_L + \mathbf{S} \left(\tilde{\nu}_R \right)^c \right) \right] \left[\cos\zeta \; W_{1\mu}^- + \sin\zeta \; W_{2\mu}^- \right] \\ & + \frac{g}{\sqrt{2}} \left[\bar{d}_R \gamma_\mu u_R + \bar{e}_R \gamma_\mu \left(\mathbf{T}^* \left(\tilde{\nu}_L \right)^c + \mathbf{V}^* \tilde{\nu}_R \right) \right] \left[-\sin\zeta \; W_{1\mu}^- + \cos\zeta \; W_{2\mu}^- \right] + h.c. \end{aligned} \tag{11}$$

In the MLRSM, the mixing angle ζ depends on the charged gauge-boson masses and on the bidoublet VEVs. Existing phenomenological constraints require this mixing to be small. Therefore, throughout the phenomenological analysis we work in the limit $\zeta \simeq 0$, so that $W_1 \simeq W_L$ and $W_2 \simeq W_R$. Corrections proportional to ζ are not included in the present analysis.

III. FLAVORED LEFT-RIGHT SYMMETRIC MODEL

Having briefly described the theoretical framework, we now comment on the additional ingredients to study fermion masses and mixing patterns. To this purpose, Φ_i $(i = 1, 2, 3)$, which are responsible for generating the fermion mixing structure. In the Majorana sector, one left-handed and one right-handed Higgs triplet are retained, as in the conventional MLRSM. In this way, we aim to preserve a minimally extended scalar sector.

Additionally, the MLRSM is supplemented with the flavor symmetry S_3. The main motivation for employing this non-Abelian discrete symmetry lies in the structure of its reducible representations, $\mathbf{3}_S$ and $\mathbf{3}_A$, which decompose as $\mathbf{3}_S = \mathbf{1}_S \oplus \mathbf{2}$ and $\mathbf{3}_A = \mathbf{1}_A \oplus \mathbf{2}$, respectively. This feature allows the three fermion families to be naturally

Matter	$Q_{I(L,R)}$	$Q_{3(L,R)}$	(L_I, R_I)	(L_3, R_3)	Φ_I	Φ_3	$\Delta_{(L,R)}$
$\mathbf{S}_3$	$\mathbf{2}$	$\mathbf{1}_S$	$\mathbf{2}$	$\mathbf{1}_S$	$\mathbf{2}$	$\mathbf{1}_S$	$\mathbf{1}_S$

TABLE II. Flavored non-minimal left-right model. Here, $I = 1, 2$.

accommodated within these decompositions, providing a framework to understand the observed hierarchies of quark and charged lepton masses.

Accordingly, the quark, lepton, and Higgs bidoublet fields are assigned under S_3 in the following way: the first and second families transform as a doublet $\mathbf{2}$, whereas the third family is assigned to the singlet representation $\mathbf{1}_S$. The complete field content and its assignments are shown in Table II. As a result of the field assignments under the flavor symmetry, the Yukawa mass terms that are invariant under both the S_3 flavor symmetry and the gauge symmetry are given by

$$\begin{aligned}
-\mathcal{L}_Y = {} & y_1^q \left[\bar{Q}_{1L}\left(\Phi_1 Q_{2R} + \Phi_2 Q_{1R}\right) + \bar{Q}_{2L}\left(\Phi_1 Q_{1R} - \Phi_2 Q_{2R}\right)\right] + y_2^q \left[\bar{Q}_{1L}\Phi_3 Q_{1R} + \bar{Q}_{2L}\Phi_3 Q_{2R}\right] \\
& + y_3^q \left[\bar{Q}_{1L}\Phi_1 + \bar{Q}_{2L}\Phi_2\right] Q_{3R} + y_4^q \bar{Q}_{3L}\left[\Phi_1 Q_{1R} + \Phi_2 Q_{2R}\right] + y_5^q \bar{Q}_{3L}\Phi_3 Q_{3R} \\
& + \tilde{y}_1^q \left[\bar{Q}_{1L}\left(\tilde{\Phi}_1 Q_{2R} + \tilde{\Phi}_2 Q_{1R}\right) + \bar{Q}_{2L}\left(\tilde{\Phi}_1 Q_{1R} - \tilde{\Phi}_2 Q_{2R}\right)\right] + \tilde{y}_2^q \left[\bar{Q}_{1L}\tilde{\Phi}_3 Q_{1R} + \bar{Q}_{2L}\tilde{\Phi}_3 Q_{2R}\right] \\
& + \tilde{y}_3^q \left[\bar{Q}_{1L}\tilde{\Phi}_1 + \bar{Q}_{2L}\tilde{\Phi}_2\right] Q_{3R} + \tilde{y}_4^q \bar{Q}_{3L}\left[\tilde{\Phi}_1 Q_{1R} + \tilde{\Phi}_2 Q_{2R}\right] + \tilde{y}_5^q \bar{Q}_{3L}\tilde{\Phi}_3 Q_{3R} \\
& + y_1^\ell \left[\bar{L}_1\left(\Phi_1 R_2 + \Phi_2 R_1\right) + \bar{L}_2\left(\Phi_1 R_1 - \Phi_2 R_2\right)\right] + y_2^\ell \left[\bar{L}_1\Phi_3 R_1 + \bar{L}_2\Phi_3 R_2\right] + y_3^\ell \left[\bar{L}_1\Phi_1 + \bar{L}_2\Phi_2\right] R_3 \\
& + y_4^\ell \bar{L}_3\left[\Phi_1 R_1 + \Phi_2 R_2\right] + y_5^\ell \bar{L}_3\Phi_3 R_3 + \tilde{y}_1^\ell \left[\bar{L}_1\left(\tilde{\Phi}_1 R_2 + \tilde{\Phi}_2 R_1\right) + \bar{L}_2\left(\tilde{\Phi}_1 R_1 - \tilde{\Phi}_2 R_2\right)\right] \\
& + \tilde{y}_2^\ell \left[\bar{L}_1\tilde{\Phi}_3 R_1 + \bar{L}_2\tilde{\Phi}_3 R_2\right] + \tilde{y}_3^\ell \left[\bar{L}_1\tilde{\Phi}_1 + \bar{L}_2\tilde{\Phi}_2\right] R_3 + \tilde{y}_4^\ell \bar{L}_3\left[\tilde{\Phi}_1 R_1 + \tilde{\Phi}_2 R_2\right] + \tilde{y}_5^\ell \bar{L}_3\tilde{\Phi}_3 R_3 \\
& + y_1^L \left[\bar{L}_1\Delta_L L_1^c + \bar{L}_2\Delta_L L_2^c\right] + y_2^L \bar{L}_3\Delta_L L_3^c + y_1^R \left[\bar{R}_1^c\Delta_R R_1 + \bar{R}_2^c\Delta_R R_2\right] + y_2^R \bar{R}_3^c\Delta_R R_3 + h.c.
\end{aligned} \tag{12}$$

As mentioned previously, after the usual spontaneous symmetry breaking in the left-right symmetric theory, the fermion mass matrices acquire the following structure[2]

$$\mathbf{M}_f = \begin{pmatrix} a_f + b'_f & b_f & c_f \\ b_f & a_f - b'_f & c'_f \\ h_f & h'_f & g_f \end{pmatrix}, \qquad \mathbf{M}_{(L,R)} = \begin{pmatrix} a_{(L,R)} & 0 & 0 \\ 0 & a_{(L,R)} & 0 \\ 0 & 0 & b_{(L,R)} \end{pmatrix}, \tag{13}$$

where $f = u,\, d,\, D,\, e$ denotes the up-type quarks, down-type quarks, Dirac neutrinos, and charged leptons, respectively. In addition, the matrix elements are given by

$$\begin{aligned}
& a_u = y_2^q k_3 + \tilde{y}_2^q k_3'^*, \quad b'_u = y_1^q k_2 + \tilde{y}_1^q k_2'^*, \quad b_u = y_1^q k_1 + \tilde{y}_1^q k_1'^*, \quad c_u = y_3^q k_1 + \tilde{y}_3^q k_1'^*, \quad c'_u = y_3^q k_2 + \tilde{y}_3^q k_2'^*; \\
& h_u = y_3^{\dagger q} k_1 + \tilde{y}_3^{\dagger q} k_1'^*, \quad h'_u = y_3^{\dagger q} k_2 + \tilde{y}_3^{\dagger q} k_2'^*, \quad g_u = y_5^q k_3 + \tilde{y}_5^q k_3'^*, \quad a_d = y_2^q k'_3 + \tilde{y}_2^q k_3^*, \quad b'_d = y_1^q k'_2 + \tilde{y}_1^q k_2^*; \\
& b_d = y_1^q k'_1 + \tilde{y}_1^q k_1^*, \quad c_d = y_3^q k'_1 + \tilde{y}_3^q k_1^*, \quad c'_d = y_3^q k'_2 + \tilde{y}_3^q k_2^*, \quad h_d = y_3^{\dagger q} k'_1 + \tilde{y}_3^{\dagger q} k_1^*, \quad h'_d = y_3^{\dagger q} k'_2 + \tilde{y}_3^{\dagger q} k_2^*; \\
& g_d = y_5^q k'_3 + \tilde{y}_5^q k_3^*, \quad a_D = y_2^\ell k_3 + \tilde{y}_2^\ell k_3'^*, \quad b'_D = y_1^\ell k_2 + \tilde{y}_1^\ell k_2'^*, \quad b_D = y_1^\ell k_1 + \tilde{y}_1^\ell k_1'^*, \quad c_D = y_3^\ell k_1 + \tilde{y}_3^\ell k_1'^*; \\
& c'_D = y_3^\ell k_2 + \tilde{y}_3^\ell k_2'^*, \quad h_D = y_3^{\dagger\ell} k_1 + \tilde{y}_3^{\dagger\ell} k_1'^*, \quad h'_D = y_3^{\dagger\ell} k_2 + \tilde{y}_3^{\dagger\ell} k_2'^*, \quad g_D = y_5^\ell k_3 + \tilde{y}_5^\ell k_3'^*, \quad a_e = y_2^\ell k'_3 + \tilde{y}_2^\ell k_3^*; \\
& b'_e = y_1^\ell k'_2 + \tilde{y}_1^\ell k_2^*, \quad b_e = y_1^\ell k'_1 + \tilde{y}_1^\ell k_1^*, \quad c_e = y_3^\ell k'_1 + \tilde{y}_3^\ell k_1^*, \quad c'_e = y_3^\ell k'_2 + \tilde{y}_3^\ell k_2^*, \quad h_e = y_3^{\dagger\ell} k'_1 + \tilde{y}_3^{\dagger\ell} k_1^*; \\
& h'_e = y_3^{\dagger\ell} k'_2 + \tilde{y}_3^{\dagger\ell} k_2^*, \quad g_e = y_5^\ell k'_3 + \tilde{y}_5^\ell k_3^*, \quad a_{(L,R)} = y_1^R v_{(L,R)}, \quad b_{(L,R)} = y_2^R v_{(L,R)}.
\end{aligned} \tag{14}$$

Here, parity symmetry has been imposed. At this stage we impose the vacuum alignment in the S_3-doublet bidoublet sector. Writing

$$\langle \Phi_I \rangle = \begin{pmatrix} k_I & 0 \\ 0 & k'_I \end{pmatrix}, \qquad I = 1, 2, \tag{15}$$

[2] The mass matrix $\mathbf{M}_f$ commonly appears in minimal extensions of the Standard Model based on the S_3 flavor symmetry [62–75]. As will be discussed below, within left-right symmetric theories this mass matrix may be either complex symmetric or Hermitian.

we choose the symmetric direction

$$k_1 = k_2 \equiv k_D, \qquad k_1' = k_2' \equiv k_D'. \tag{16}$$

while the VEVs of the S_3-singlet bidoublet Φ_3 remain independent. This alignment identifies the matrix elements generated by Φ_1 and Φ_2, reducing the number of independent entries of Eq. (13). Together with the parity conditions and the defining properties of the pseudomanifest and manifest realizations, it leads to the reduced mass-matrix structures given below. We emphasize that the symmetric direction is adopted as a vacuum ansatz and is not derived here from the minimization of the complete scalar potential. Consequently, if the VEVs are complex, the fermion mass matrices become complex symmetric. In the literature, this scenario is commonly referred to as the **pseudomanifest left-right symmetric framework** [76, 77]. On the other hand, if the VEVs are real, the fermion mass matrices are Hermitian and the number of CP-violating phases is significantly reduced. This case is known as the **manifest left-right symmetric framework** [76, 78]. Explicitly, the mass matrices have the form

- **Pseudomanifest left-right theory (PLRT)**.

$$\mathbf{M}_f = \begin{pmatrix} a_f + b_f & b_f & c_f \\ b_f & a_f - b_f & c_f \\ c_f & c_f & g_f \end{pmatrix}, \quad \mathbf{M}_{(L,R)} = \begin{pmatrix} a_{(L,R)} & 0 & 0 \\ 0 & a_{(L,R)} & 0 \\ 0 & 0 & b_{(L,R)} \end{pmatrix}. \tag{17}$$

  Here, the $\mathbf{M}_f$ is a complex symmetric matrix.

- **Manifest left-right theory (MLRT)**.

$$\mathbf{M}_f = \begin{pmatrix} a_f + b_f & b_f & c_f \\ b_f^* & a_f - b_f & c_f \\ c_f^* & c_f^* & g_f \end{pmatrix}, \quad \mathbf{M}_{(L,R)} = \begin{pmatrix} a_{(L,R)} & 0 & 0 \\ 0 & a_{(L,R)} & 0 \\ 0 & 0 & b_{(L,R)} \end{pmatrix}. \tag{18}$$

  Here, $\mathbf{M}_f$ is a Hermitian matrix. Therefore, if both combinations $(a_f + b_f)$ and $(a_f - b_f)$ are simultaneously real, then the parameters a_f and b_f must necessarily be real as well. As a consequence, c_f remains as the only complex parameter in the above mass matrix.

As can be observed, the Majorana neutrino mass matrices, $\mathbf{M}_{(L,R)}$, are diagonal. This implies that neutrino mixing arises from the interplay between the type-I seesaw mechanism and the charged-lepton sector. Furthermore, in the right-handed sector, the corresponding PMNS mixing matrix is completely determined by the charged-lepton sector, as will be shown below.

The effective neutrino mass matrix is generated through the combined type-I and type-II seesaw mechanism and is given by

$$\mathbf{M}_\nu = \mathbf{M}_L - \mathbf{M}_D \mathbf{M}_R^{-1} \mathbf{M}_D^T, \tag{19}$$

where $\mathbf{M}_L$, $\mathbf{M}_D$, and $\mathbf{M}_R$ denote the left-handed Majorana, Dirac, and right-handed Majorana neutrino mass matrices, respectively. In both the **PLRT** and **MLRT** frameworks, the mass matrices entering Eq. (19), together with the charged-lepton mass matrix $\mathbf{M}_e$, are given in Eqs. (17) and (18). The main distinction between the fermion mass matrices $\mathbf{M}_f$ in these two scenarios lies in their mathematical structure: in the **PLRT** framework they are complex symmetric matrices, whereas in the **MLRT** framework they are Hermitian. Nevertheless, in both cases the effective neutrino mass matrix $\mathbf{M}_\nu$ resulting from the seesaw mechanism is a complex symmetric matrix, as required for Majorana neutrinos. The explicit form of $\mathbf{M}_\nu$ is given by

$$\mathbf{M}_\nu^{(\mathtt{j})} = \begin{pmatrix} f_\nu^{(\mathtt{j})} & a_\nu^{(\mathtt{j})} & d_\nu^{(\mathtt{j})} \\ a_\nu^{(\mathtt{j})} & b_\nu^{(\mathtt{j})} & c_\nu^{(\mathtt{j})} \\ d_\nu^{(\mathtt{j})} & c_\nu^{(\mathtt{j})} & g_\nu^{(\mathtt{j})} \end{pmatrix} \tag{20}$$

where $\mathtt{j} = 1$ denotes the **PLRT** framework, while $\mathtt{j} = 2$ denotes the **MLRT** scenario. For the PLRT framework

$$\begin{aligned} a_\nu^{(1)} &= -\tfrac{c_D^2}{b_R} - \tfrac{b_D(a_D - b_D)}{a_R} - \tfrac{b_D(a_D + b_D)}{a_R}, \quad b_\nu^{(1)} = a_L - \tfrac{c_D^2}{b_R} - \tfrac{b_D^2}{a_R} - \tfrac{(a_D - b_D)^2}{a_R}, \\ c_\nu^{(1)} &= -\tfrac{c_D g_D}{b_R} - \tfrac{b_D c_D}{a_R} - \tfrac{c_D(a_D - b_D)}{a_R}, \quad d_\nu^{(1)} = -\tfrac{c_D g_D}{b_R} - \tfrac{b_D c_D}{a_R} - \tfrac{c_D(a_D + b_D)}{a_R}, \\ f_\nu^{(1)} &= a_L - \tfrac{c_D^2}{b_R} - \tfrac{b_D^2}{a_R} - \tfrac{(a_D + b_D)^2}{a_R}, \quad g_\nu^{(1)} = b_L - \tfrac{g_D^2}{b_R} - \tfrac{2c_D^2}{a_R}. \end{aligned} \tag{21}$$

While for the MLRT framework

$$\begin{aligned}
a_\nu^{(2)} &= -\tfrac{c_D^2}{b_R} - \tfrac{b_D^*(a_D+b_D)}{a_R} - \tfrac{b_D(a_D-b_D)}{a_R}, \quad b_\nu^{(2)} = a_L - \tfrac{c_D^2}{b_R} - \tfrac{b_D^{*2}}{a_R} - \tfrac{(a_D-b_D)^2}{a_R}, \\
c_\nu^{(2)} &= -\tfrac{c_D g_D}{b_R} - \tfrac{b_D^* c_D^*}{a_R} - \tfrac{c_D^*(a_D-b_D)}{a_R}, \quad d_\nu^{(2)} = -\tfrac{c_D g_D}{b_R} - \tfrac{c_D^* b_D}{a_R} - \tfrac{c_D^*(a_D+b_D)}{a_R}, \\
f_\nu^{(2)} &= a_L - \tfrac{c_D^2}{b_R} - \tfrac{b_D^2}{a_R} - \tfrac{(a_D+b_D)^2}{a_R}, \quad g_\nu^{(2)} = b_L - \tfrac{g_D^2}{b_R} - \tfrac{2c_D^{*2}}{a_R}.
\end{aligned} \tag{22}$$

Within the PLRT framework, the fermion mass matrices $\mathbf{M}_f$ can be brought into diagonal form through a unitary transformation which is [56, 79]

$$\mathbf{M}_q = \mathbf{U}_q^\top \hat{\mathbf{M}}_q \mathbf{U}_q \;\text{ for quarks,} \quad \text{and} \quad \mathbf{M}_e = \mathbf{U}_e \hat{\mathbf{M}}_e \mathbf{U}_e^\top \;\text{ for charged leptons,} \tag{23}$$

with $q = u, d$. On the other hand, within the MLRT framework, we have

$$\mathbf{M}_q = \mathbf{U}_q^\dagger \hat{\mathbf{M}}_q \mathbf{U}_q \;\text{ for quarks,} \quad \text{and} \quad \mathbf{M}_e = \mathbf{U}_e \hat{\mathbf{M}}_e \mathbf{U}_e^\dagger \;\text{ for charged leptons.} \tag{24}$$

In the above expressions $\hat{\mathbf{M}}_f$, with $f = u, d, e, D$, is a diagonal matrix whose non-negative real entries correspond to the physical fermion masses. Also,

$$\begin{aligned}
&\mathbf{U}_q = \mathbf{O}_q^\top \mathbf{P}_q \mathbf{R}_{\frac{\pi}{4}} \quad \text{and} \quad \mathbf{U}_e = \mathbf{R}_{\frac{\pi}{4}}^\top \mathbf{P}_e^\top \mathbf{O}_e \qquad \text{for PLRT.} \\
&\mathbf{U}_q = \mathbf{O}_q^\top \mathbf{P}_q \mathbf{R}_{\frac{\pi}{4}} \quad \text{and} \quad \mathbf{U}_e = \mathbf{R}_{\frac{\pi}{4}}^\top \mathbf{P}_e^\dagger \mathbf{O}_e \qquad \text{for MLRT.}
\end{aligned} \tag{25}$$

In both theoretical frameworks, the effective neutrino mass matrix is diagonalized by a unitary transformation of the form [79]

$$\mathbf{M}_\nu = \mathbf{U}_\nu^{(\mathrm{j})} \hat{\mathbf{M}}_\nu \mathbf{U}_\nu^{(\mathrm{j})\top} \quad \text{with} \quad \mathbf{U}_\nu^{(\mathrm{j})} = \mathbf{R}_{\beta_\nu}^{(\mathrm{j})\top} \mathbf{P}_\nu^{(\mathrm{j})\top} \mathbf{O}_\nu \tag{26}$$

In the above expressions, $\mathbf{R}_{\frac{\pi}{4}}$ and $\mathbf{R}_{\beta_\nu}$ represent the rotation matrices that bring the fermion mass matrices to a basis where the $(1,3)$ and $(3,1)$ matrix elements are identically zero. Their explicit forms are given by

$$\mathbf{R}_{\frac{\pi}{4}} = \begin{pmatrix} \cos\left(\frac{\pi}{4}\right) & -\sin\left(\frac{\pi}{4}\right) & 0 \\ \sin\left(\frac{\pi}{4}\right) & \cos\left(\frac{\pi}{4}\right) & 0 \\ 0 & 0 & 1 \end{pmatrix} \quad \text{and} \quad \mathbf{R}_{\beta_\nu}^{(\mathrm{j})} = \begin{pmatrix} \cos\beta_\nu^{(\mathrm{j})} & -\sin\beta_\nu^{(\mathrm{j})} & 0 \\ \sin\beta_\nu^{(\mathrm{j})} & \cos\beta_\nu^{(\mathrm{j})} & 0 \\ 0 & 0 & 1 \end{pmatrix}. \tag{27}$$

where $\tan\beta_\nu^{(\mathrm{j})} = \frac{|d_\nu^{(\mathrm{j})}|}{|c_\nu^{(\mathrm{j})}|}$ with $\arg\{c_\nu^{(\mathrm{j})}\} = \arg\{d_\nu^{(\mathrm{j})}\}$. The matrices $\mathbf{O}_\ell$ correspond to the real orthogonal matrices entering the decomposition of the unitary matrices $\mathbf{U}_\ell$. Here, the index $\ell = u, d, e, \nu$ refers to the up-type quark, down-type quark, charged-lepton, and neutrino sectors, respectively. Their explicit form is given by

$$\mathbf{O}_\ell = \begin{pmatrix} \sqrt{\frac{\sigma_{\ell2}\sigma_{\ell3}\xi_{\ell1}}{\mathtt{D}_{\ell1}}} & -\sqrt{\frac{\sigma_{\ell1}\sigma_{\ell3}\xi_{\ell2}}{\mathtt{D}_{\ell2}}} & \sqrt{\frac{\sigma_{\ell1}\sigma_{\ell2}\xi_{\ell3}}{\mathtt{D}_{\ell3}}} \\ \sqrt{\frac{\sigma_{\ell1}\mathcal{D}_\ell\xi_{\ell1}}{\mathtt{D}_{\ell1}}} & \sqrt{\frac{\sigma_{\ell2}\mathcal{D}_\ell\xi_{\ell2}}{\mathtt{D}_{\ell2}}} & \sqrt{\frac{\sigma_{\ell3}\mathcal{D}_\ell\xi_{\ell3}}{\mathtt{D}_{\ell3}}} \\ -\sqrt{\frac{\sigma_{\ell1}\xi_{\ell3}\xi_{\ell2}}{\mathtt{D}_{\ell1}}} & -\sqrt{\frac{\sigma_{\ell2}\xi_{\ell3}\xi_{\ell1}}{\mathtt{D}_{\ell2}}} & \sqrt{\frac{\sigma_{\ell3}\xi_{\ell1}\xi_{\ell2}}{\mathtt{D}_{\ell3}}} \end{pmatrix}, \tag{28}$$

where $\sigma_{\ell1} = m_{\ell1} - m_{11}^\ell$, $\sigma_{\ell2} = m_{\ell2} + m_{11}^\ell$, $\sigma_{\ell3} = m_{\ell3} - m_{11}^\ell$, $\xi_{\ell1} = (\mathcal{D}_\ell - \sigma_{\ell1})$, $\xi_{\ell2} = (\mathcal{D}_\ell + \sigma_{\ell2})$, $\xi_{\ell3} = (\sigma_{\ell3} - \mathcal{D}_\ell)$, $\mathtt{D}_{\ell1} = \mathcal{D}_\ell\,(\sigma_{\ell2} + \sigma_{\ell1})\,(\sigma_{\ell3} - \sigma_{\ell1})$, $\mathtt{D}_{\ell2} = \mathcal{D}_\ell\,(\sigma_{\ell3} + \sigma_{\ell2})\,(\sigma_{\ell2} + \sigma_{\ell1})$, $\mathtt{D}_{\ell3} = \mathcal{D}_\ell\,(\sigma_{\ell3} + \sigma_{\ell2})\,(\sigma_{\ell3} - \sigma_{\ell1})$. The quantities $\sigma_{\ell i}$, with $i = 1, 2, 3$, correspond to the shifted masses of fermions and are related to the physical fermion masses through the expressions $\sigma_{\ell1} = m_{\ell1} - m_{11}^\ell$, $\sigma_{\ell2} = m_{\ell2} + m_{11}^\ell$, $\sigma_{\ell3} = m_{\ell3} - m_{11}^\ell$. The parameter m_{11}^ℓ denotes the $(1,1)$ entry of the rotated fermion mass matrix. After extracting this contribution, the resulting mass matrix acquires an effective two texture zeros structure, which considerably simplifies its analytical diagonalization. [79]. The explicit form of m_{11}^ℓ is: $m_{11}^f = |a_f - b_f|$ for PLRT, $m_{11}^f = a_f - b_f$ for MLRT and $m_{11}^\nu = |b_\nu^{(\mathrm{j})} \sin^2\beta_\nu^{(\mathrm{j})} + f_\nu^{(\mathrm{j})} \cos^2\beta_\nu^{(\mathrm{j})} - a_\nu^{(\mathrm{j})} \sin 2\beta_\nu^{(\mathrm{j})}|$ for neutrinos in both theoretical frameworks. The parameter $\mathcal{D}_f$ is explicitly given by $\mathcal{D}_f = |g_f| + |a_f - b_f|$ for PLRT, $\mathcal{D}_f = g_f + b_f - a_f$ for MLRT, and $\mathcal{D}_\nu = |g_\nu^{(\mathrm{j})}| - |b_\nu^{(\mathrm{j})} \sin^2\beta_\nu^{(\mathrm{j})} + f_\nu^{(\mathrm{j})} \cos^2\beta_\nu^{(\mathrm{j})} - a_\nu^{(\mathrm{j})} \sin 2\beta_\nu^{(\mathrm{j})}|$ for neutrinos in both theoretical frameworks. For a normal fermion mass hierarchy, these parameters m_{11}^ℓ and $\mathcal{D}_\ell$ satisfy $m_{\ell1} > m_{11}^\ell$,

$\sigma_{\ell 3} > \mathcal{D}_\ell > \sigma_{\ell 1}$, and $\mathcal{D}_\ell \neq \sigma_{\ell 1} - \sigma_{\ell 2} + \sigma_{\ell 3}$. For an inverted hierarchy, which occurs only in the neutrino sector, the corresponding conditions are $m_{\ell 3} > m_{11}^{\ell}$, $\sigma_{\ell 1} > \mathcal{D}_\ell > \sigma_{\ell 3}$, and $\mathcal{D}_\ell \neq \sigma_{\ell 1} - \sigma_{\ell 2} + \sigma_{\ell 3}$. Finally,

$$\mathbf{P}_f = \text{diag}\left(e^{i\frac{\alpha_f}{2}}, e^{i\frac{\beta_f}{2}}, e^{i\frac{\gamma_f}{2}}\right) \quad \text{for PLRT}, \qquad \mathbf{P}_f = \text{diag}\left(1, 1, e^{i\phi_{fc}}\right) \quad \text{for MLRT}, \tag{29}$$

where $\alpha_f = \arg\{a_f - b_f\}$, $\beta_f = \arg\{a_f + b_f\}$, and $\gamma_f = \arg\{g_f\}$, while $\phi_{fc} = \arg\{c_f\}$. Also, for the PLRT we have $\arg\{a_f - b_f\} + \arg\{a_f + b_f\} = 2\arg\{b_f\}$, $\arg\{a_f + b_f\} + \arg\{g_f\} = 2\arg\{c_f\}$. For neutrinos in both theoretical frameworks

$$\mathbf{P}_\nu^{(\mathtt{j})} = \text{diag}\left(e^{i\frac{\alpha_\nu^{(\mathtt{j})}}{2}}, e^{i\frac{\beta_\nu^{(\mathtt{j})}}{2}}, e^{i\frac{\gamma_\nu^{(\mathtt{j})}}{2}}\right), \tag{30}$$

where $\alpha_\nu^{(\mathtt{j})} = \arg\{m_{11}^\nu\}$, $\beta_\nu^{(\mathtt{j})} = \arg\{m_{22}^\nu\}$, $\gamma_\nu^{(\mathtt{j})} = \arg\{m_{33}^\nu\}$, $\arg\{m_{11}^\nu\} + \arg\{m_{22}^\nu\} = 2\arg\{m_{12}^\nu\}$, $\arg\{m_{11}^\nu\} + \arg\{m_{33}^\nu\} = \arg\{m_{23}^\nu\}$. The m_{ij}^ν are the elements of the rotated neutrino mass matrix. An important result of our analysis is that the unitary matrices arising in the PLRT and MLRT frameworks differ only in the number of independent CP-violating phase factors they contain. In particular, from a model-independent perspective, the unitary matrix obtained in the MLRT framework emerges naturally as a more restrictive realization of the general structure derived in the PLRT case. This highlights the fact that the MLRT scenario can be understood as a specific limit of the broader PLRT framework [56, 79]. Also, in general terms we can say that in this left-right model, we have a unified treatment of the fermion mass matrices since these can be reduced to a matrix with two texture zeros.

A. Flavor mixing matrix in quark sector

In this section, our primary objective is to derive the theoretical expressions for the left- and right-handed quark flavor mixing matrices, commonly known as the CKM matrices. These mixing matrices originate from the mismatch between the diagonalization of the up- and down-type quark mass matrices. Consequently, by virtue of the singular value decomposition theorem, the following bilinear forms are obtained:

$$\hat{\mathbf{M}}_q \hat{\mathbf{M}}_q^\dagger = \mathbf{U}_{qL}^\dagger \mathbf{M}_q \mathbf{M}_q^\dagger \mathbf{U}_{qL} \qquad \text{and} \qquad \hat{\mathbf{M}}_q^\dagger \hat{\mathbf{M}}_q = \mathbf{U}_{qR}^\dagger \mathbf{M}_q^\dagger \mathbf{M}_q \mathbf{U}_{qR}, \tag{31}$$

where $\hat{\mathbf{M}}_q = \text{diag}(m_{q_1}, m_{q_2}, m_{q_3})$ and $\mathbf{U}_{q(L,R)}$ are unitary matrices. We obtain that the left- and right-handed CKM matrices have the form [80]

$$\mathbf{V}_{CKM}^L = \mathbf{U}_{uL}\mathbf{U}_{dL}^\dagger \qquad \text{and} \qquad \mathbf{V}_{CKM}^R = \mathbf{U}_{uR}\mathbf{U}_{dR}^\dagger \tag{32}$$

As discussed above, the left- and right-handed CKM matrices are related differently in the PLRT and MLRT frameworks. In the MLRT case, where the quark mass matrices are Hermitian, $\mathbf{M}_q = \mathbf{M}_q^\dagger$, the diagonalization matrices satisfy $\mathbf{U}_{qL} = \mathbf{U}_{qR}$. Consequently, $\mathbf{V}_{\text{CKM}}^L = \mathbf{V}_{\text{CKM}}^R = \mathbf{U}_{uL}\mathbf{U}_{dL}^\dagger$. In this theoretical framework, the left- and right-handed quark mixing matrices are equal to each other. On the other hand, in the **PLRT** framework, where the quark mass matrices are complex symmetric, $\mathbf{M}_q = \mathbf{M}_q^\top$, the unitary matrices satisfy the relation $\mathbf{U}_{qL} = \mathbf{U}_{qR}^*$. As a consequence, the CKM matrices take the form $\mathbf{V}_{\text{CKM}}^R = \left(\mathbf{V}_{\text{CKM}}^L\right)^* = \mathbf{U}_{uL}^*\mathbf{U}_{dL}^\top$. In this scenario, after performing the polar decomposition of the unitary matrices that diagonalize the quark mass matrices, one obtains $\mathbf{V}_{\text{CKM}}^L = \mathbf{O}_u^\top \mathbf{P}^{(u-d)} \mathbf{O}_d$ and $\mathbf{V}_{\text{CKM}}^R = \mathbf{O}_u^\top \mathbf{P}^{(u-d)\dagger} \mathbf{O}_d$, where $\mathbf{O}_q$ denotes a real orthogonal matrix and $\mathbf{P}^{(u-d)} = \mathbf{P}_u\mathbf{P}_d^\dagger$ is a diagonal matrix of phase factors. Hence, the only difference between $\mathbf{V}_{\text{CKM}}^L$ and $\mathbf{V}_{\text{CKM}}^R$ lies in the sign of the phase factors. The explicit form of the left-handed CKM mixing matrix is given by [56]

$$\mathbf{V}_{\text{CKM}}^{L(\mathtt{j})} = e^{i\zeta_\mathtt{j}}\, \mathbf{O}_u^\top \mathbf{P}_\mathtt{j}^{(u-d)} \mathbf{O}_d, \tag{33}$$

where

$$\mathbf{P}_\mathtt{j}^{(u-d)} = \text{diag}\left(1, e^{i\Theta_\mathtt{j}}, e^{i\Gamma_\mathtt{j}}\right), \tag{34}$$

here $\mathtt{j} = 1$ denotes the **PLRT** framework, while $\mathtt{j} = 2$ denotes the **MLRT** scenario, and

$$\begin{array}{lll} \Theta_1 = \frac{\alpha_{d1} - \alpha_{u1} + \beta_{u1} - \beta_{d1}}{2}, & \Gamma_1 = \frac{\alpha_{d1} - \alpha_{u1} + \gamma_{u1} - \gamma_{d1}}{2}, & \zeta_1 = \alpha_{u1} - \alpha_{d1}, \\ \Theta_2 = 0, & \Gamma_2 = \phi_{uc} - \phi_{dc}, & \zeta_2 = 0. \end{array} \tag{35}$$

It is worth noting that the rotation matrix $R_{\frac{\pi}{4}}$ does not contribute to the CKM matrix, since it appears identically in the diagonalization of both the up- and down-quark sectors. As a consequence, this common rotation cancels out in the construction of the CKM matrix. This feature constitutes a non-trivial prediction of the underlying S_3 flavor symmetry and indicates that the experimentally observed quark mixing is generated solely by the symmetry-breaking effects encoded in the fermion mass eigenvalues and phase factors. Therefore, the flavor symmetry naturally removes an otherwise large mixing contribution, providing a possible explanation for the hierarchical structure of the CKM matrix [62, 75, 81]. Consequently, from expressions in Eqs. (25)-(29), the explicit form of the CKM mixing in both frameworks is [56, 79]:

$$\mathbf{V}_{\rm CKM}^{L(\mathrm{j})} = e^{i\zeta_{\mathrm{j}}} \begin{pmatrix} V_{ud}^{(\mathrm{j})} & V_{us}^{(\mathrm{j})} & V_{ub}^{(\mathrm{j})} \\ V_{cd}^{(\mathrm{j})} & V_{cs}^{(\mathrm{j})} & V_{cb}^{(\mathrm{j})} \\ V_{td}^{(\mathrm{j})} & V_{ts}^{(\mathrm{j})} & V_{tb}^{(\mathrm{j})} \end{pmatrix} \tag{36}$$

where

$$V_{ud}^{(\mathrm{j})} = \sqrt{\frac{\widetilde{\sigma}_c\widetilde{\sigma}_s\widetilde{\sigma}_t\widetilde{\sigma}_b\widetilde{\xi}_{d1}\widetilde{\xi}_{u1}}{\widetilde{\mathtt{D}}_{u1}\widetilde{\mathtt{D}}_{d1}}} + \sqrt{\frac{\widetilde{\sigma}_u\widetilde{\sigma}_d}{\widetilde{\mathtt{D}}_{u1}\widetilde{\mathtt{D}}_{d1}}}\varepsilon_{ud}^{(\mathrm{j})},\ V_{us}^{(\mathrm{j})} = -\sqrt{\frac{\widetilde{\sigma}_c\widetilde{\sigma}_d\widetilde{\sigma}_t\widetilde{\sigma}_b\widetilde{\xi}_{u1}\widetilde{\xi}_{d2}}{\widetilde{\mathtt{D}}_{u1}\widetilde{\mathtt{D}}_{d2}}} + \sqrt{\frac{\widetilde{\sigma}_u\widetilde{\sigma}_s}{\widetilde{\mathtt{D}}_{u1}\widetilde{\mathtt{D}}_{d2}}}\varepsilon_{us}^{(\mathrm{j})}, \tag{37}$$

$$V_{ub}^{(\mathrm{j})} = \sqrt{\frac{\widetilde{\sigma}_c\widetilde{\sigma}_d\widetilde{\sigma}_s\widetilde{\sigma}_t\widetilde{\xi}_{u1}\widetilde{\xi}_{d3}}{\widetilde{\mathtt{D}}_{u1}\widetilde{\mathtt{D}}_{d3}}} - \sqrt{\frac{\widetilde{\sigma}_u\widetilde{\sigma}_b}{\widetilde{\mathtt{D}}_{u1}\widetilde{\mathtt{D}}_{d3}}}\varepsilon_{ub}^{(\mathrm{j})},\ V_{cd}^{(\mathrm{j})} = -\sqrt{\frac{\widetilde{\sigma}_u\widetilde{\sigma}_s\widetilde{\sigma}_t\widetilde{\sigma}_b\widetilde{\xi}_{u2}\widetilde{\xi}_{d1}}{\widetilde{\mathtt{D}}_{u2}\widetilde{\mathtt{D}}_{d1}}} + \sqrt{\frac{\widetilde{\sigma}_c\widetilde{\sigma}_d}{\widetilde{\mathtt{D}}_{u2}\widetilde{\mathtt{D}}_{d1}}}\varepsilon_{cd}^{(\mathrm{j})}, \tag{38}$$

$$V_{cs}^{(\mathrm{j})} = \sqrt{\frac{\widetilde{\sigma}_u\widetilde{\sigma}_d\widetilde{\sigma}_t\widetilde{\sigma}_b\widetilde{\xi}_{u2}\widetilde{\xi}_{d2}}{\widetilde{\mathtt{D}}_{u2}\widetilde{\mathtt{D}}_{d2}}} + \sqrt{\frac{\widetilde{\sigma}_c\widetilde{\sigma}_s}{\widetilde{\mathtt{D}}_{u2}\widetilde{\mathtt{D}}_{d2}}}\varepsilon_{cs}^{(\mathrm{j})},\ V_{cb}^{(\mathrm{j})} = -\sqrt{\frac{\widetilde{\sigma}_u\widetilde{\sigma}_d\widetilde{\sigma}_s\widetilde{\sigma}_t\widetilde{\xi}_{u2}\widetilde{\xi}_{d3}}{\widetilde{\mathtt{D}}_{u2}\widetilde{\mathtt{D}}_{d3}}} - \sqrt{\frac{\widetilde{\sigma}_c\widetilde{\sigma}_b}{\widetilde{\mathtt{D}}_{u2}\widetilde{\mathtt{D}}_{d3}}}\varepsilon_{cb}^{(\mathrm{j})}, \tag{39}$$

$$V_{td}^{(\mathrm{j})} = \sqrt{\frac{\widetilde{\sigma}_u\widetilde{\sigma}_c\widetilde{\sigma}_s\widetilde{\sigma}_b\widetilde{\xi}_{u3}\widetilde{\xi}_{d1}}{\widetilde{\mathtt{D}}_{u3}\widetilde{\mathtt{D}}_{d1}}} - \sqrt{\frac{\widetilde{\sigma}_d\widetilde{\sigma}_t}{\widetilde{\mathtt{D}}_{u3}\widetilde{\mathtt{D}}_{d1}}}\varepsilon_{td}^{(\mathrm{j})},\ V_{ts}^{(\mathrm{j})} = -\sqrt{\frac{\widetilde{\sigma}_u\widetilde{\sigma}_c\widetilde{\sigma}_d\widetilde{\sigma}_b\widetilde{\xi}_{u3}\widetilde{\xi}_{d2}}{\widetilde{\mathtt{D}}_{u3}\widetilde{\mathtt{D}}_{d2}}} - \sqrt{\frac{\widetilde{\sigma}_s\widetilde{\sigma}_t}{\widetilde{\mathtt{D}}_{u3}\widetilde{\mathtt{D}}_{d2}}}\varepsilon_{ts}^{(\mathrm{j})}, \tag{40}$$

$$V_{tb}^{(\mathrm{j})} = \sqrt{\frac{\widetilde{\sigma}_u\widetilde{\sigma}_c\widetilde{\sigma}_d\widetilde{\sigma}_s\widetilde{\xi}_{u3}\widetilde{\xi}_{d3}}{\widetilde{\mathtt{D}}_{u3}\widetilde{\mathtt{D}}_{d3}}} + \sqrt{\frac{\widetilde{\sigma}_t\widetilde{\sigma}_b}{\widetilde{\mathtt{D}}_{u3}\widetilde{\mathtt{D}}_{d3}}}\varepsilon_{tb}^{(\mathrm{j})}, \tag{41}$$

where

$$\varepsilon_{ud}^{(\mathrm{j})} = \sqrt{\widetilde{\xi}_{u2}\widetilde{\xi}_{u3}\widetilde{\xi}_{d2}\widetilde{\xi}_{d3}}e^{i\Gamma_{\mathrm{j}}} + \sqrt{\widetilde{\mathcal{D}}_u\widetilde{\mathcal{D}}_d\widetilde{\xi}_{u1}\widetilde{\xi}_{d1}}e^{i\Theta_{\mathrm{j}}},\ \varepsilon_{us}^{(\mathrm{j})} = \sqrt{\widetilde{\xi}_{u2}\widetilde{\xi}_{u3}\widetilde{\xi}_{d1}\widetilde{\xi}_{d3}}e^{i\Gamma_{\mathrm{j}}} + \sqrt{\widetilde{\mathcal{D}}_u\widetilde{\mathcal{D}}_d\widetilde{\xi}_{u1}\widetilde{\xi}_{d2}}e^{i\Theta_{\mathrm{j}}}, \tag{42}$$

$$\varepsilon_{ub}^{(\mathrm{j})} = \sqrt{\widetilde{\xi}_{u2}\widetilde{\xi}_{u3}\widetilde{\xi}_{d1}\widetilde{\xi}_{d2}}e^{i\Gamma_{\mathrm{j}}} - \sqrt{\widetilde{\mathcal{D}}_u\widetilde{\mathcal{D}}_d\widetilde{\xi}_{u1}\widetilde{\xi}_{d3}}e^{i\Theta_{\mathrm{j}}},\ \varepsilon_{cd}^{(\mathrm{j})} = \sqrt{\widetilde{\xi}_{u1}\widetilde{\xi}_{u3}\widetilde{\xi}_{d2}\widetilde{\xi}_{d3}}e^{i\Gamma_{\mathrm{j}}} + \sqrt{\widetilde{\mathcal{D}}_u\widetilde{\mathcal{D}}_d\widetilde{\xi}_{u2}\widetilde{\xi}_{d1}}e^{i\Theta_{\mathrm{j}}}, \tag{43}$$

$$\varepsilon_{cs}^{(\mathrm{j})} = \sqrt{\widetilde{\xi}_{u1}\widetilde{\xi}_{u3}\widetilde{\xi}_{d1}\widetilde{\xi}_{d3}}e^{i\Gamma_{\mathrm{j}}} + \sqrt{\widetilde{\mathcal{D}}_u\widetilde{\mathcal{D}}_d\widetilde{\xi}_{u2}\widetilde{\xi}_{d2}}e^{i\Theta_{\mathrm{j}}},\ \varepsilon_{cb}^{(\mathrm{j})} = \sqrt{\widetilde{\xi}_{u1}\widetilde{\xi}_{u3}\widetilde{\xi}_{d1}\widetilde{\xi}_{d2}}e^{i\Gamma_{\mathrm{j}}} - \sqrt{\widetilde{\mathcal{D}}_u\widetilde{\mathcal{D}}_d\widetilde{\xi}_{u2}\widetilde{\xi}_{d3}}e^{i\Theta_{\mathrm{j}}}, \tag{44}$$

$$\varepsilon_{td}^{(\mathrm{j})} = \sqrt{\widetilde{\xi}_{u1}\widetilde{\xi}_{u2}\widetilde{\xi}_{d2}\widetilde{\xi}_{d3}}e^{i\Gamma_{\mathrm{j}}} - \sqrt{\widetilde{\mathcal{D}}_u\widetilde{\mathcal{D}}_d\widetilde{\xi}_{u3}\widetilde{\xi}_{d1}}e^{i\Theta_{\mathrm{j}}},\ \varepsilon_{ts}^{(\mathrm{j})} = \sqrt{\widetilde{\xi}_{u1}\widetilde{\xi}_{u2}\widetilde{\xi}_{d1}\widetilde{\xi}_{d3}}e^{i\Gamma_{\mathrm{j}}} - \sqrt{\widetilde{\mathcal{D}}_u\widetilde{\mathcal{D}}_d\widetilde{\xi}_{u3}\widetilde{\xi}_{d2}}e^{i\Theta_{\mathrm{j}}}, \tag{45}$$

$$\varepsilon_{tb}^{(\mathrm{j})} = \sqrt{\widetilde{\xi}_{u1}\widetilde{\xi}_{u2}\widetilde{\xi}_{d1}\widetilde{\xi}_{d2}}e^{i\Gamma_{\mathrm{j}}} + \sqrt{\widetilde{\mathcal{D}}_u\widetilde{\mathcal{D}}_d\widetilde{\xi}_{u3}\widetilde{\xi}_{d3}}e^{i\Theta_{\mathrm{j}}}. \tag{46}$$

Here, $\widetilde{\sigma}_u = \widetilde{m}_u - \widetilde{m}_{11}^u$, $\widetilde{\sigma}_c = \widetilde{m}_c + \widetilde{m}_{11}^u$, $\widetilde{\sigma}_t = 1 - \widetilde{m}_{11}^u$, $\widetilde{\sigma}_d = \widetilde{m}_d - \widetilde{m}_{11}^d$, $\widetilde{\sigma}_s = \widetilde{m}_s + \widetilde{m}_{11}^d$, $\widetilde{\sigma}_b = 1 - \widetilde{m}_{11}^d$,

$$\widetilde{\xi}_{u1} = \widetilde{\mathcal{D}}_u - \widetilde{\sigma}_u, \quad \widetilde{\xi}_{u2} = \widetilde{\mathcal{D}}_u + \widetilde{\sigma}_c, \quad \widetilde{\xi}_{u3} = \widetilde{\sigma}_t - \widetilde{\mathcal{D}}_u, \quad \widetilde{\xi}_{d1} = \widetilde{\mathcal{D}}_d - \widetilde{\sigma}_d, \quad \widetilde{\xi}_{d2} = \widetilde{\mathcal{D}}_d + \widetilde{\sigma}_s, \quad \widetilde{\xi}_{d3} = \widetilde{\sigma}_b - \widetilde{\mathcal{D}}_d, \tag{47}$$

$$\begin{aligned} &\widetilde{\mathtt{D}}_{u1} = \widetilde{\mathcal{D}}_u\left(\widetilde{\sigma}_c + \widetilde{\sigma}_u\right)\left(\widetilde{\sigma}_t - \widetilde{\sigma}_u\right), \quad \widetilde{\mathtt{D}}_{u2} = \widetilde{\mathcal{D}}_u\left(\widetilde{\sigma}_t + \widetilde{\sigma}_c\right)\left(\widetilde{\sigma}_c + \widetilde{\sigma}_u\right), \quad \widetilde{\mathtt{D}}_{u3} = \widetilde{\mathcal{D}}_u\left(\widetilde{\sigma}_t + \widetilde{\sigma}_c\right)\left(\widetilde{\sigma}_t - \widetilde{\sigma}_u\right), \\ &\widetilde{\mathtt{D}}_{d1} = \widetilde{\mathcal{D}}_d\left(\widetilde{\sigma}_s + \widetilde{\sigma}_d\right)\left(\widetilde{\sigma}_b - \widetilde{\sigma}_d\right), \quad \widetilde{\mathtt{D}}_{d2} = \widetilde{\mathcal{D}}_d\left(\widetilde{\sigma}_b + \widetilde{\sigma}_s\right)\left(\widetilde{\sigma}_s + \widetilde{\sigma}_d\right), \quad \widetilde{\mathtt{D}}_{d3} = \widetilde{\mathcal{D}}_d\left(\widetilde{\sigma}_b + \widetilde{\sigma}_s\right)\left(\widetilde{\sigma}_b - \widetilde{\sigma}_d\right). \end{aligned} \tag{48}$$

Also, $\widetilde{m}_u = \frac{m_u}{m_t}$, $\widetilde{m}_c = \frac{m_c}{m_t}$, $\widetilde{m}_d = \frac{m_d}{m_b}$, $\widetilde{m}_s = \frac{m_s}{m_b}$, $\widetilde{\mathcal{D}}_u = \frac{\mathcal{D}_u}{m_t}$, $\widetilde{\mathcal{D}}_d = \frac{\mathcal{D}_d}{m_b}$, $\widetilde{m}^u_{11} = \frac{m^u_{11}}{m_t}$, $\widetilde{m}^d_{11} = \frac{m^d_{11}}{m_b}$, $\widetilde{\sigma}_u = \frac{\sigma_u}{m_t}$, $\widetilde{\sigma}_c = \frac{\sigma_c}{m_t}$, $\widetilde{\sigma}_t = \frac{\sigma_t}{m_t}$, $\widetilde{\sigma}_d = \frac{\sigma_d}{m_b}$, $\widetilde{\sigma}_s = \frac{\sigma_s}{m_b}$, $\widetilde{\sigma}_b = \frac{\sigma_b}{m_b}$, $\widetilde{\xi}_{u1} = \frac{\xi_{u1}}{m_t}$, $\widetilde{\xi}_{u2} = \frac{\xi_{u2}}{m_t}$, $\widetilde{\xi}_{u3} = \frac{\xi_{u3}}{m_t}$, $\widetilde{\xi}_{d1} = \frac{\xi_{d1}}{m_b}$, $\widetilde{\xi}_{d2} = \frac{\xi_{d2}}{m_b}$, $\widetilde{\xi}_{d3} = \frac{\xi_{d3}}{m_b}$. Finally, the parameter $\widetilde{\mathcal{D}}_q$, where $q = u, d$, is required to satisfy the following conditions:

$$\widetilde{\sigma}_{q3} > \widetilde{\mathcal{D}}_q > \widetilde{\sigma}_{q1}, \qquad \widetilde{\mathcal{D}}_q \neq +\widetilde{\sigma}_{q1} - \widetilde{\sigma}_{q2} + \widetilde{\sigma}_{q3}. \tag{49}$$

The above expressions are formulated in terms of mass ratios since both the PDG and recent analyses indicate that the hierarchical structure of quark masses is largely preserved under the renormalization-group evolution. Consequently, the quark mass ratios remain approximately invariant over a wide range of energy scales. [82–84].

1. *Likelihood Test* χ^2

A crucial test of the proposed model is its ability to reproduce the observed phenomenology of the quark sector. Our first objective is therefore to determine whether the fermion mass matrices and the corresponding CKM mixing matrices derived within the **PLRT** and **MLRT** frameworks are consistent with the current experimental information on quark masses and flavor mixing. To this end, we perform a likelihood analysis based on the following χ^2 function:

$$\chi^2 = \frac{\left(|V^{\rm th}_{us}| - |V^{\rm exp}_{us}|\right)^2}{\sigma^2_{us}} + \frac{\left(|V^{\rm th}_{ub}| - |V^{\rm exp}_{ub}|\right)^2}{\sigma^2_{ub}} + \frac{\left(|V^{\rm th}_{cb}| - |V^{\rm exp}_{cb}|\right)^2}{\sigma^2_{cb}}. \tag{50}$$

In the above expression, the superscripts "th" and "exp" denote the theoretical predictions and the corresponding experimental measurements, respectively.

The observables entering the likelihood function are the magnitudes of the CKM matrix elements $|V_{us}|$, $|V_{ub}|$, and $|V_{cb}|$. These quantities are among the most precisely measured flavor observables and are extracted from independent experimental processes, including kaon decays and semileptonic B-meson decays. Owing to their different experimental origins and distinct sources of systematic uncertainty, they can be regarded as effectively uncorrelated in the statistical analysis. Their current experimental values are [85]

$$|V_{us}| = 0.22431 \pm 0.00085, \;\; |V_{ub}| = (3.82 \pm 0.20) \times 10^{-3}, \;\; |V_{cb}| = (41.1 \pm 1.2) \times 10^{-3}. \tag{51}$$

The likelihood function depends on a set of ten free parameters,

$$\chi^2 = \chi^2\left(\widetilde{m}_u, \widetilde{m}_c, \widetilde{m}_d, \widetilde{m}_s, \widetilde{m}^u_{11}, \widetilde{m}^d_{11}, \widetilde{\mathcal{D}}_u, \widetilde{\mathcal{D}}_d, \Gamma_{\rm j}, \Theta_{\rm j}\right). \tag{52}$$

However, it is constrained by only three independent experimental observables. Consequently, the fit is intrinsically underconstrained and the corresponding χ^2 function has no statistical degrees of freedom. As a result, confidence intervals or confidence regions cannot be assigned to the fitted parameters in a statistically meaningful way. Therefore, our analysis is restricted to determining the Best Fit Point (BFP), defined as the parameter configuration that minimizes the χ^2 function and hence provides the best overall agreement between the theoretical predictions and the available experimental data. For the purpose of characterizing the local structure of the numerical fit, we define $\Delta\chi^2(\boldsymbol{\lambda}) = \chi^2(\boldsymbol{\lambda}) - \chi^2_{\rm min}$, where $\boldsymbol{\lambda}$ denotes the set of model parameters. In the two-dimensional slices discussed below, the two displayed parameters are varied simultaneously while the remaining eight parameters are kept fixed at their BFP values. The conventional two-parameter thresholds are used only as reference numerical cuts and should not be interpreted as statistically rigorous confidence levels, since the global fit is underconstrained.

The likelihood analysis also requires the values of the quark masses. We adopt the values reported in Ref. [85] and evolve them to the top-quark mass scale using the *RunDec* package [86]. The resulting quark mass ratios are

$$\begin{aligned} &\widetilde{m}_u = (1.26 \pm 0.22) \times 10^{-5}, \;\; \widetilde{m}_c = (6.35 \pm 0.13) \times 10^{-3}, \\ &\widetilde{m}_d = (1.12 \pm 0.08) \times 10^{-3}, \;\; \widetilde{m}_s = (2.25 \pm 0.16) \times 10^{-2}. \end{aligned} \tag{53}$$

Since these mass ratios are approximately invariant under renormalization-group evolution over a broad range of energy scales [82–84], they are treated as free parameters within the numerical intervals

$$\begin{aligned} &\widetilde{m}_u \in [0.9 \times 10^{-5}, \, 10.0 \times 10^{-5}], \;\; \widetilde{m}_c \in [0.9 \times 10^{-3}, \, 10.0 \times 10^{-3}], \\ &\widetilde{m}_d \in [0.9 \times 10^{-3}, \, 10.0 \times 10^{-3}], \;\; \widetilde{m}_s \in [0.9 \times 10^{-2}, \, 10.0 \times 10^{-2}]. \end{aligned} \tag{54}$$

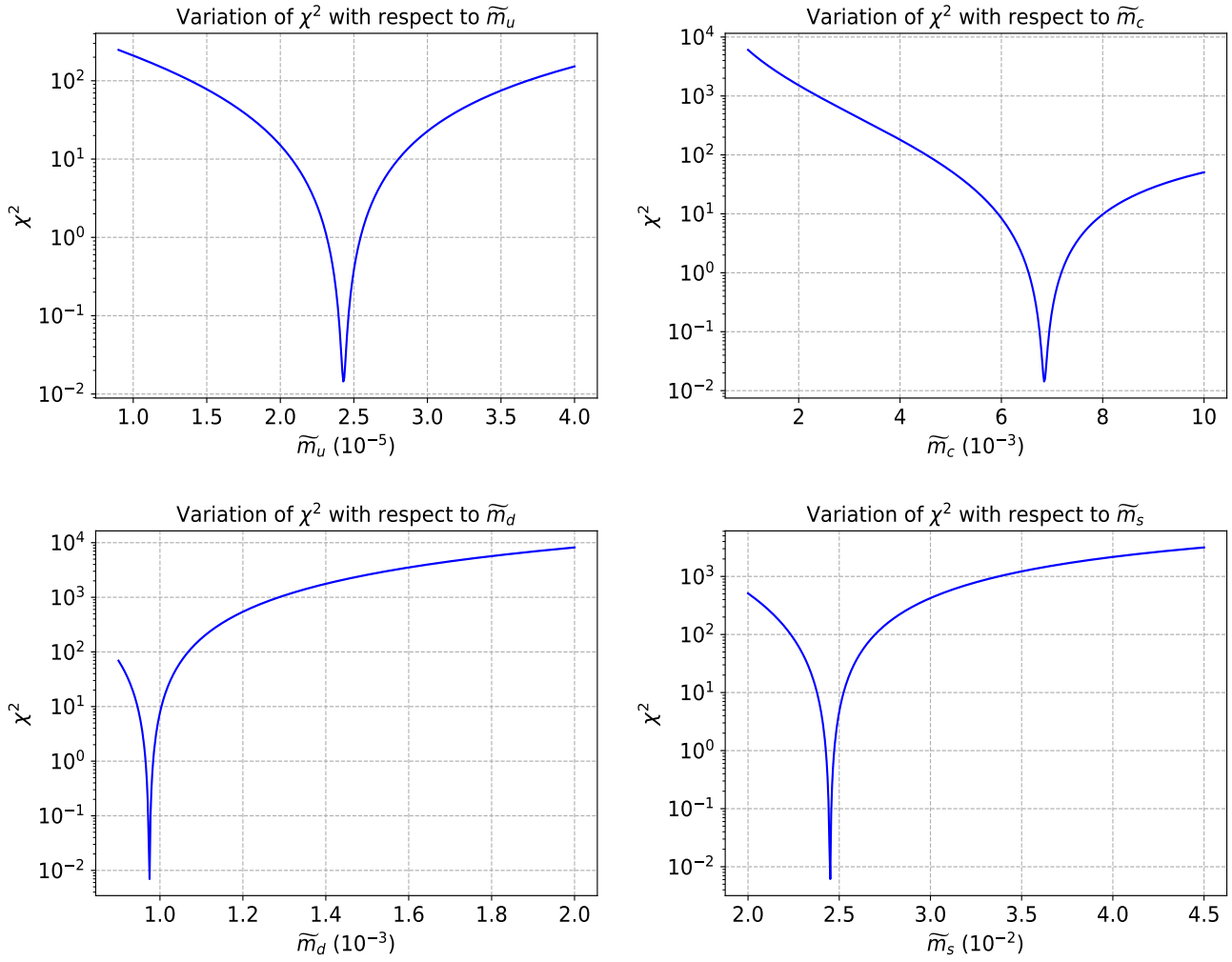

FIG. 1. One-dimensional slices of the χ^2 statistic as a function of the quark mass ratios $\widetilde{m}_u$, $\widetilde{m}_d$, $\widetilde{m}_c$, and $\widetilde{m}_s$. Each panel is obtained by varying a single mass ratio while keeping the remaining free parameters fixed at their Best Fit Point (BFP) values. The location of the minima reveals the preferred regions of the parameter space and illustrates the sensitivity of the likelihood function to each quark mass ratio.

The remaining free parameters are varied within their corresponding physically allowed domains, subject to the algebraic constraints imposed by the singular-value parametrization. These constraints guarantee the consistency of the fermion mass matrices and ensure that the diagonalization procedure remains well defined throughout the parameter space.

Finally, we carry out a comprehensive scan of the allowed parameter space by evaluating the χ^2 function over a large number of randomly generated parameter configurations. The parameter set that yields a minimum of the χ^2 function is identified as the Best Fit Point (BFP). The resulting values of the ten free parameters are

$$\begin{aligned}
&\widetilde{m}_u = 2.4510 \times 10^{-5}, \quad \widetilde{m}_c = 6.7886 \times 10^{-3}, \quad \widetilde{m}_d = 0.9763 \times 10^{-3}, \quad \widetilde{m}_s = 2.4444 \times 10^{-2}, \\
&\widetilde{m}^u_{11} = 1.3507 \times 10^{-9}, \quad \widetilde{m}^d_{11} = 1.0850 \times 10^{-8}, \quad \widetilde{\mathcal{D}}_u = 9.1694 \times 10^{-1}, \quad \widetilde{\mathcal{D}}_d = 9.1620 \times 10^{-1}, \\
&\Theta_{\mathrm{j}} = 111.196^\circ, \quad \Gamma_{\mathrm{j}} = 119.803^\circ, \quad \chi^2 = 4.67 \times 10^{-2}
\end{aligned} \tag{55}$$

Figure 1 shows the dependence of the χ^2 statistic on each of the quark mass ratios included in the likelihood analysis. Each panel is obtained by performing a one-dimensional scan of the corresponding mass ratio while fixing the remaining nine free parameters at their Best Fit Point (BFP) values. Consequently, the resulting curves represent one-dimensional χ^2 slices that illustrate the sensitivity of the fit to variations of each mass ratio in the vicinity of the minimum. In all cases, a well-defined minimum is observed near the corresponding BFP value, indicating that the

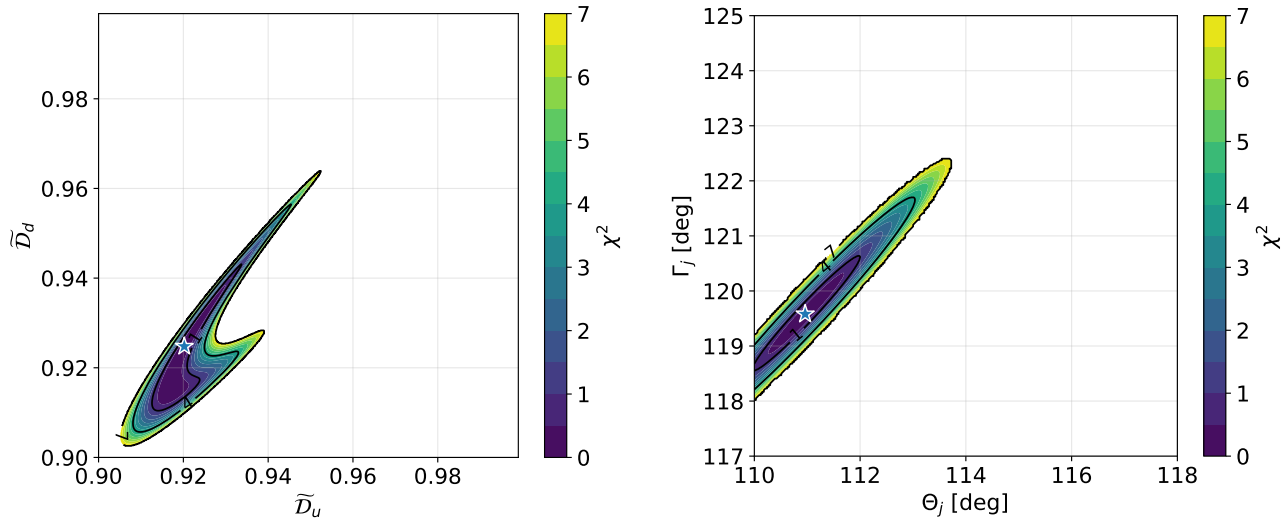

FIG. 2. Two-dimensional slices of the χ^2 function in the $(\widetilde{\mathcal{D}}_u, \widetilde{\mathcal{D}}_d)$ (left panel) and $(\Theta_{\rm j}, \Gamma_{\rm j})$ (right panel) planes. For each slice, the displayed parameters are varied simultaneously over their allowed ranges, while the remaining eight free parameters are fixed at their BFP values. The color map represents the value of the χ^2 function, the black contour denotes the $\chi^2 = 1$ region, and the white star marks the global BFP. The elongated contours reveal the correlations between the corresponding parameters and characterize the local structure of the likelihood function around its global minimum.

quark mass ratios are tightly constrained by the structure of the model and play a non-trivial role in reproducing the experimentally measured CKM matrix elements. The asymmetric shape exhibited by some of the slices reflects the nonlinear dependence of the χ^2 function on the mass ratios, as well as the pronounced hierarchical structure of the quark mass spectrum.

Figure 2 displays the two-dimensional χ^2 slices in the $(\widetilde{D}_u, \widetilde{D}_d)$ and $(\Theta_{\rm j}, \Gamma_{\rm j})$ parameter planes. These slices are obtained by simultaneously varying the two parameters shown in each panel while fixing the remaining eight free parameters at their BFP values. Unlike the one-dimensional slices, these contour plots provide direct information on the local correlations between pairs of parameters and on the geometry of the χ^2 function around its minimum. For the parameter pairs $(\widetilde{D}_u, \widetilde{D}_d)$, $(\widetilde{m}^u_{11}, \widetilde{m}^d_{11})$, and $(\Theta_{\rm j}, \Gamma_{\rm j})$, using the reference two-parameter threshold $\Delta\chi^2 \leq 6.18$, we obtain

$$\begin{aligned} \widetilde{\mathcal{D}}_u &= \left(9.169^{+0.821}_{-0.020}\right) \times 10^{-1}, \;\; \widetilde{m}^u_{11} = \left(1.351^{+1.865}_{-0.351}\right) \times 10^{-9}, \;\; \Theta_{\rm j}(^\circ) = 111.20^{+23.52}_{-16.61}, \\ \widetilde{\mathcal{D}}_d &= \left(9.162^{+0.821}_{-0.162}\right) \times 10^{-1}, \;\; \widetilde{m}^d_{11} = \left(1.085^{+0.985}_{-0.915}\right) \times 10^{-8}, \;\; \Gamma_{\rm j}(^\circ) = 119.20^{+20.20}_{-13.41}. \end{aligned} \tag{56}$$

Here, $\chi^2 = 4.67 \times 10^{-2}$. For each two-dimensional $\Delta\chi^2$ contour, we also compute the induced ranges of the nine CKM matrix elements. These ranges should be interpreted as the variation of the CKM predictions within fixed-$\Delta\chi^2$ regions rather than as statistically rigorous confidence intervals, since the global fit is underconstrained.

When the two parameters $(\widetilde{D}_u, \widetilde{D}_d)$ are varied simultaneously, while the remaining eight free parameters are fixed at their BFP values, we obtain

$$\left|\mathbf{V}^{L({\rm j})}_{\rm CKM}\right| = \begin{pmatrix} 0.97447 \pm 0.00014 & 0.22449 \pm 0.00063 & (3.88 \pm 0.40) \times 10^{-3} \\ 0.22437 \pm 0.00058 & 0.97364 \pm 0.00022 & (4.11 \pm 0.30) \times 10^{-2} \\ (8.38 \pm 2.90) \times 10^{-3} & (4.04 \pm 0.31) \times 10^{-2} & 0.999148 \pm 0.00018 \end{pmatrix}. \tag{57}$$

These results for the magnitudes of all nine CKM elements are in good agreement with the results obtained in the global fit [85].

B. Leptonic Sector

The matrices $\mathbf{M}_\nu$ and $\mathbf{M}_e$ can be brought to diagonal form through unitary transformations,

$$\mathbf{U}_{\nu L}^{\top}\,\mathbf{M}_\nu\,\mathbf{U}_{\nu L}=\hat{\mathbf{M}}_\nu,\qquad \mathbf{U}_{eL}^{\dagger}\mathbf{M}_e\mathbf{M}_e^{\dagger}\mathbf{U}_{eL}=\hat{\mathbf{M}}_e\hat{\mathbf{M}}_e^{\dagger}\qquad\text{and}\qquad \mathbf{U}_{eR}^{\dagger}\mathbf{M}_e^{\dagger}\mathbf{M}_e\mathbf{U}_{eR}=\hat{\mathbf{M}}_e^{\dagger}\hat{\mathbf{M}}_e, \tag{58}$$

where $\mathbf{U}_{\nu L}$ and $\mathbf{U}_{e(L,R)}$ are unitary matrices, while $\hat{\mathbf{M}}_e=\mathrm{diag}(m_e,m_\mu,m_\tau)$ and $\hat{\mathbf{M}}_\nu$ is a diagonal matrix whose elements are the physical neutrino masses. Similarly, the diagonal Majorana mass matrix $\mathbf{M}_R$ satisfies $\mathbf{U}_{\nu R}^{\top}\,\mathbf{M}_R\,\mathbf{U}_{\nu R}=\hat{\mathbf{M}}_R$ where the diagonal entries of $\hat{\mathbf{M}}_R$ are the physical heavy-neutrino masses. The left- and right-handed PMNS mixing matrices are then defined as [80]

$$\mathbf{U}_{\rm PMNS}^{L}=\mathbf{U}_{eL}^{\dagger}\mathbf{U}_{\nu L},\qquad \mathbf{U}_{\rm PMNS}^{R}=\mathbf{U}_{eR}^{\dagger}\mathbf{U}_{\nu R}^{*}. \tag{59}$$

Let us emphasize that the structure of $\mathbf{U}_{\rm PMNS}^{R}$ is determined by the charged-lepton sector because $\mathbf{M}_R$ is diagonal, as discussed above. The explicit form of the PMNS matrix depends on whether the **PLRT** or **MLRT** framework is considered. In analogy with the quark sector, a relation between the left- and right-handed leptonic mixing matrices can be established by exploiting the properties of the charged lepton mass matrix in the MLRT and PLRT scenarios. In the MLRT framework, where the charged-lepton mass matrix is Hermitian, $\mathbf{M}_e=\mathbf{M}_e^{\dagger}$, one has $\mathbf{U}_{eL}=\mathbf{U}_{eR}$. Therefore, $\mathbf{U}_{\rm PMNS}^{R}=\mathbf{U}_{\rm PMNS}^{L}\mathbf{U}_{\nu L}^{\dagger}\mathbf{U}_{\nu R}^{*}$. On the other hand, in the PLRT framework, where the charged-lepton mass matrix is complex symmetric, $\mathbf{M}_e=\mathbf{M}_e^{\top}$, the diagonalization matrices satisfy $\mathbf{U}_{eR}=\mathbf{U}_{eL}^{*}$, leading to $\mathbf{U}_{\rm PMNS}^{R}=\left(\mathbf{U}_{\rm PMNS}^{L}\right)^{*}\mathbf{U}_{\nu L}^{T}\mathbf{U}_{\nu R}^{*}$. Since in the present model the right-handed Majorana neutrino mass matrix $\mathbf{M}_R$ is diagonal, one may choose $\mathbf{U}_{\nu R}=\mathbb{I}_{3\times3}$, up to unphysical phase conventions. Consequently, the above relations reduce to $\mathbf{U}_{\rm PMNS}^{R}=\mathbf{U}_{\rm PMNS}^{L}\mathbf{U}_{\nu L}^{\dagger}$, $\mathbf{U}_{\rm PMNS}^{R}=\mathbf{U}_{eL}^{\dagger}$, so $\mathbf{U}_{\rm PMNS}^{R}=\mathbf{O}_{eL}^{\top}\mathbf{P}_e\mathbf{R}_{\frac{\pi}{4}}$ for MLRT. And $\mathbf{U}_{\rm PMNS}^{R}=\left(\mathbf{U}_{\rm PMNS}^{L}\right)^{*}\mathbf{U}_{\nu L}^{T}$, $\mathbf{U}_{\rm PMNS}^{R}=\mathbf{U}_{eL}^{\top}$, so $\mathbf{U}_{\rm PMNS}^{R}=\mathbf{O}_{eL}^{\top}\mathbf{P}_e\mathbf{R}_{\frac{\pi}{4}}$ for PLRT. Thus, unlike in the quark sector, the left- and right-handed PMNS matrices are not, in general, directly equal or complex conjugates of each other. This difference originates from the distinct diagonalization matrices associated with the light and heavy Majorana neutrino sectors. In particular, because M_R is diagonal, the right-handed leptonic mixing matrix is entirely determined by the charged-lepton sector. From the unitary matrices in Eqs. (25) and (26) the explicit form of the left-handed PMNS flavor mixing matrix is given by

$$\mathbf{U}_{\rm PMNS}^{L(1)}=\mathbf{O}_e^{\top}\mathbf{P}_e^{\dagger}\mathbf{R}_{\beta\frac{\pi}{4}}\mathbf{P}_\nu^{1}\mathbf{O}_\nu\quad\text{for PLRT,}\quad\text{and}\quad\mathbf{U}_{\rm PMNS}^{L(2)}=\mathbf{O}_e^{\top}\mathbf{P}_e\mathbf{R}_{\beta\frac{\pi}{4}}\mathbf{P}_\nu^{2}\mathbf{O}_\nu\quad\text{for MLRT,} \tag{60}$$

where $\mathbf{R}_{\beta\frac{\pi}{4}}=\mathbf{R}_{\frac{\pi}{4}}\mathbf{R}_{\beta_\nu}^{(\mathrm{j})\top}$

$$\mathbf{R}_{\beta\frac{\pi}{4}}=\begin{pmatrix}\cos\left(\frac{\pi}{4}-\beta_\nu^{(\mathrm{j})}\right) & -\sin\left(\frac{\pi}{4}-\beta_\nu^{(\mathrm{j})}\right) & 0\\ \sin\left(\frac{\pi}{4}-\beta_\nu^{(\mathrm{j})}\right) & \cos\left(\frac{\pi}{4}-\beta_\nu^{(\mathrm{j})}\right) & 0\\ 0 & 0 & 1\end{pmatrix}. \tag{61}$$

In the particular case when the rotation angle is the same in both lepton sectors, $\beta_\nu^{(\mathrm{j})}=\frac{\pi}{4}$, we have $\mathbf{R}_{\beta\frac{\pi}{4}}=\mathrm{diag}\,(1,1,1)$. Then the left-handed PMNS mixing matrix takes the form

$$\mathbf{U}_{\rm PMNS}^{L(\mathrm{j})}=e^{i\Xi_{\mathrm{j}}}\mathbf{O}_e^{\top}\mathbf{P}_{\mathrm{j}}^{(\nu-e)}\mathbf{O}_\nu, \tag{62}$$

where

$$\mathbf{P}_j^{(\nu-e)}=\mathrm{diag}\left(1,e^{i\varsigma_{\mathrm{j}}},e^{i\varrho_{\mathrm{j}}}\right), \tag{63}$$

with

$$\begin{aligned}&\Xi_1=\tfrac{1}{2}\left(\alpha_{\nu1}-\alpha_{e1}\right),\ \varsigma_1=\tfrac{1}{2}\left(\beta_{\nu1}-\beta_e-\alpha_{\nu1}+\alpha_{e1}\right),\ \varrho_1=\tfrac{1}{2}\left(\gamma_{\nu1}-\gamma_{e1}-\alpha_{\nu1}+\alpha_{e1}\right),\\ &\Xi_2=\tfrac{1}{2}\alpha_{\nu2},\qquad\qquad \varsigma_2=\tfrac{1}{2}\left(\beta_{\nu2}-\alpha_{\nu2}\right),\qquad\qquad \varrho_2=\tfrac{1}{2}\left(2\phi_{ec}+\gamma_{e2}-\alpha_{\nu2}\right).\end{aligned} \tag{64}$$

It is worth noting that the choice $\beta_\nu^{(\mathrm{j})}=\pi/4$ is not arbitrary. In fact, it emerges naturally when the effective neutrino mass matrix preserves the residual S_3 structure inherited from the underlying flavor symmetry. Under this condition,

the matrix elements responsible for the rotation satisfy $d_\nu = c_\nu$, leading to $\tan\beta_\nu^{(\mathrm{j})} = 1$ and therefore $\beta_\nu^{(\mathrm{j})} = \pi/4$. This result reflects a maximal mixing within the **2** representation of S_3 and constitutes the neutrino-sector analogue of the universal $R_{\pi/4}$ rotation that appears in the quark sector. The explicit form of the PMNS mixing matrix elements in both theoretical frameworks is:

$$\mathbf{U}_{\mathrm{PMNS}}^{L(\mathrm{j})} = e^{i\Xi_{\mathrm{j}}} \begin{pmatrix} V_{e1}^{\mathrm{th}} & V_{e2}^{\mathrm{th}} & V_{e3}^{\mathrm{th}} \\ V_{\mu1}^{\mathrm{th}} & V_{\mu2}^{\mathrm{th}} & V_{\mu3}^{\mathrm{th}} \\ V_{\tau1}^{\mathrm{th}} & V_{\tau2}^{\mathrm{th}} & V_{\tau3}^{\mathrm{th}} \end{pmatrix}, \tag{65}$$

The entries of the PMNS mixing matrix are given by

$$V_{e1}^{(\mathrm{j})} = \sqrt{\frac{\widetilde{\sigma}_\mu\widetilde{\sigma}_\tau\widetilde{\sigma}_{\nu2}\widetilde{\sigma}_{\nu3}\widetilde{\xi}_{\ell1}\widetilde{\xi}_{\nu1}}{\widetilde{\mathtt{D}}_{\ell1}\widetilde{\mathtt{D}}_{\nu1}}} + \sqrt{\frac{\widetilde{\sigma}_e\widetilde{\sigma}_{\nu1}}{\widetilde{\mathtt{D}}_{\ell1}\widetilde{\mathtt{D}}_{\nu1}}}\varepsilon_{e1}^{(\mathrm{j})}, \quad V_{e2}^{(\mathrm{j})} = -\sqrt{\frac{\widetilde{\sigma}_\mu\widetilde{\sigma}_\tau\widetilde{\sigma}_{\nu1}\widetilde{\sigma}_{\nu3}\widetilde{\xi}_{\ell1}\widetilde{\xi}_{\nu2}}{\widetilde{\mathtt{D}}_{\ell1}\widetilde{\mathtt{D}}_{\nu2}}} + \sqrt{\frac{\widetilde{\sigma}_e\widetilde{\sigma}_{\nu2}}{\widetilde{\mathtt{D}}_{\ell1}\widetilde{\mathtt{D}}_{\nu2}}}\varepsilon_{e2}^{(\mathrm{j})}, \tag{66}$$

$$V_{e3}^{(\mathrm{j})} = \sqrt{\frac{\widetilde{\sigma}_\mu\widetilde{\sigma}_\tau\widetilde{\sigma}_{\nu1}\widetilde{\sigma}_{\nu2}\widetilde{\xi}_{\ell1}\widetilde{\xi}_{\nu3}}{\widetilde{\mathtt{D}}_{\ell1}\widetilde{\mathtt{D}}_{\nu3}}} + \sqrt{\frac{\widetilde{\sigma}_e\widetilde{\sigma}_{\nu3}}{\widetilde{\mathtt{D}}_{\ell1}\widetilde{\mathtt{D}}_{\nu3}}}\varepsilon_{e3}^{(\mathrm{j})}, \quad V_{\mu1}^{(\mathrm{j})} = -\sqrt{\frac{\widetilde{\sigma}_e\widetilde{\sigma}_\tau\widetilde{\sigma}_{\nu2}\widetilde{\sigma}_{\nu3}\widetilde{\xi}_{\ell2}\widetilde{\xi}_{\nu1}}{\widetilde{\mathtt{D}}_{\ell2}\widetilde{\mathtt{D}}_{\nu1}}} + \sqrt{\frac{\widetilde{\sigma}_\mu\widetilde{\sigma}_{\nu1}}{\widetilde{\mathtt{D}}_{\ell2}\widetilde{\mathtt{D}}_{\nu1}}}\varepsilon_{\mu1}^{(\mathrm{j})}, \tag{67}$$

$$V_{\mu2}^{(\mathrm{j})} = \sqrt{\frac{\widetilde{\sigma}_e\widetilde{\sigma}_\tau\widetilde{\sigma}_{\nu1}\widetilde{\sigma}_{\nu3}\widetilde{\xi}_{\ell2}\widetilde{\xi}_{\nu2}}{\widetilde{\mathtt{D}}_{\ell2}\widetilde{\mathtt{D}}_{\nu2}}} + \sqrt{\frac{\widetilde{\sigma}_\mu\widetilde{\sigma}_{\nu2}}{\widetilde{\mathtt{D}}_{\ell2}\widetilde{\mathtt{D}}_{\nu2}}}\varepsilon_{\mu2}^{(\mathrm{j})}, \quad V_{\mu3}^{(\mathrm{j})} = -\sqrt{\frac{\widetilde{\sigma}_e\widetilde{\sigma}_\tau\widetilde{\sigma}_{\nu1}\widetilde{\sigma}_{\nu2}\widetilde{\xi}_{\ell2}\widetilde{\xi}_{\nu3}}{\widetilde{\mathtt{D}}_{\ell2}\widetilde{\mathtt{D}}_{\nu3}}} + \sqrt{\frac{\widetilde{\sigma}_\mu\widetilde{\sigma}_{\nu3}}{\widetilde{\mathtt{D}}_{\ell2}\widetilde{\mathtt{D}}_{\nu3}}}\varepsilon_{\mu3}^{(\mathrm{j})}, \tag{68}$$

$$V_{\tau1}^{(\mathrm{j})} = \sqrt{\frac{\widetilde{\sigma}_e\widetilde{\sigma}_\mu\widetilde{\sigma}_{\nu2}\widetilde{\sigma}_{\nu3}\widetilde{\xi}_{\ell3}\widetilde{\xi}_{\nu1}}{\widetilde{\mathtt{D}}_{\ell3}\widetilde{\mathtt{D}}_{\nu1}}} + \sqrt{\frac{\widetilde{\sigma}_\tau\widetilde{\sigma}_{\nu1}}{\widetilde{\mathtt{D}}_{\ell3}\widetilde{\mathtt{D}}_{\nu1}}}\varepsilon_{\tau1}^{(\mathrm{j})}, \quad V_{\tau2}^{(\mathrm{j})} = -\sqrt{\frac{\widetilde{\sigma}_e\widetilde{\sigma}_\mu\widetilde{\sigma}_{\nu1}\widetilde{\sigma}_{\nu3}\widetilde{\xi}_{\ell3}\widetilde{\xi}_{\nu2}}{\widetilde{\mathtt{D}}_{\ell3}\widetilde{\mathtt{D}}_{\nu2}}} + \sqrt{\frac{\widetilde{\sigma}_\tau\widetilde{\sigma}_{\nu2}}{\widetilde{\mathtt{D}}_{\ell3}\widetilde{\mathtt{D}}_{\nu2}}}\varepsilon_{\tau2}^{(\mathrm{j})}, \tag{69}$$

$$V_{\tau3}^{(\mathrm{j})} = \sqrt{\frac{\widetilde{\sigma}_e\widetilde{\sigma}_\mu\widetilde{\sigma}_{\nu1}\widetilde{\sigma}_{\nu2}\widetilde{\xi}_{\ell3}\widetilde{\xi}_{\nu3}}{\widetilde{\mathtt{D}}_{\ell3}\widetilde{\mathtt{D}}_{\nu3}}} + \sqrt{\frac{\widetilde{\sigma}_\tau\widetilde{\sigma}_{\nu3}}{\widetilde{\mathtt{D}}_{\ell3}\widetilde{\mathtt{D}}_{\nu3}}}\varepsilon_{\tau3}^{(\mathrm{j})}. \tag{70}$$

where

$$\varepsilon_{e1}^{(\mathrm{j})} = \sqrt{\widetilde{\mathcal{D}}_\ell\widetilde{\mathcal{D}}_\nu\widetilde{\xi}_{\ell1}\widetilde{\xi}_{\nu1}}e^{i\varsigma_{\mathrm{j}}} + \sqrt{\widetilde{\xi}_{\ell2}\widetilde{\xi}_{\ell3}\widetilde{\xi}_{\nu2}\widetilde{\xi}_{\nu3}}e^{i\varrho_{\mathrm{j}}}, \quad \varepsilon_{e2}^{(\mathrm{j})} = \sqrt{\widetilde{\mathcal{D}}_\ell\widetilde{\mathcal{D}}_\nu\widetilde{\xi}_{\ell1}\widetilde{\xi}_{\nu2}}e^{i\varsigma_{\mathrm{j}}} + \sqrt{\widetilde{\xi}_{\ell2}\widetilde{\xi}_{\ell3}\widetilde{\xi}_{\nu1}\widetilde{\xi}_{\nu3}}e^{i\varrho_{\mathrm{j}}}, \tag{71}$$

$$\varepsilon_{e3}^{(\mathrm{j})} = \sqrt{\widetilde{\mathcal{D}}_\ell\widetilde{\mathcal{D}}_\nu\widetilde{\xi}_{\ell1}\widetilde{\xi}_{\nu3}}e^{i\varsigma_{\mathrm{j}}} - \sqrt{\widetilde{\xi}_{\ell2}\widetilde{\xi}_{\ell3}\widetilde{\xi}_{\nu1}\widetilde{\xi}_{\nu2}}e^{i\varrho_{\mathrm{j}}}, \quad \varepsilon_{\mu1}^{(\mathrm{j})} = \sqrt{\widetilde{\mathcal{D}}_\ell\widetilde{\mathcal{D}}_\nu\widetilde{\xi}_{\ell2}\widetilde{\xi}_{\nu1}}e^{i\varsigma_{\mathrm{j}}} + \sqrt{\widetilde{\xi}_{\ell1}\widetilde{\xi}_{\ell3}\widetilde{\xi}_{\nu2}\widetilde{\xi}_{\nu3}}e^{i\varrho_{\mathrm{j}}}, \tag{72}$$

$$\varepsilon_{\mu2}^{(\mathrm{j})} = \sqrt{\widetilde{\mathcal{D}}_\ell\widetilde{\mathcal{D}}_\nu\widetilde{\xi}_{\ell2}\widetilde{\xi}_{\nu2}}e^{i\varsigma_{\mathrm{j}}} + \sqrt{\widetilde{\xi}_{\ell1}\widetilde{\xi}_{\ell3}\widetilde{\xi}_{\nu1}\widetilde{\xi}_{\nu3}}e^{i\varrho_{\mathrm{j}}}, \quad \varepsilon_{\mu3}^{(\mathrm{j})} = \sqrt{\widetilde{\mathcal{D}}_\ell\widetilde{\mathcal{D}}_\nu\widetilde{\xi}_{\ell2}\widetilde{\xi}_{\nu3}}e^{i\varsigma_{\mathrm{j}}} - \sqrt{\widetilde{\xi}_{\ell1}\widetilde{\xi}_{\ell3}\widetilde{\xi}_{\nu1}\widetilde{\xi}_{\nu2}}e^{i\varrho_{\mathrm{j}}}, \tag{73}$$

$$\varepsilon_{\tau1}^{(\mathrm{j})} = \sqrt{\widetilde{\mathcal{D}}_\ell\widetilde{\mathcal{D}}_\nu\widetilde{\xi}_{\ell3}\widetilde{\xi}_{\nu1}}e^{i\varsigma_{\mathrm{j}}} - \sqrt{\widetilde{\xi}_{\ell1}\widetilde{\xi}_{\ell2}\widetilde{\xi}_{\nu2}\widetilde{\xi}_{\nu3}}e^{i\varrho_{\mathrm{j}}}, \quad \varepsilon_{\tau2}^{(\mathrm{j})} = \sqrt{\widetilde{\mathcal{D}}_\ell\widetilde{\mathcal{D}}_\nu\widetilde{\xi}_{\ell3}\widetilde{\xi}_{\nu2}}e^{i\varsigma_{\mathrm{j}}} - \sqrt{\widetilde{\xi}_{\ell1}\widetilde{\xi}_{\ell2}\widetilde{\xi}_{\nu1}\widetilde{\xi}_{\nu3}}e^{i\varrho_{\mathrm{j}}}, \tag{74}$$

$$\varepsilon_{\tau3}^{(\mathrm{j})} = \sqrt{\widetilde{\mathcal{D}}_\ell\widetilde{\mathcal{D}}_\nu\widetilde{\xi}_{\ell3}\widetilde{\xi}_{\nu3}}e^{i\varsigma_{\mathrm{j}}} + \sqrt{\widetilde{\xi}_{\ell1}\widetilde{\xi}_{\ell2}\widetilde{\xi}_{\nu1}\widetilde{\xi}_{\nu2}}e^{i\varrho_{\mathrm{j}}}. \tag{75}$$

Here, $\widetilde{\sigma}_e = \widetilde{m}_e - \widetilde{m}_{11}^\ell$, $\widetilde{\sigma}_\mu = \widetilde{m}_\mu + \widetilde{m}_{11}^\ell$, $\widetilde{\sigma}_\tau = 1 - \widetilde{m}_{11}^\ell$, $\widetilde{\xi}_{\ell1} = \widetilde{\mathcal{D}}_\ell - \widetilde{\sigma}_e$, $\widetilde{\xi}_{\ell2} = \widetilde{\mathcal{D}}_\ell + \widetilde{\sigma}_\mu$, $\widetilde{\xi}_{\ell3} = \widetilde{\sigma}_\tau - \widetilde{\mathcal{D}}_\ell$,

$$\begin{aligned} &\widetilde{\mathtt{D}}_{\ell1} = \widetilde{\mathcal{D}}_\ell\left(\widetilde{\sigma}_\mu + \widetilde{\sigma}_e\right)\left(\widetilde{\sigma}_\tau - \widetilde{\sigma}_e\right), \quad \widetilde{\mathtt{D}}_{\ell2} = \widetilde{\mathcal{D}}_\ell\left(\widetilde{\sigma}_\tau + \widetilde{\sigma}_\mu\right)\left(\widetilde{\sigma}_\mu + \widetilde{\sigma}_e\right), \quad \widetilde{\mathtt{D}}_{\ell3} = \widetilde{\mathcal{D}}_\ell\left(\widetilde{\sigma}_\tau + \widetilde{\sigma}_\mu\right)\left(\widetilde{\sigma}_\tau - \widetilde{\sigma}_e\right), \\ &\widetilde{\mathtt{D}}_{\nu1} = \widetilde{\mathcal{D}}_\nu\left(\widetilde{\sigma}_{\nu2} + \widetilde{\sigma}_{\nu1}\right)\left(\widetilde{\sigma}_{\nu3} - \widetilde{\sigma}_{\nu1}\right), \quad \widetilde{\mathtt{D}}_{\nu2} = \widetilde{\mathcal{D}}_\nu\left(\widetilde{\sigma}_{\nu3} + \widetilde{\sigma}_{\nu2}\right)\left(\widetilde{\sigma}_{\nu2} + \widetilde{\sigma}_{\nu1}\right), \quad \widetilde{\mathtt{D}}_{\nu3} = \widetilde{\mathcal{D}}_\nu\left(\widetilde{\sigma}_{\nu3} + \widetilde{\sigma}_{\nu2}\right)\left(\widetilde{\sigma}_{\nu3} - \widetilde{\sigma}_{\nu1}\right), \end{aligned} \tag{76}$$

where $\widetilde{m}_e = \frac{m_e}{m_\tau}$, $\widetilde{m}_\mu = \frac{m_\mu}{m_\tau}$, $\widetilde{m}_{11}^\ell = \frac{m_{11}^\ell}{m_\tau}$, $\widetilde{\sigma}_e = \frac{\sigma_e}{m_\tau}$, $\widetilde{\sigma}_\mu = \frac{\sigma_\mu}{m_\tau}$, $\widetilde{\sigma}_\tau = \frac{\sigma_\tau}{m_\tau}$, $\widetilde{\xi}_{\ell1} = \frac{\xi_{\ell1}}{m_\tau}$, $\widetilde{\xi}_{\ell2} = \frac{\xi_{\ell2}}{m_\tau}$, $\widetilde{\xi}_{\ell3} = \frac{\xi_{\ell3}}{m_\tau}$, $\widetilde{\mathcal{D}}_\ell = \frac{\mathcal{D}_\ell}{m_\tau}$. For the normal neutrino mass ordering, $m_{\nu3} > m_{\nu2} > m_{\nu1}$, the following relations hold: $\widetilde{\sigma}_{\nu1} = \widetilde{m}_{\nu1} - \widetilde{m}_{11}^\nu$, $\widetilde{\sigma}_{\nu2} = \widetilde{m}_{\nu2} + \widetilde{m}_{11}^\nu$, $\widetilde{\sigma}_{\nu3} = 1 - \widetilde{m}_{11}^\nu$, $\widetilde{\xi}_{\nu1} = \widetilde{\mathcal{D}}_\nu - \widetilde{\sigma}_{\nu1}$, $\widetilde{\xi}_{\nu2} = \widetilde{\mathcal{D}}_\nu + \widetilde{\sigma}_{\nu2}$, $\widetilde{\xi}_{\nu3} = \widetilde{\sigma}_{\nu3} - \widetilde{\mathcal{D}}_\nu$, where $\widetilde{m}_{\nu1} = \frac{m_{\nu1}}{m_{\nu3}}$, $\widetilde{m}_{\nu2} = \frac{m_{\nu2}}{m_{\nu3}}$, $\widetilde{m}_{11}^\nu = \frac{m_{11}^\nu}{m_{\nu3}}$, $\widetilde{\sigma}_{\nu1} = \frac{\sigma_{\nu1}}{m_{\nu3}}$, $\widetilde{\sigma}_{\nu2} = \frac{\sigma_{\nu2}}{m_{\nu3}}$, $\widetilde{\sigma}_{\nu3} = \frac{\sigma_{\nu3}}{m_{\nu3}}$, $\widetilde{\xi}_{\nu1} = \frac{\xi_{\nu1}}{m_{\nu3}}$, $\widetilde{\xi}_{\nu2} = \frac{\xi_{\nu2}}{m_{\nu3}}$, $\widetilde{\xi}_{\nu3} = \frac{\xi_{\nu3}}{m_{\nu3}}$, $\widetilde{\mathcal{D}}_\nu = \frac{\mathcal{D}_\nu}{m_{\nu3}}$. For the inverted neutrino mass ordering, $m_{\nu2} > m_{\nu1} > m_{\nu3}$: $\widetilde{\sigma}_{\nu1} = \widetilde{m}_{\nu1} - \widetilde{m}_{11}^\nu$, $\widetilde{\sigma}_{\nu2} = 1 + \widetilde{m}_{11}^\nu$, $\widetilde{\sigma}_{\nu3} = \widetilde{m}_{\nu3} - \widetilde{m}_{11}^\nu$, $\widetilde{\xi}_{\nu1} = \widetilde{\mathcal{D}}_\nu - \widetilde{\sigma}_{\nu1}$,

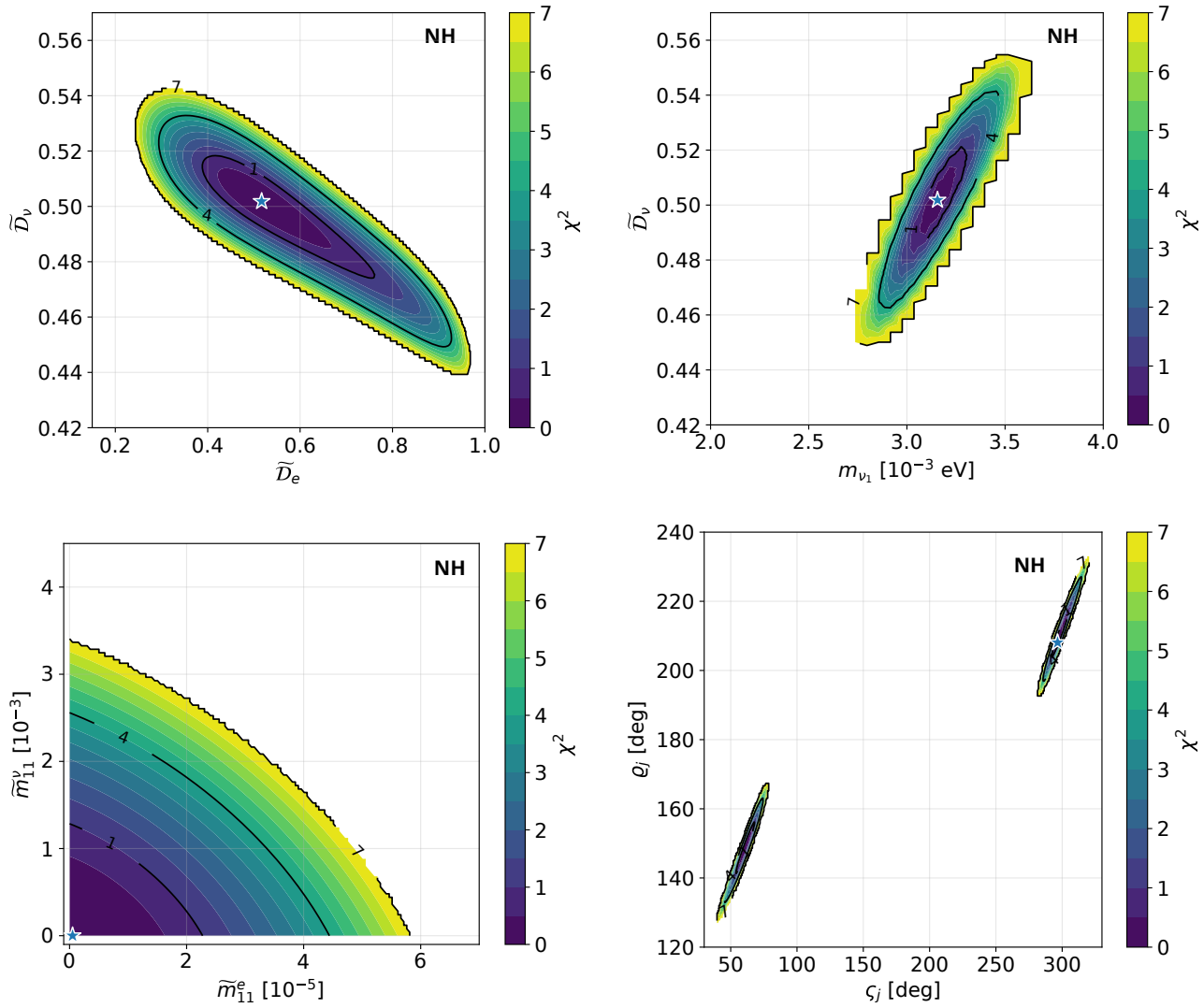

FIG. 3. The two-dimensional χ^2 slices for the normal neutrino mass ordering (NH). The star indicates the BFP, while the colored regions represent the variation of χ^2 around the global minimum.

$\widetilde{\xi}_{\nu 2} = \widetilde{\mathcal{D}}_\nu + \widetilde{\sigma}_{\nu 2}$, $\widetilde{\xi}_{\nu 3} = \widetilde{\sigma}_{\nu 3} - \widetilde{\mathcal{D}}_\nu$, where $\widetilde{m}_{\nu 1} = \frac{m_{\nu 1}}{m_{\nu 2}}$, $\widetilde{m}_{\nu 3} = \frac{m_{\nu 3}}{m_{\nu 2}}$, $\widetilde{m}^{\nu}_{11} = \frac{m^{\nu}_{11}}{m_{\nu 2}}$, $\widetilde{\sigma}_{\nu 1} = \frac{\sigma_{\nu 1}}{m_{\nu 2}}$, $\widetilde{\sigma}_{\nu 2} = \frac{\sigma_{\nu 2}}{m_{\nu 2}}$, $\widetilde{\sigma}_{\nu 3} = \frac{\sigma_{\nu 3}}{m_{\nu 2}}$, $\widetilde{\xi}_{\nu 1} = \frac{\xi_{\nu 1}}{m_{\nu 2}}$, $\widetilde{\xi}_{\nu 2} = \frac{\xi_{\nu 2}}{m_{\nu 2}}$, $\widetilde{\xi}_{\nu 3} = \frac{\xi_{\nu 3}}{m_{\nu 2}}$, $\widetilde{\mathcal{D}}_\nu = \frac{\mathcal{D}_\nu}{m_{\nu 2}}$.

For the normal neutrino mass ordering, the parameter $\widetilde{\mathcal{D}}_\ell$, with $\ell = e, \nu$, is required to satisfy the following condition: $\widetilde{m}^{l}_{11} < \widetilde{m}_{l1}, \widetilde{\sigma}_{l3} > \widetilde{\mathcal{D}}_l > \widetilde{\sigma}_{l1}$, and $\widetilde{\mathcal{D}}_l \neq +\widetilde{\sigma}_{l1} - \widetilde{\sigma}_{l2} + \widetilde{\sigma}_{l3}$. For the inverted neutrino mass ordering, the following condition is required to hold: $\widetilde{m}^{\nu}_{11} < \widetilde{m}_{\nu 3}, \widetilde{\sigma}_{\nu 1} > \widetilde{\mathcal{D}}_\nu > \widetilde{\sigma}_{\nu 3}$, and $\widetilde{\mathcal{D}}_\nu \neq +\widetilde{\sigma}_{\nu 1} - \widetilde{\sigma}_{\nu 2} + \widetilde{\sigma}_{\nu 3}$.

As in the quark sector, the main distinction between the PMNS matrices obtained within the **PLRT** and **MLRT** frameworks resides in their phase structure. Nevertheless, both scenarios contain the same number of effective physical phases, which are related through the definitions given in Eq. (64). Consequently, a numerical analysis based solely on the PMNS matrix is unable to discriminate between the two frameworks. This result indicates that neutrino mixing observables alone do not provide sufficient information to distinguish whether the underlying theory corresponds to the **PLRT** or the **MLRT** scenario.

1. Likelihood Test

To confront the model with the latest neutrino oscillation data, we construct a χ^2 function using the experimental determinations of the three leptonic mixing angles reported by NuFIT 6.1 [87, 88]. The neutrino mass-squared differences are used as fixed experimental inputs to reconstruct the neutrino mass spectrum for a given value of the lightest neutrino mass, while they do not enter directly into the χ^2 function defined below.

By minimizing the χ^2 function over the free parameters of the model, we determine the Best-Fit Point (BFP). Since the number of free parameters exceeds the number of observables entering the fit, the system is statistically underconstrained. Consequently, the numerical regions discussed below should not be interpreted as conventional confidence regions of the full parameter space. Instead, we use one- and two-dimensional χ^2 slices around the BFP to study the local sensitivity to the model parameters and their correlations. In this case the χ^2 function has the form:

$$\chi^2 = \frac{\left(\sin^2\theta_{12}^{\rm exp} - \sin^2\theta_{12}^{\rm th}\right)^2}{\sigma^2_{\theta_{12}}} + \frac{\left(\sin^2\theta_{13}^{\rm exp} - \sin^2\theta_{13}^{\rm th}\right)^2}{\sigma^2_{\theta_{13}}} + \frac{\left(\sin^2\theta_{23}^{\rm exp} - \sin^2\theta_{23}^{\rm th}\right)^2}{\sigma^2_{\theta_{23}}} \tag{77}$$

where θ_{ij} are the lepton flavor mixing angles. In the above expression, the "th" superscript denotes the theoretical expressions of leptonic mixing angles, while the "exp" superscript denotes the experimental data for lepton mixing angles with an uncertainty $\sigma_{\theta_{ij}}$. The corresponding experimental best-fit values and their 1σ uncertainties are [87, 88]:

$$\sin^2\theta_{12}^{\rm exp} = 0.3088^{+0.0067}_{-0.0066}, \qquad \sin^2\theta_{13}^{\rm exp} = \begin{cases} 0.02248^{+0.00055}_{-0.00059} \\ 0.02262^{+0.00057}_{-0.00056} \end{cases}, \qquad \sin^2\theta_{23}^{\rm exp} = \begin{cases} 0.470^{+0.017}_{-0.014} \\ 0.550^{+0.013}_{-0.016} \end{cases}. \tag{78}$$

The other neutrino oscillation parameters are [87, 88]:

$$\Delta m^2_{21}\,[10^{-5}\,{\rm eV}^2] = 7.537^{+0.094}_{-0.10}, \qquad \Delta m^2_{31}\,[10^{-3}\,{\rm eV}^2] = \begin{cases} +2.511^{+0.021}_{-0.020} \\ -2.483^{+0.020}_{-0.020} \end{cases}, \qquad \delta_{\rm CP}\,[^\circ] = \begin{cases} 212^{+26}_{-36} \\ 274^{+22}_{-25} \end{cases}. \tag{79}$$

where $\Delta m^2_{21} = m^2_{\nu_2} - m^2_{\nu_1}$ and $\Delta m^2_{31} = m^2_{\nu_3} - m^2_{\nu_1}$ are the neutrino mass-squared differences, while $\delta_{\rm CP}$ is the Dirac CP-violating phase. The upper and lower entries correspond to the normal and inverted neutrino mass orderings (NH and IH), respectively. The neutrino masses are given by

$$\begin{aligned} &m_{\nu_2} = \sqrt{\Delta m^2_{21} + m^2_{\nu_1}}, \quad m_{\nu_3} = \sqrt{\Delta m^2_{31} + m^2_{\nu_1}} \quad \text{for NH}, \\ &m_{\nu_1} = \sqrt{\Delta m^2_{13} + m^2_{\nu_3}}, \quad m_{\nu_2} = \sqrt{\Delta m^2_{23} + m^2_{\nu_3}} \quad \text{for IH}. \end{aligned} \tag{80}$$

In the above expressions, the atmospheric mass-squared difference satisfies the relation $\Delta m^2_{23} = \Delta m^2_{21} + \Delta m^2_{13}$. Moreover, m_{ν_1} and m_{ν_3} correspond to the lightest neutrino mass eigenvalues for the NH and IH, respectively. The expressions in Eq. (80) allow two of the neutrino masses to be expressed in terms of the experimentally measured neutrino mass-squared differences and the lightest neutrino mass.

On the other hand, the charged-lepton masses are [82]

$$m_e = 0.5109998928 \pm 0.000000011, \quad m_\mu = 105.6583715 \pm 0.0000035, \quad m_\tau = 1776.82 \pm 0.16. \tag{81}$$

In the numerical analysis that we perform, the charged lepton masses and the neutrino mass-squared differences are not varied, but are instead fixed to their experimental central values. The physical motivation for this treatment is that charged lepton masses are known with a precision much higher than that required for the present analysis, and moreover, their mass ratios are only weakly affected by renormalization-group evolution over a broad range of energy scales [82–84]. Therefore, allowing them to vary within their experimental uncertainties would have a negligible impact on the determination of the remaining model parameters. Similarly, once the lightest neutrino mass is specified, the other two neutrino masses are determined through the measured mass-squared differences. Consequently, varying these differences within their experimental uncertainties would mainly introduce additional nuisance directions in the numerical analysis, while having only a subleading effect on the determination of the flavor parameters considered here.

The lightest neutrino mass determines the absolute neutrino mass scale, whereas the measured mass-squared differences determine the remaining two neutrino masses. The parameters $\widetilde{m}^e_{11}$, $\widetilde{m}^\nu_{11}$, $\widetilde{\mathcal{D}}_e$ and $\widetilde{\mathcal{D}}_\nu$ control the structure of

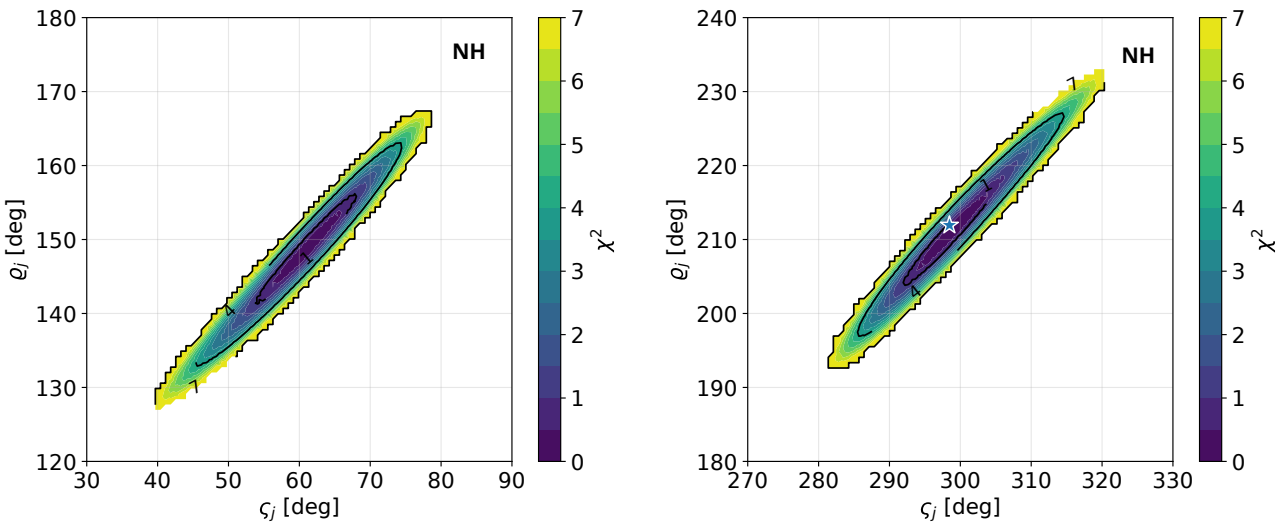

FIG. 4. The two-dimensional χ^2 slices for the normal neutrino mass ordering (NH). The star indicates the BFP, while the colored regions represent the variation of χ^2 around the global minimum.

the corresponding charged lepton and neutrino mass matrices, while $\varsigma_{\rm j}$ and $\varrho_{\rm j}$ contain the independent phase information relevant to lepton mixing. Hence, the χ^2 function explored in the numerical analysis is effectively a function of these seven independent parameters, $\left\{m_{\nu_{\rm lightest}}, \widetilde{m}^e_{11}, \widetilde{m}^\nu_{11}, \widetilde{\mathcal{D}}_e, \widetilde{\mathcal{D}}_\nu, \varsigma_{\rm j}, \varrho_{\rm j}\right\}$. The lightest neutrino mass determines the absolute neutrino-mass scale, whereas the measured mass-squared differences determine the remaining two neutrino masses. Since the χ^2 function depends on seven free parameters, while only three experimental observables are included in the fit, Eq. (77), the system is statistically underconstrained. Therefore, when all seven parameters are simultaneously varied, the analysis only allows us to identify the BFP, but not to determine statistically meaningful confidence intervals for each individual parameter. For the purpose of exploring the local structure of the numerical fit, we define $\Delta\chi^2(\boldsymbol{\lambda}) = \chi^2(\boldsymbol{\lambda}) - \chi^2_{\rm min}$, where $\boldsymbol{\lambda}$ denotes the set of model parameters. In the two-dimensional scans shown below, the two displayed parameters are varied simultaneously, while the remaining five parameters are kept fixed at their BFP values. We use the reference values $\Delta\chi^2 = 2.30,\ \ 6.18,\ \ 11.83$, which, for a regular likelihood with two fitted parameters, would conventionally correspond to the 68.27%, 95.45%, and 99.73% confidence levels, respectively. In the present underconstrained fit, however, these values are used only as convenient numerical thresholds to characterize the local χ^2 structure and should not be interpreted as statistically rigorous confidence levels.

In the numerical analysis performed assuming the normal neutrino mass ordering (NH), $m_{\nu_1} < m_{\nu_2} < m_{\nu_3}$. We obtain that the seven free parameters in the BFP, with a minimum χ^2 value of $\chi^2_{\rm min} = 1.41558 \times 10^{-4}$, have the values

$$\begin{aligned} &m_{\nu_1} = 3.155 \times 10^{-3}\ \text{eV}, \quad \widetilde{m}^e_{11} = 2.16 \times 10^{-7}, \quad \widetilde{m}^\nu_{11} = 3.25 \times 10^{-8}, \\ &\widetilde{\mathcal{D}}_e = 0.5192, \quad \widetilde{\mathcal{D}}_\nu = 0.5015, \quad \varsigma_{\rm j} = 298.79^\circ, \quad \varrho_{\rm j} = 211.05^\circ. \end{aligned} \tag{82}$$

The corresponding mixing angles are

$$\sin^2\theta_{12} = 0.308771, \qquad \sin^2\theta_{13} = 0.022486, \qquad \sin^2\theta_{23} = 0.469933. \tag{83}$$

In Figures 3 and 4, we show the two-dimensional χ^2 slices for the free parameters of the model in the vicinity of the BFP. These slices illustrate the local correlations among the free parameters.

The numerical ranges induced by the innermost reference region, $\Delta\chi^2 \leq 2.30$, for the seven free parameters of the model and the three flavor mixing angles are:

$$\begin{aligned} &m_{\nu_1} = \left(3.155^{+0.241}_{-0.179}\right) \times 10^{-3}\ \text{eV}, \quad \widetilde{m}^e_{11} \lesssim 3.36 \times 10^{-5}, \quad \widetilde{m}^\nu_{11} \lesssim 1.92 \times 10^{-3}, \\ &\widetilde{\mathcal{D}}_e = 0.5192^{+0.3550}_{-0.1812}, \quad \widetilde{\mathcal{D}}_\nu = 0.5015^{+0.0292}_{-0.0418}, \quad \varsigma_{\rm j} = \left(298.79^{+11.43}_{-10.22}\right)^\circ, \quad \varrho_{\rm j} = \left(211.05^{+11.87}_{-10.49}\right)^\circ. \end{aligned} \tag{84}$$

$$\sin^2\theta_{12} = 0.3088^{+0.0085}_{-0.0102}, \qquad \sin^2\theta_{13} = 0.02249^{+0.00085}_{-0.00086}, \qquad \sin^2\theta_{23} = 0.4699^{+0.0218}_{-0.0170}. \tag{85}$$

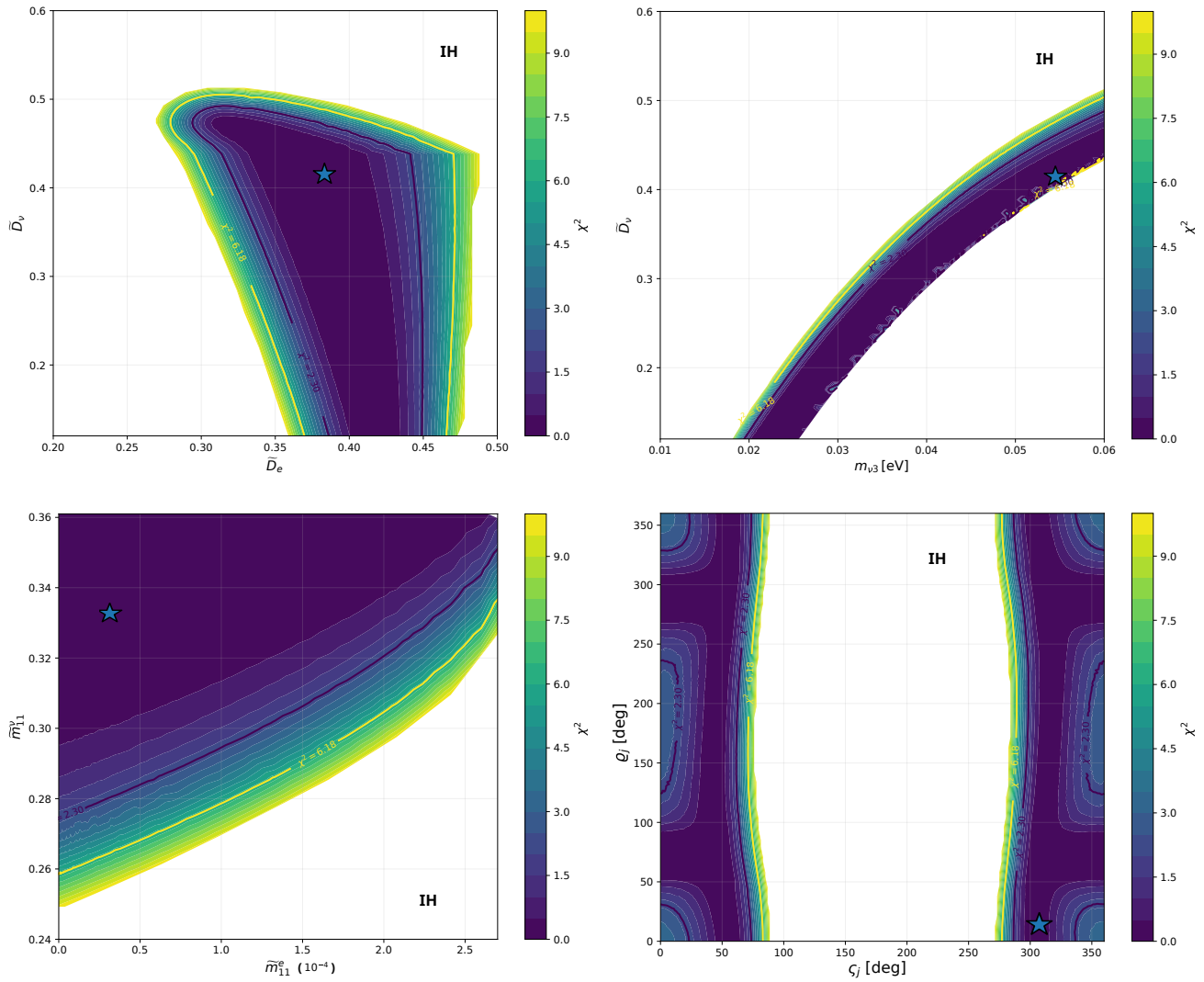

FIG. 5. The two-dimensional χ^2 slices for IH. The star indicates the BFP, while the colored regions represent the variation of χ^2 around the global minimum.

These ranges were obtained by projecting the two-dimensional slices satisfying $\Delta\chi^2 \leq 2.30$ onto the corresponding parameter axes. For the phases $\varsigma_{\rm j}$ and $\varrho_{\rm j}$, the quoted intervals correspond to the disconnected branch containing the global best-fit point; an additional disconnected branch is also present within the same reference region, $\Delta\chi^2 \leq 2.30$, as shown in Figure 4. In the cases of $\widetilde{m}^{e}_{11}$ and $\widetilde{m}^{\nu}_{11}$, the allowed regions extend down to the lower boundary of the numerical scan, indicating that values compatible with zero cannot be excluded. Therefore, these two parameters are more appropriately reported in terms of upper bounds rather than as central values with two-sided uncertainties.

The numerical ranges of the elements of the real orthogonal matrices $\mathbf{O}_e$ and $\mathbf{O}_\nu$ are obtained by propagating the parameter regions defined by the two-dimensional slices satisfying the reference condition $\Delta\chi^2 \leq 2.30$. Therefore, the resulting intervals should be interpreted as induced ranges rather than as independent statistical uncertainties. In particular, the matrix elements are strongly correlated through the orthogonality conditions, and hence they do not represent independent degrees of freedom. The corresponding numerical results are

$$\mathbf{O}_e = \begin{pmatrix} 0.997460^{+0.000295}_{-0.000148} & -0.071130^{+0.004255}_{-0.001933} & 0.003865^{+0.001756}_{-0.002341} \\ 0.049962^{+0.014875}_{-0.009657} & 0.737245^{+0.199214}_{-0.126240} & 0.673776^{+0.116824}_{-0.329042} \\ -0.050775^{+0.025344}_{-0.010423} & -0.671871^{+0.328073}_{-0.116377} & 0.738926^{+0.199774}_{-0.126618} \end{pmatrix}. \tag{86}$$

$$\mathbf{O}_{\nu} = \begin{pmatrix} 0.834104^{+0.005378}_{-0.005446} & -0.542139^{+0.008130}_{-0.006571} & 0.101765^{+0.008887}_{-0.004843} \\ 0.345206^{+0.009454}_{-0.016849} & 0.656932^{+0.011569}_{-0.020333} & 0.670279^{+0.027521}_{-0.016579} \\ -0.430237^{+0.013258}_{-0.023094} & -0.523953^{+0.011268}_{-0.017951} & 0.735098^{+0.015423}_{-0.027404} \end{pmatrix}. \tag{87}$$

Once the numerical ranges associated with the reference condition $\Delta\chi^2 \leq 2.30$ have been determined, their impact on the leptonic mixing matrix can be evaluated. We propagate the corresponding parameter ranges to the elements of the PMNS matrix. Since $\mathbf{U}_{\rm PMNS}$ is in general complex, we report separately its real and imaginary parts. Thus, we have

$$\mathbf{U}_{\rm PMNS} = {\rm Re}(\mathbf{U}_{\rm PMNS}) + i\ {\rm Im}(\mathbf{U}_{\rm PMNS})\,, \tag{88}$$

where

$${\rm Re}(\mathbf{U}_{\rm PMNS}) = \begin{pmatrix} 0.82158^{+0.00598}_{-0.00591} & -0.54774^{+0.00903}_{-0.00886} & 0.14961^{+0.00267}_{-0.00302} \\ -0.18438^{+0.14209}_{-0.06452} & -0.02973^{+0.19628}_{-0.10701} & 0.65389^{+0.03711}_{-0.13860} \\ 0.38761^{+0.03315}_{-0.02845} & 0.54278^{+0.02991}_{-0.04137} & -0.24741^{+0.14169}_{-0.20721} \end{pmatrix}, \tag{89}$$

and

$${\rm Im}(\mathbf{U}_{\rm PMNS}) = \begin{pmatrix} -0.02638^{+0.00243}_{-0.00174} & -0.04249^{+0.00270}_{-0.00155} & -0.01009^{+0.01049}_{-0.02027} \\ -0.37214^{+0.03042}_{-0.02087} & -0.60602^{+0.04013}_{-0.02285} & -0.17829^{+0.13733}_{-0.26887} \\ -0.03984^{+0.16015}_{-0.07208} & -0.18818^{+0.25826}_{-0.11076} & -0.67597^{+0.12248}_{-0.04119} \end{pmatrix}. \tag{90}$$

The moduli of the matrix elements are

$$|\mathbf{U}_{\rm PMNS}| = \begin{pmatrix} 0.82200^{+0.00593}_{-0.00462} & 0.54939^{+0.00730}_{-0.00892} & 0.14995^{+0.00280}_{-0.00291} \\ 0.41531^{+0.01862}_{-0.06280} & 0.60675^{+0.03493}_{-0.02961} & 0.67777^{+0.01523}_{-0.01205} \\ 0.38965^{+0.04757}_{-0.01346} & 0.57448^{+0.02602}_{-0.03029} & 0.71983^{+0.01119}_{-0.01469} \end{pmatrix}. \tag{91}$$

For the inverted neutrino mass ordering (IH), $m_{\nu_3} < m_{\nu_1} < m_{\nu_2}$. We obtain that the seven free parameters in the BFP, with a minimum χ^2 value of $\chi^2_{\rm min} = 1.5907417 \times 10^{-4}$, have the values

$$\begin{aligned} &m_{\nu_3} = 0.0549332\ {\rm eV}, \quad \widetilde{m}^{e}_{11} = 3.08403 \times 10^{-5}, \quad \widetilde{m}^{\nu}_{11} = 0.332738, \\ &\widetilde{D}_{e} = 0.384517, \quad \widetilde{D}_{\nu} = 0.411413, \quad \varsigma_{\rm j} = 303.859^{\circ}, \quad \varrho_{\rm j} = 9.11931^{\circ}. \end{aligned} \tag{92}$$

The corresponding mixing angles are

$$\sin^2\theta_{12} = 0.3088268, \quad \sin^2\theta_{13} = 0.0226219, \quad \sin^2\theta_{23} = 0.5501664. \tag{93}$$

In Figure 5, we show the two-dimensional χ^2 slices for the free parameters of the model in the vicinity of the BFP. The numerical ranges induced by the innermost reference region, $\Delta\chi^2 \leq 2.30$, for the seven free parameters of the model and the three flavor mixing angles are:

$$\begin{aligned} &m_{\nu_3} = \left(5.493^{+0.507}_{-1.193}\right) \times 10^{-2}\ {\rm eV}, \quad \widetilde{m}^{e}_{11} \lesssim 2.5 \times 10^{-4}, \quad \widetilde{m}^{\nu}_{11} = 0.332^{+0.027}_{-0.055}, \\ &\widetilde{\mathcal{D}}_{e} = 0.3845^{+0.0455}_{-0.0744}, \quad \widetilde{\mathcal{D}}_{\nu} = 0.4114^{+0.0708}_{-0.0776}, \quad \varsigma_{\rm j} = \left(303.86^{+8.18}_{-7.42}\right)^{\circ}, \quad \varrho_{\rm j} = \left(9.12^{+5.60}_{-9.12}\right)^{\circ}. \end{aligned} \tag{94}$$

$$\sin^2\theta_{12} = 0.3088^{+0.0066}_{-0.0067}, \quad \sin^2\theta_{13} = 0.02262^{+0.00056}_{-0.00057}, \quad \sin^2\theta_{23} = 0.5502^{+0.0143}_{-0.0146}. \tag{95}$$

These ranges were obtained by projecting the two-dimensional slices satisfying $\Delta\chi^2 \leq 2.30$ onto the corresponding parameter axes. For $\widetilde{m}^{e}_{11}$, the numerical region extends down to the lower boundary of the scan, indicating that values compatible with zero cannot be excluded. Therefore, this parameter is more appropriately reported as an upper bound rather than as a central value with a two-sided uncertainty.

The absolute neutrino-mass scale obtained in the flavor analysis can also be confronted with cosmological constraints. Defining $\Sigma_\nu = m_{\nu_1} + m_{\nu_2} + m_{\nu_3}$, the neutrino mass spectra at the best-fit points yield $\Sigma_\nu^{\rm NH,BFP} \simeq 0.0626$ eV and $\Sigma_\nu^{\rm IH,BFP} \simeq 0.2038$ eV. For the inverted ordering, the range of the lightest neutrino mass induced by the reference region $\Delta\chi^2 \leq 2.30$, $0.0430\ \text{eV} \lesssim m_{\nu_3} \lesssim 0.0600$ eV, corresponds approximately to $0.175\ \text{eV} \lesssim \Sigma_\nu^{\rm IH} \lesssim 0.216$ eV. These results should be compared with cosmological constraints with some caution, since limits on the sum of neutrino masses depend on the assumed cosmological model. Within the ΛCDM framework, the recent DESI DR2 analysis combined with CMB and neutrino-oscillation data gives the ordering-dependent bounds $\Sigma_\nu < 0.101$ eV for normal ordering and $\Sigma_\nu < 0.133$ eV for inverted ordering at 95% probability [89]. Consequently, while the NH best-fit region obtained here is compatible with these constraints, the IH region selected by our flavor analysis is in strong tension with the corresponding ΛCDM cosmological bound.

We emphasize, however, that this tension should not be interpreted as a model-independent exclusion of the inverted-ordering solution. Cosmological neutrino-mass bounds are sensitive to assumptions about the background cosmology. Therefore, we retain the IH solution as a viable realization at the level of neutrino oscillation and flavor data, while explicitly noting its tension with standard ΛCDM cosmology.

Following the same procedure as for the normal-ordering case, using the reference condition $\Delta\chi^2 \leq 2.30$, we obtain

$$\mathbf{O}_e = \begin{pmatrix} 0.997644^{+0.001620}_{-0.000373} & -0.0684331^{+0.0302020}_{-0.0051466} & 0.0048043^{+0.0011889}_{-0.0019149} \\ 0.0406399^{+0.0048442}_{-0.0196380} & 0.6459788^{+0.0326320}_{-0.0568164} & 0.7622727^{+0.0448186}_{-0.0286910} \\ -0.0552681^{+0.0232249}_{-0.0076462} & -0.7602817^{+0.0288000}_{-0.0445256} & 0.6472381^{+0.0323495}_{-0.0568419} \end{pmatrix}. \tag{96}$$

$$\mathbf{O}_\nu = \begin{pmatrix} 0.7957468^{+0.0117998}_{-0.0172680} & -0.5710577^{+0.0135330}_{-0.0214910} & 0.2016932^{+0.0077675}_{-0.0276733} \\ [2mm] 0.5660641^{+0.0237243}_{-0.0123978} & 0.8197016^{+0.0086162}_{-0.0162914} & 0.0875254^{+0.0106723}_{-0.0138411} \\ -0.2153102^{+0.0238787}_{-0.0090654} & -0.0445232^{+0.0110747}_{-0.0157682} & 0.9755302^{+0.0054007}_{-0.0022041} \end{pmatrix}. \tag{97}$$

Also we have

$$\mathbf{U}_{\rm PMNS} = {\rm Re}(\mathbf{U}_{\rm PMNS}) + i\ {\rm Im}(\mathbf{U}_{\rm PMNS})\,, \tag{98}$$

where

$${\rm Re}(\mathbf{U}_{\rm PMNS}) = \begin{pmatrix} 0.81844^{+0.00383}_{-0.00530} & -0.54872^{+0.00562}_{-0.00750} & 0.14997^{+0.00184}_{-0.00137} \\ 0.31090^{+0.06102}_{-0.08390} & 0.36752^{+0.08943}_{-0.11912} & -0.71460^{+0.02608}_{-0.02038} \\ 0.10663^{+0.07465}_{-0.09740} & 0.31693^{+0.10607}_{-0.14023} & 0.66156^{+0.01502}_{-0.02504} \end{pmatrix}. \tag{99}$$

$${\rm Im}(\mathbf{U}_{\rm PMNS}) = \begin{pmatrix} -0.01722^{+0.04163}_{-0.00720} & -0.02727^{+0.05922}_{-0.00468} & -0.01150^{+0.02963}_{-0.00663} \\ -0.27771^{+0.65941}_{-0.10399} & -0.43435^{+0.94107}_{-0.07237} & -0.16450^{+0.42032}_{-0.09132} \\ -0.38041^{+0.80242}_{-0.04161} & -0.52344^{+1.10900}_{-0.06212} & 0.04467^{+0.17531}_{-0.26464} \end{pmatrix}. \tag{100}$$

Finally, the moduli of the matrix elements are

$$|\mathbf{U}_{\rm PMNS}| = \begin{pmatrix} 0.8186196^{+0.0053820}_{-0.0054242} & 0.5494002^{+0.0058543}_{-0.0059597} & 0.1504057^{+0.0018598}_{-0.0018937} \\ 0.4168717^{+0.0587493}_{-0.0840141} & 0.5689692^{+0.0245705}_{-0.0281937} & 0.7332944^{+0.0094788}_{-0.0098193} \\ 0.3950695^{+0.0732944}_{-0.0725278} & 0.6119097^{+0.0241320}_{-0.0230531} & 0.6630667^{+0.0107076}_{-0.0106420} \end{pmatrix}. \tag{101}$$

IV. SOME PHENOMENOLOGICAL ASPECTS

In the previous section, we supplemented an extended left-right symmetric model with the S_3 flavor symmetry and analyzed the CKM and PMNS flavor mixing matrices in the quark and lepton sectors. Having determined these matrices numerically, we now study their impact on selected observables. For the phenomenological analysis presented below, we adopt two simplifying approximations:

1. The mixing between the left- and right-handed charged gauge bosons is neglected, $\zeta \simeq 0$, consistently with the stringent phenomenological constraints on this parameter [90].

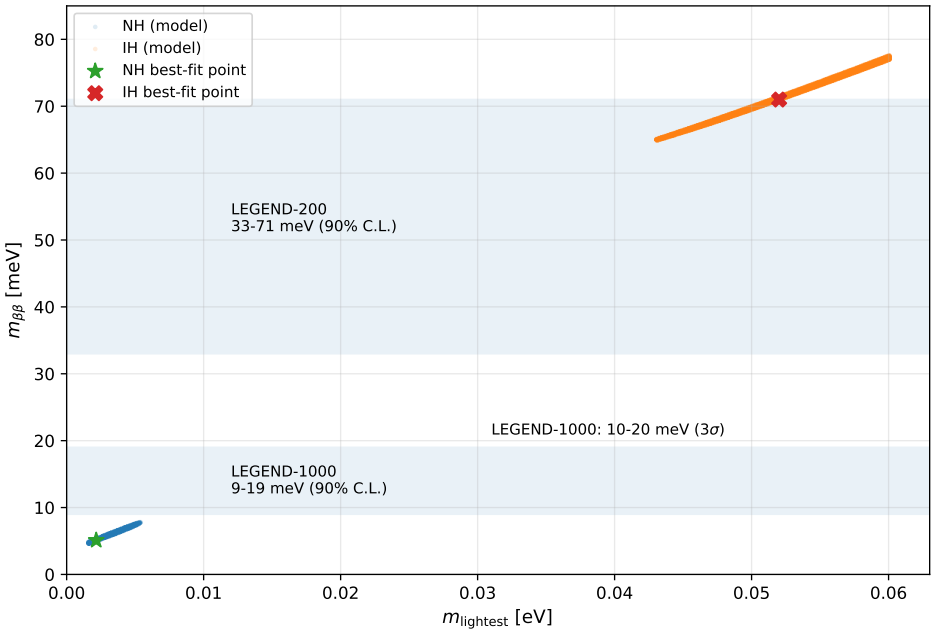

FIG. 6. Effective Majorana neutrino mass $m_{\beta\beta}$ as a function of the lightest neutrino mass for NH and IH. The points correspond to the parameter configurations satisfying $\chi^2 < 1$, while the markers indicate the corresponding BFP. The shaded regions illustrate the projected sensitivity to $m_{\beta\beta}$ of the LEGEND experimental program. The conversion between the neutrinoless double-beta decay half-life and $m_{\beta\beta}$ depends on the adopted nuclear matrix elements.

2. The light-heavy neutrino mixing is neglected, $\theta \simeq 0$. This approximation is appropriate for the regime in which the heavy-neutrino scale is sufficiently above the electroweak scale and is consistent with existing constraints on heavy-light neutrino mixing [91].

These assumptions allow us to isolate the purely left-handed and right-handed contributions considered below. Mixed-current contributions proportional to ζ, θ, or their products are therefore outside the scope of the present analysis. With these assumptions in place, we now determine the allowed ranges of the observables considered below.

A. Neutrinoless double beta decay

It should be kept in mind that the IH region displayed here is obtained from the flavor and oscillation analysis alone. Its comparatively large absolute neutrino-mass scale is in tension with current cosmological bounds within ΛCDM, as discussed above. Therefore, the $0\nu\beta\beta$ predictions for IH should be understood conditionally on either a relaxation of the standard cosmological assumptions or future changes in the cosmological neutrino-mass constraints.

Neutrinoless double-beta decay is a promising process for probing whether neutrinos are Majorana fermions [35–38]. In general, the decay width for $0\nu\beta\beta$ can be written as

$$\Gamma^{0\nu} = \sum_j G_j\,(Q, Z)\,|\mathcal{M}_j \eta_j|^2. \tag{102}$$

In this expression, $\mathcal{M}_j$ denotes the nuclear matrix element associated with the j-th mechanism, η_j is the corresponding dimensionless particle-physics parameter, and $G_j(Q, Z)$ is a phase-space factor that may also depend on the underlying mechanism [35–38].

Under the approximations $\zeta \simeq 0$ and $\theta \simeq 0$, one has $W_1 \simeq W_L$, $W_2 \simeq W_R$, $\mathbf{S} \simeq \mathbf{T} \simeq 0$, $\mathbf{U} \simeq \mathbf{U}_{\nu L}$, and $\mathbf{V} \simeq \mathbf{U}_{\nu R}$. Therefore, the leptonic charged current in Eq. (11) reduces to

$$\mathcal{L}_{CC} \simeq \frac{g}{\sqrt{2}} \left[\bar{\tilde{e}}_L \gamma_\mu \mathbf{U}^L_{\text{PMNS}} \tilde{\nu}_L\, W_1^{-\mu} + \bar{\tilde{e}}_R \gamma_\mu \mathbf{U}^R_{\text{PMNS}} \tilde{\nu}_R\, W_2^{-\mu}\right] + h.c. \tag{103}$$

In the MLRSM, the additional scalar and fermionic degrees of freedom give rise to several contributions to the decay amplitude [92–94]. Under the assumptions adopted in our analysis, some of these contributions are neglected. The

relevant contributions are then those involving the left- and right-handed PMNS mixing matrices, namely,

$$\Gamma^{0\nu} = G_{01}^{0\nu} \left[|\mathcal{M}_{\nu}^{0\nu} \eta_{\nu}|^2 + |\mathcal{M}_{N}^{0\nu} \eta_{\nu R}^{R}|^2 \right] \tag{104}$$

with

$$\eta_{\nu} = \frac{1}{m_e} \sum_{i=1}^{3} \left(\mathbf{U}_{PMNS}^{L} \right)_{ei}^{2} m_i; \tag{105}$$

$$\eta_{\nu R}^{R} = m_p \left(\frac{m_{W_L}}{m_{W_R}} \right)^4 \sum_{i=1}^{3} \frac{\left(\mathbf{U}_{PMNS}^{R} \right)_{ei}^{2}}{M_{\nu_{iR}}}, \tag{106}$$

where m_e and m_p are the electron and proton masses, respectively. From Eq. (105), we obtain

$$|\eta_{\nu}| = \frac{m_{\beta\beta}}{m_e} \tag{107}$$

where $m_{\beta\beta}$ is the effective Majorana mass, defined as

$$m_{\beta\beta} = \left| \sum_{i=1}^{3} \left(U_{\mathrm{PMNS}}^{L} \right)_{ei}^{2} m_{\nu_i} \right|. \tag{108}$$

The effective Majorana mass $m_{\beta\beta}$ connects the low-energy neutrino parameters with the $0\nu\beta\beta$ decay rate when the process is dominated by the exchange of light Majorana neutrinos [95]. For the parameter points satisfying $\chi^2 < 1$, our numerical analysis predicts for NH 4.63 meV $\lesssim m_{\beta\beta}^{\mathrm{NH}} \lesssim$ 7.74 meV, with a best-fit value $m_{\beta\beta}^{\mathrm{NH,BFP}} \simeq 5.10$ meV. For IH, a significantly larger and rather narrow interval is obtained, 64.85 meV $\lesssim m_{\beta\beta}^{\mathrm{IH}} \lesssim$ 77.52 meV, with $m_{\beta\beta}^{\mathrm{IH,BFP}} \simeq$ 71.00 meV. Therefore, within the parameter region selected by our numerical analysis, the two neutrino mass orderings lead to clearly separated predictions for the effective Majorana mass. Notice that the quoted intervals correspond to the envelope of the accepted points satisfying $\chi^2 < 1$ and should not be interpreted as conventional statistical 1σ confidence intervals.

The predicted regions can be confronted with the current experimental limits on neutrinoless double-beta decay. The KamLAND-Zen Collaboration, using the complete KamLAND-Zen dataset, obtained a lower limit on the ^{136}Xe neutrinoless double-beta decay half-life of $T_{1/2}^{0\nu} > 3.8 \times 10^{26}$ yr (90% C.L.), which, under the standard light-Majorana-neutrino exchange mechanism, corresponds to an upper bound on the effective Majorana mass in the range $m_{\beta\beta} < 28 - 122$ meV. The range reflects the theoretical uncertainty associated with the nuclear matrix elements (NMEs) entering the conversion between $T_{1/2}^{0\nu}$ and $m_{\beta\beta}$ [96]. The first results from LEGEND-200, based on ^{76}Ge, yield $T_{1/2}^{0\nu} > 1.9 \times 10^{26}$ yr (90% C.L.), corresponding to $m_{\beta\beta} < 75 - 200$ meV, depending on the adopted nuclear matrix element [97].

Consequently, the NH region predicted by the present model lies well below the sensitivity of current neutrinoless double-beta decay searches. In contrast, the IH prediction, $m_{\beta\beta}^{\mathrm{IH}} \simeq 65 - 78$ meV, lies in the mass range currently being approached by these experiments. Because the translation from a half-life limit into a constraint on $m_{\beta\beta}$ depends significantly on the nuclear matrix elements, the present experimental results do not provide a nuclear-matrix-element-independent exclusion of the IH region predicted by the model. This situation becomes particularly interesting for the next-generation neutrinoless double-beta decay experiments. LEGEND-1000 is designed to probe half-lives at the 10^{28} yr scale, corresponding to a sensitivity to the effective Majorana mass at the level of $m_{\beta\beta} \sim \mathcal{O}(10)$ meV, depending on the nuclear matrix elements employed in the conversion from the half-life sensitivity [98]. Therefore, the IH region predicted by the present model, $m_{\beta\beta}^{\mathrm{IH}} \simeq 65 - 78$ meV, lies well within the mass scale expected to be explored by next-generation experiments, under the assumption that light Majorana-neutrino exchange is the dominant mechanism responsible for $0\nu\beta\beta$ decay. On the other hand, the NH prediction, $m_{\beta\beta}^{\mathrm{NH}} \simeq 4.6 - 7.7$ meV, lies below the nominal projected sensitivity of LEGEND-1000 and would therefore require experiments capable of probing the few-meV region.

Figure 6 summarizes these results by showing the predicted effective Majorana mass as a function of the lightest neutrino mass for both mass orderings, together with the experimental sensitivity ranges. The strong separation between the NH and IH regions constitutes a distinctive phenomenological feature of the present flavored left-right symmetric scenario and provides a direct connection between the model predictions and forthcoming searches for neutrinoless double-beta decay.

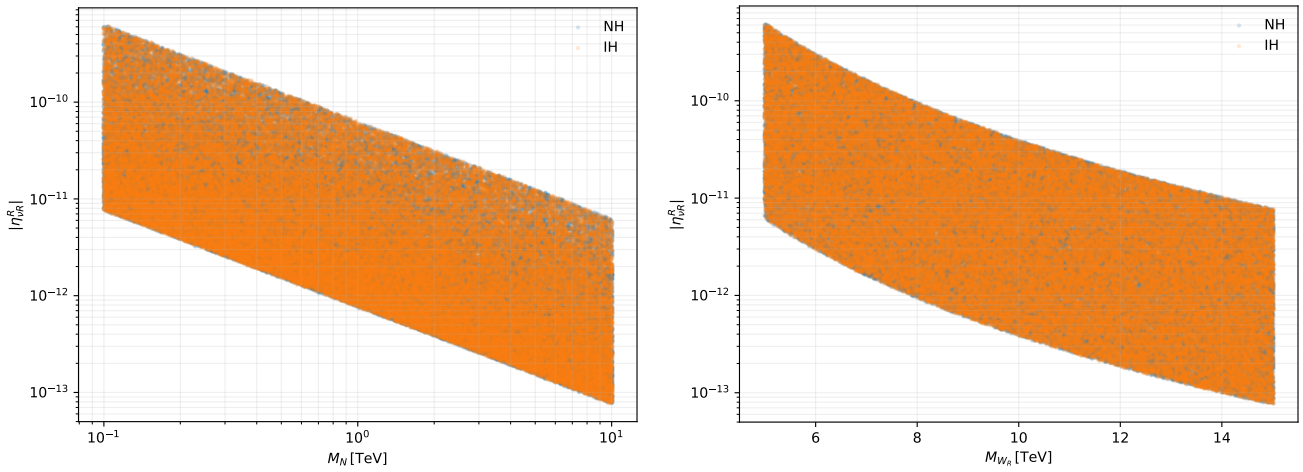

FIG. 7. Right-handed contribution to neutrinoless double-beta decay, $|\eta^R_{\nu R}|$, as a function of the common heavy-neutrino mass scale $M_N = M_{\nu_1^R} = M_{\nu_2^R}$ (left panel) and the right-handed charged gauge boson mass M_{W_R} (right panel), for the normal (NH) and inverted (IH) neutrino mass orderings. The points correspond to parameter configurations satisfying $\chi^2 < 1$ in the lepton-sector analysis, while the remaining heavy-sector parameters are varied within the ranges adopted in the numerical scan.

In this model, the right-handed PMNS matrix is completely determined by the charged lepton sector, since the right-handed Majorana neutrino mass matrix is diagonal. Thus, one has $\mathbf{U}^R_{\rm PMNS} = \mathbf{O}_e^\top \mathbf{P}_e \mathbf{R}_{\pi/4}$, where $\mathbf{O}_e$ is the real orthogonal matrix associated with the charged-lepton sector, $\mathbf{P}_e$ contains the corresponding phase factors, and $\mathbf{R}_{\pi/4}$ is the maximal rotation defined in Eq. (27). Writing $\mathbf{P}_e = \mathrm{diag}(p_1, p_2, p_3)$, the elements of the first row of $\mathbf{U}^R_{\rm PMNS}$, which are the ones entering Eq. (106), are

$$\begin{aligned}
\left(\mathbf{U}^R_{\rm PMNS}\right)_{e1} &= \frac{1}{\sqrt{2}}\left(O_{11}p_1 + O_{21}p_2\right), \\
\left(\mathbf{U}^R_{\rm PMNS}\right)_{e2} &= \frac{1}{\sqrt{2}}\left(-O_{11}p_1 + O_{21}p_2\right), \\
\left(\mathbf{U}^R_{\rm PMNS}\right)_{e3} &= O_{31}p_3.
\end{aligned} \tag{109}$$

Therefore, the right-handed contribution to neutrinoless double-beta decay can be expressed as

$$\eta^R_{\nu R} = m_p \left(\frac{m_{W_L}}{m_{W_R}}\right)^4 \left[\frac{(O_{11}p_1 + O_{21}p_2)^2}{2M_{\nu_{1R}}} + \frac{(-O_{11}p_1 + O_{21}p_2)^2}{2M_{\nu_{2R}}} + \frac{O_{31}^2 p_3^2}{M_{\nu_{3R}}}\right]. \tag{110}$$

This form makes explicit that the contribution $\eta^R_{\nu R}$ depends simultaneously on the right-handed gauge boson mass scale, the heavy neutrino mass spectrum, and the flavor structure predicted by the charged lepton sector. In particular, since eq. (106) involves $\left(\mathbf{U}^R_{\rm PMNS}\right)^2_{ei}$ rather than $\left|\left(\mathbf{U}^R_{\rm PMNS}\right)_{ei}\right|^2$, the phases contained in $\mathbf{P}_e$ may lead to constructive or destructive interference among the different heavy neutrino contributions. The corresponding phase matrices are those defined in Eq. (29), namely $\mathbf{P}_e = \mathrm{diag}(e^{i\alpha_e/2}, e^{i\beta_e/2}, e^{i\gamma_e/2})$ for PLRT and $\mathbf{P}_e = \mathrm{diag}(1, 1, e^{i\varphi_{ec}})$ for MLRT. Also, the right-handed Majorana neutrino mass matrix has the S_3-induced structure $\mathbf{M}_R = \mathrm{diag}(a_R, a_R, b_R)$, with $a_R = y_1^R v_R$ and $b_R = y_2^R v_R$. Therefore, taking the physical masses to be positive, $M_{\nu_{1R}} = M_{\nu_{2R}} \equiv M_N = |a_R|$ and $M_{\nu_{3R}} = |b_R|$. Defining $r_R \equiv M_{\nu_{3R}}/M_N = |b_R/a_R|$, the twofold degeneracy of the first two right-handed neutrinos considerably simplifies Eq. (110), since the interference terms between the first two contributions cancel. As a result,

$$\eta^R_{\nu R} = \frac{m_p}{M_N}\left(\frac{m_{W_L}}{m_{W_R}}\right)^4 \left[O_{11}^2 p_1^2 + O_{21}^2 p_2^2 + \frac{O_{31}^2 p_3^2}{r_R}\right]. \tag{111}$$

Thus, the right-handed contribution is controlled by the overall heavy neutrino mass scale M_N, the mass ratio r_R, the right-handed gauge boson mass, and the flavor structure encoded in $\mathbf{O}_e$ and $\mathbf{P}_e$. In particular, for the MLRT case, where $\mathbf{P}_e = \mathrm{diag}(1, 1, e^{i\varphi_{ec}})$, this expression can be rewritten using the orthogonality of O_e as

$$\eta^{R,\rm MLRT}_{\nu R} = \frac{m_p}{M_N}\left(\frac{m_{W_L}}{m_{W_R}}\right)^4 \left[1 - O_{31}^2 + \frac{O_{31}^2}{r_R} e^{2i\varphi_{ec}}\right], \tag{112}$$

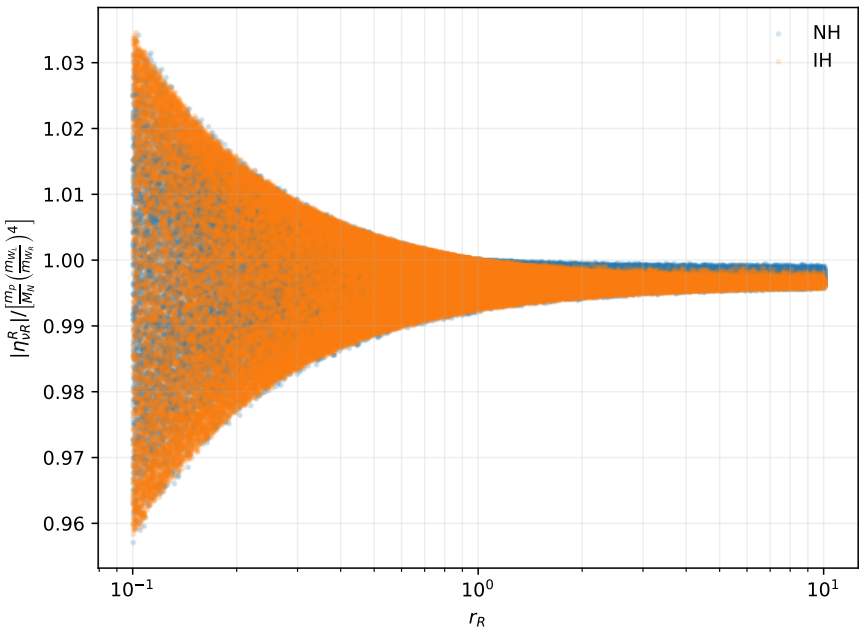

FIG. 8. Flavor-dependent correction factor $\mathcal{F}_R = |\eta^R_{\nu R}|/\left[\frac{m_p}{M_N}\left(\frac{m_{W_L}}{m_{W_R}}\right)^4\right]$ as a function of the heavy-neutrino mass ratio $r_R = M_{\nu_3^R}/M_N$ for the normal (NH) and inverted (IH) neutrino mass orderings. The proximity of $\mathcal{F}_R$ to unity shows that the dependence on r_R, O_{31}, and φ_{ec} provides only a subleading correction to the dominant heavy mass scaling.

making explicit the interplay between the heavy neutrino mass hierarchy and the phase structure of the charged lepton sector.

Figures 7 and 8 summarize the behavior of the right-handed contribution to neutrinoless double-beta decay in the parameter region compatible with the lepton-sector fit. The left panel of Figure 7 shows $|\eta^R_{\nu R}|$ as a function of the common heavy-neutrino mass scale $M_N = M_{\nu_1^R} = M_{\nu_2^R}$, whereas the right panel displays its dependence on the right-handed charged gauge-boson mass M_{W_R}. As follows from Eq. (112), the dominant scaling is approximately $|\eta^R_{\nu R}| \propto M_N^{-1} M_{W_R}^{-4}$. Accordingly, the left panel exhibits the expected inverse dependence on M_N, while the right panel shows the much stronger suppression associated with increasing M_{W_R}. The vertical spread in each panel originates from the simultaneous variation of the remaining heavy-sector parameters, while the normal and inverted light-neutrino mass orderings largely overlap. This indicates that the magnitude of the right-handed contribution is controlled mainly by the heavy-neutrino and right-handed gauge-boson mass scales, with only a weak residual dependence on the light-neutrino ordering. The latter feature can be understood more clearly from Figure 8, where we isolate the flavor-dependent part by defining

$$\mathcal{F}_R \equiv \frac{|\eta^R_{\nu R}|}{\dfrac{m_p}{M_N}\left(\dfrac{m_{W_L}}{m_{W_R}}\right)^4}. \tag{113}$$

For the MLRT framework, Eq. (112) gives

$$\mathcal{F}_R = \left|1 - O_{31}^2 + \frac{O_{31}^2}{r_R} e^{2i\varphi_{ec}}\right|, \tag{114}$$

so that this quantity contains the dependence on the heavy neutrino mass ratio r_R, the charged lepton mixing parameter O_{31}, and the phase φ_{ec}. As shown in Figure 8, the numerical points remain close to $\mathcal{F}_R = 1$ over most of the scanned region. This behavior is a consequence of the small value of O_{31}^2 in the parameter space selected by the lepton sector fit. Therefore, the flavor-dependent correction is generally subleading, and the right-handed contribution can be approximated to a good accuracy by

$$|\eta^R_{\nu R}| \simeq \frac{m_p}{M_N}\left(\frac{m_{W_L}}{m_{W_R}}\right)^4. \tag{115}$$

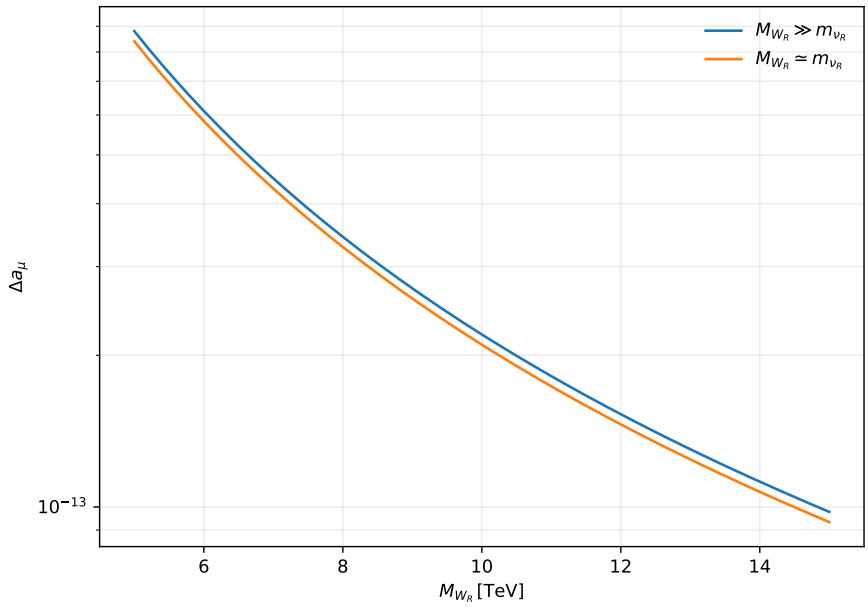

FIG. 9. Contribution of the right-handed neutrinos and the W_R gauge boson to the muon anomalous magnetic moment, $\Delta a_\mu(\nu_R, W_R)$, as a function of the right-handed charged gauge-boson mass M_{W_R}. The two curves correspond to the limiting regimes $M_{W_R} \gg m_{\nu_R}$ and $M_{W_R} \simeq m_{\nu_R}$ appearing in Eq. (116). Parity symmetry, $g_R = g_L$, and the unitarity relation $\sum_i |(U^R_{\rm PMNS})_{\mu i}|^2 = 1$ have been used. Both regimes show the characteristic behavior $\Delta a_\mu \propto M^{-2}_{W_R}$ and differ only slightly in their overall normalization.

The nearly coincident NH and IH regions observed in both figures are thus a natural consequence of the dominant dependence on the heavy right-handed sector rather than on the ordering of the light neutrino masses.

B. Muon anomalous magnetic moment and lepton-flavor violation

In this section, we examine the impact of lepton mixing on the muon anomalous magnetic moment, $(g-2)_\mu$ (for a recent review, see [99]), and on the lepton-flavor-violating decay $\mu \to e\gamma$. Fermilab reported a measurement of the muon anomalous magnetic moment [100] which, when combined with the BNL data [101], showed a discrepancy with the SM prediction. More recently, this tension has disappeared [102], and the Muon $g-2$ Collaboration has reported the most precise measurement of this quantity to date. With this motivation, we briefly examine the role of left-right interactions in these observables. In particular, right-handed charged currents can contribute to $(g-2)_\mu$ and to the $\mu \to e\gamma$ decay. The relevant contributions involve the W_R gauge boson and right-handed neutrinos ν_R. Approximate expressions were obtained in Ref. [41] for two limiting regimes:

$$\Delta a_\mu\,(\nu_R, W_R) = \begin{cases} 2.2\times 10^{-11}\left(\frac{g_R}{g_L}\right)^2\left(\frac{1\text{TeV}}{M_{W_R}}\right)^2 \sum_{i=1}^{3} |\left(\mathbf{U}^R_{\rm PMNS}\right)_{\mu i}|^2, & \text{if} \qquad M_{W_R} \gg m_{\nu_R} \\ 2.1\times 10^{-11}\left(\frac{g_R}{g_L}\right)^2\left(\frac{1\text{TeV}}{M_{W_R}}\right)^2 \sum_{i=1}^{3} |\left(\mathbf{U}^R_{\rm PMNS}\right)_{\mu i}|^2, & \text{if} \qquad M_{W_R} \approx m_{\nu_R}. \end{cases} \tag{116}$$

The observable Δa_μ depends on the W_R gauge-boson mass and on the right-handed PMNS mixing matrix, with the sum running over the three right-handed neutrino species, $i = 1, 2, 3$. In the present model, the right-handed leptonic mixing matrix is given by $\mathbf{U}^R_{\rm PMNS} = \mathbf{O}_e^\top \mathbf{P}_e \mathbf{R}_{\pi/4}$. Although $\mathbf{U}^R_{\rm PMNS}$ is in general nontrivial, it is a unitary matrix. Therefore, the normalization of its muon row implies

$$\sum_{i=1}^{3} \left|\left(U^R_{\rm PMNS}\right)_{\mu i}\right|^2 = 1. \tag{117}$$

Furthermore, parity symmetry implies $g_R = g_L$. Consequently, within the two limiting regimes considered in Eq. (116), the contribution of the right-handed neutrinos and the W_R gauge boson to the muon anomalous magnetic moment

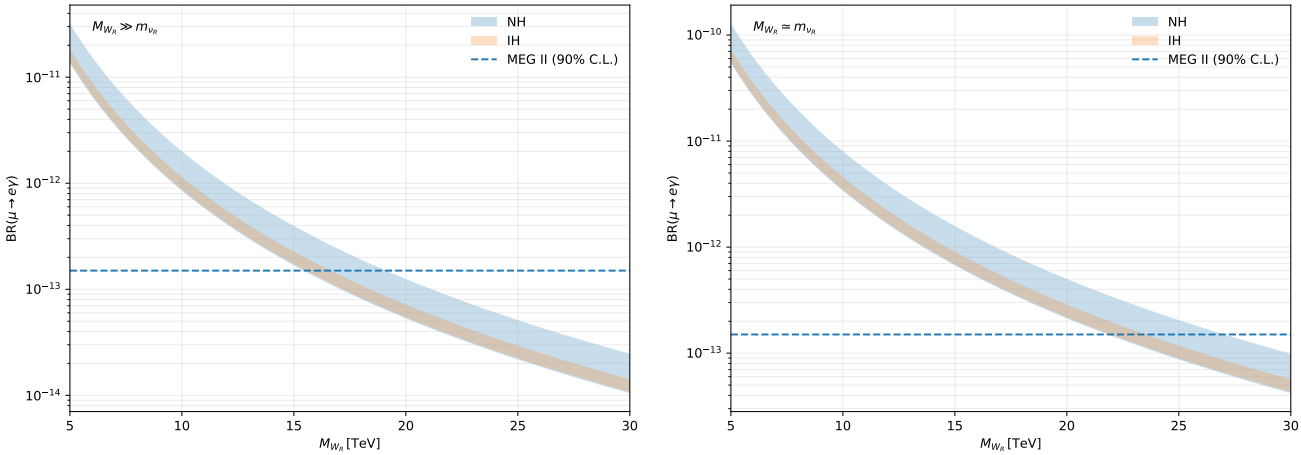

FIG. 10. Branching ratio for the lepton-flavor-violating decay $\mu \to e\gamma$ as a function of the right-handed charged gauge-boson mass M_{W_R} for NH and IH. The left panel corresponds to the regime $M_{W_R} \gg m_{\nu_R}$, whereas the right panel corresponds to $M_{W_R} \simeq m_{\nu_R}$. The shaded bands are obtained from the variation of the charged-lepton flavor factor $S^R_{e\mu}$ over the parameter configurations satisfying the numerical selection criterion $\chi^2 < 1$ in the lepton-sector analysis. Parity symmetry, $g_R = g_L$, has been assumed. The horizontal dashed line represents the current MEG II upper bound, $\mathrm{BR}(\mu^+ \to e^+\gamma) < 1.5 \times 10^{-13}$ at 90% C.L. Parameter configurations lying above this line are excluded by the present experimental limit.

reduces to

$$\Delta a_\mu(\nu_R, W_R) = \begin{cases} 2.2 \times 10^{-11} \left(\dfrac{1\ \mathrm{TeV}}{M_{W_R}}\right)^2, & M_{W_R} \gg m_{\nu_R}, \\ 2.1 \times 10^{-11} \left(\dfrac{1\ \mathrm{TeV}}{M_{W_R}}\right)^2, & M_{W_R} \simeq m_{\nu_R}. \end{cases} \tag{118}$$

Thus, under the approximations entering in Eq. (116), the dependence on the right-handed flavor-mixing parameters disappears after summing over the three neutrino states. The resulting contribution is controlled only by the right-handed gauge-boson mass and exhibits the characteristic scaling $\Delta a_\mu \propto M_{W_R}^{-2}$. Figure 9 shows this behavior for 5 TeV $\leq M_{W_R} \leq$ 15 TeV. The two limiting cases follow nearly parallel curves and differ only slightly in their normalization. In particular, for $M_{W_R} = 5$ TeV one obtains $\Delta a_\mu \simeq 8.8 \times 10^{-13}$ and 8.4×10^{-13} for the $M_{W_R} \gg m_{\nu_R}$ and $M_{W_R} \simeq m_{\nu_R}$ regimes, respectively, whereas for $M_{W_R} = 15$ TeV these contributions decrease to approximately 9.8×10^{-14} and 9.3×10^{-14}. Hence, the contribution considered here becomes rapidly suppressed as the right-handed gauge boson mass increases.

Lepton-flavor violation occurs in the neutrino sector through neutrino oscillations, but has not been observed in charged-lepton processes. The observation of charged-lepton flavor violation would therefore provide a clear signal of physics beyond the SM. In particular, the decay $\mu \to e\gamma$ has been extensively studied, and stringent upper limits on its branching ratio have been established (see Ref. [41]). Within the MLRSM, the branching ratio for this lepton-flavor-violating process is given by

$$\mathrm{BR}\left(\mu \to e\gamma\right) = \begin{cases} 5 \times 10^{-8} \left(\frac{g_R}{g_L}\right)^4 \left(\frac{1\mathrm{TeV}}{M_{W_R}}\right)^4 \sum_{i=1}^{3} |\left(\mathbf{U}^{*R}_{\mathrm{PMNS}}\right)_{ei} \left(\mathbf{U}^{R}_{\mathrm{PMNS}}\right)_{\mu i}|^2, & \text{if} \quad M_{W_R} \gg m_{\nu_R} \\ 2 \times 10^{-7} \left(\frac{g_R}{g_L}\right)^4 \left(\frac{1\mathrm{TeV}}{M_{W_R}}\right)^4 \sum_{i=1}^{3} |\left(\mathbf{U}^{*R}_{\mathrm{PMNS}}\right)_{ei} \left(\mathbf{U}^{R}_{\mathrm{PMNS}}\right)_{\mu i}|^2, & \text{if} \quad M_{W_R} \approx m_{\nu_R}. \end{cases} \tag{119}$$

For the lepton-flavor-violating decay $\mu \to e\gamma$, the right-handed contribution depends on the combination

$$\mathcal{S}^R_{e\mu} = \sum_{i=1}^{3} \left|\left(\mathbf{U}^R_{\mathrm{PMNS}}\right)^*_{ei} \left(\mathbf{U}^R_{\mathrm{PMNS}}\right)_{\mu i}\right|^2 = \sum_{i=1}^{3} \left|\left(\mathbf{U}^R_{\mathrm{PMNS}}\right)_{ei}\right|^2 \left|\left(\mathbf{U}^R_{\mathrm{PMNS}}\right)_{\mu i}\right|^2. \tag{120}$$

In the MLRT scenario, using $\mathbf{U}^R_{\mathrm{PMNS}} = \mathbf{O}_e^\top \mathbf{P}_e \mathbf{R}_{\pi/4}$ with $\mathbf{P}_e = \mathrm{diag}(1, 1, e^{i\varphi_{ec}})$, this quantity reduces to

$$\mathcal{S}^R_{e\mu} = \frac{1}{4}(O_{11} + O_{21})^2 (O_{12} + O_{22})^2 + \frac{1}{4}(O_{21} - O_{11})^2 (O_{22} - O_{12})^2 + O_{31}^2 O_{32}^2. \tag{121}$$

Therefore, within the approximation adopted in Eq. (119), the branching ratio can be written as

$$\mathrm{BR}(\mu \to e\gamma) = \begin{cases} 5 \times 10^{-8} \left(\dfrac{1\ \mathrm{TeV}}{M_{W_R}} \right)^4 \mathcal{S}^R_{e\mu}, & M_{W_R} \gg m_{\nu_R}, \\ 2 \times 10^{-7} \left(\dfrac{1\ \mathrm{TeV}}{M_{W_R}} \right)^4 \mathcal{S}^R_{e\mu}, & M_{W_R} \simeq m_{\nu_R}, \end{cases} \tag{122}$$

where parity symmetry, $g_R = g_L$, has been used. The predictions shown in Fig. 10 can be directly confronted with the current MEG II upper bound, $\mathrm{BR}(\mu^+ \to e^+\gamma) < 1.5 \times 10^{-13}$ (90% C.L.) [103]. Within the limiting approximation adopted in Eq. (119), and using parity symmetry, $g_R = g_L$, the branching ratio can be written as

$$\mathrm{BR}(\mu \to e\gamma) = C \left(\frac{1\ \mathrm{TeV}}{M_{W_R}} \right)^4 S^R_{e\mu}, \tag{123}$$

where $C = 5 \times 10^{-8}$ for $M_{W_R} \gg m_{\nu_R}$ and $C = 2 \times 10^{-7}$ for $M_{W_R} \simeq m_{\nu_R}$. Therefore, the MEG II limit translates into the lower bound

$$M_{W_R} > 1\ \mathrm{TeV} \left[\frac{C\, S^R_{e\mu}}{1.5 \times 10^{-13}} \right]^{1/4}. \tag{124}$$

For the parameter configurations satisfying $\chi^2 < 1$, the charged-lepton flavor factor lies in the intervals $0.1701 \lesssim S^R_{e\mu} \lesssim 0.4006$ (NH), and $0.1748 \lesssim S^R_{e\mu} \lesssim 0.2298$ (IH). Consequently, in the regime $M_{W_R} \gg m_{\nu_R}$, the first allowed parameter configurations appear at $M_{W_R} \simeq 15.43$ TeV for NH and $M_{W_R} \simeq 15.54$ TeV for IH. Requiring the entire flavor band to satisfy the MEG II bound gives the more conservative constraints $M_{W_R} \gtrsim 19.12$ TeV (NH), and $M_{W_R} \gtrsim 16.64$ TeV (IH). For the regime $M_{W_R} \simeq m_{\nu_R}$, the larger normalization of the branching ratio strengthens these limits. The first allowed configurations occur at approximately 21.82 TeV for NH and 21.97 TeV for IH, whereas requiring the complete flavor bands to lie below the MEG II limit yields $M_{W_R} \gtrsim 27.03$ TeV (NH), and $M_{W_R} \gtrsim 23.53$ TeV (IH). Thus, within the approximation used in Eq. (119), the present $\mu \to e\gamma$ limit already provides a stringent constraint on the right-handed scale of the model. In particular, the interval 5 TeV $\leq M_{W_R} \leq$ 15 TeV previously considered lies below the value at which even the first allowed flavor configurations become compatible with MEG II. The different widths of the NH and IH bands originate from the different ranges of the charged-lepton mixing matrix allowed by the corresponding lepton-sector fits.

V. CONCLUSIONS

We have investigated the origin of fermion mixing in a non-minimal left-right symmetric framework supplemented by the non-Abelian flavor symmetry S_3. The three fermion families are organized as $\mathbf{2} \oplus \mathbf{1}_S$, while the scalar sector is extended to three Higgs bidoublets together with one left-handed and one right-handed triplet. After imposing parity symmetry and a specific alignment of the bidoublet vacuum expectation values, the quark and lepton mass matrices acquire a common structure that can be treated analytically. An important consequence is that all fermion mass matrices can be reduced to an effective two texture zeros form, providing a unified description of the flavor sector in terms of fermion masses, a small number of additional mass parameters, and CP-violating phases.

In the pseudomanifest left-right theory (PLRT), the fermion mass matrices are complex symmetric, whereas in the manifest left-right theory (MLRT) they are Hermitian. Despite this difference, their diagonalization reveals a close connection between the two frameworks. In particular, the MLRT mixing structure emerges as a more restrictive realization of the PLRT one, with fewer independent phase factors. In the quark sector, the common $R_{\pi/4}$ rotation induced by the S_3 structure cancels from the CKM matrix, so that the observed quark mixing originates from fermion mass hierarchies and relative phases. Our numerical analysis reproduces the observed CKM matrix, including all nine magnitudes, in agreement with current global-fit values. In the lepton sector, both NH and IH can reproduce the observed PMNS mixing pattern. Moreover, although the PLRT and MLRT parametrizations have different underlying phase structures, they contain the same number of effective phases entering the left-handed PMNS matrix. Consequently, neutrino oscillation data alone cannot distinguish between the two realizations. At the level of the absolute neutrino-mass scale, however, the two orderings behave quite differently. The NH best-fit point gives $\Sigma_\nu \simeq 0.063$ eV and is compatible with current ordering-dependent cosmological constraints. In contrast, the IH best-fit point yields $\Sigma_\nu \simeq 0.204$ eV, with the local parameter region considered here corresponding approximately to $\Sigma_\nu \simeq 0.175$–0.216 eV. This region is in strong tension with current DESI+CMB limits within ΛCDM. Since

these bounds are cosmological-model dependent, we do not regard this as a model-independent exclusion of the IH realization, but rather as an important complementary constraint on this branch of the model. The phenomenological analysis provides additional ways of probing the model. For neutrinoless double-beta decay mediated by light Majorana neutrinos, the parameter configurations satisfying $\chi^2 < 1$ predict

$$4.63 \text{ meV} \lesssim m_{\beta\beta}^{\rm NH} \lesssim 7.74 \text{ meV}, \qquad 64.85 \text{ meV} \lesssim m_{\beta\beta}^{\rm IH} \lesssim 77.52 \text{ meV},$$

with best-fit values of approximately 5.10 meV and 71.00 meV, respectively. The strong separation between the two orderings is one of the most distinctive predictions of the model. In particular, the IH region lies within the mass scale expected to be explored by next-generation neutrinoless double-beta decay experiments, whereas testing the NH prediction would require sensitivity at the few-meV level. The contribution from right-handed neutrinos is governed predominantly by the heavy-neutrino scale and the right-handed charged gauge-boson mass, $|\eta^R_{\nu R}| \propto M_N^{-1} M_{W_R}^{-4}$. The numerical analysis further shows that the flavor-dependent correction remains close to unity over most of the allowed parameter space, explaining the nearly overlapping NH and IH predictions for this contribution.

The same right-handed flavor structure also leaves characteristic signatures in other low-energy observables. Within the limiting expressions considered here, the (ν_R, W_R) contribution to the muon anomalous magnetic moment scales as $\Delta a_\mu \propto M_{W_R}^{-2}$ and becomes strongly suppressed as the right-handed scale increases. In contrast, $\mu \to e\gamma$ retains a direct sensitivity to the charged-lepton flavor structure through $\mathcal{S}^R_{e\mu}$ and exhibits the stronger scaling $\text{BR}(\mu \to e\gamma) \propto M_{W_R}^{-4}$. The present MEG II bound already imposes stringent constraints on the right-handed scale. In the regime $M_{W_R} \gg m_{\nu_R}$, requiring the full flavor bands obtained from the lepton sector analysis to satisfy the MEG II limit leads to the conservative lower bounds $M_{W_R} \gtrsim 19.1$ TeV (NH), $M_{W_R} \gtrsim 16.6$ TeV (IH). For the regime $M_{W_R} \simeq m_{\nu_R}$, the larger normalization of the branching ratio strengthens these constraints to approximately $M_{W_R} \gtrsim 27.0$ TeV (NH), $M_{W_R} \gtrsim 23.5$ TeV (IH). These bounds should be understood within the limiting approximation adopted for the $\mu \to e\gamma$ rate and correspond to requiring the complete flavor bands to lie below the present experimental upper limit. Thus, the current MEG II result already probes the right-handed parameter space of the model beyond the 5–15 TeV interval initially explored. Future improvements in searches for $0\nu\beta\beta$, $\mu \to e\gamma$, and right-handed charged currents will provide complementary and increasingly stringent tests of the flavored left-right symmetric framework developed here.

ACKNOWLEDGEMENTS

This work was partially supported by SIP-IPN 20261005. FGC acknowledges the financial support from *SECIHTI* under Grant CBF-2025-G-1187.

Appendix A: The discrete S_3 flavor symmetry

The non-Abelian group S_3 is the permutation group of three objects [42] and has three irreducible representations: two 1-dimensional, $\mathbf{1}_S$ and $\mathbf{1}_A$, and one 2-dimensional representation, $\mathbf{2}$. We list the multiplication rules among them

$$\begin{aligned}
&\mathbf{1}_S \otimes \mathbf{1}_S = \mathbf{1}_S, \qquad \mathbf{1}_A \otimes \mathbf{1}_S = \mathbf{1}_A, \qquad \mathbf{1}_S \otimes \mathbf{1}_A = \mathbf{1}_A, \\
&\mathbf{1}_A \otimes \mathbf{1}_A = \mathbf{1}_S, \qquad \mathbf{1}_S \otimes \mathbf{2} = \mathbf{2}, \qquad \mathbf{1}_A \otimes \mathbf{2} = \mathbf{2} \\
&\begin{pmatrix} a_1 \\ a_2 \end{pmatrix}_{\mathbf{2}} \otimes \begin{pmatrix} b_1 \\ b_2 \end{pmatrix}_{\mathbf{2}} = (a_1 b_1 + a_2 b_2)_{\mathbf{1}_S} \oplus (a_1 b_2 - a_2 b_1)_{\mathbf{1}_A} \oplus \begin{pmatrix} a_1 b_2 + a_2 b_1 \\ a_1 b_1 - a_2 b_2 \end{pmatrix}_{\mathbf{2}}.
\end{aligned} \tag{A1}$$

[1] G. Aad et al. (ATLAS), *Observation of a new particle in the search for the Standard Model Higgs boson with the ATLAS detector at the LHC*, Phys. Lett. B **716** (2012) 1–29, arXiv:1207.7214 [hep-ex].
[2] S. Chatrchyan et al. (CMS), *Observation of a New Boson at a Mass of 125 GeV with the CMS Experiment at the LHC*, Phys. Lett. B **716** (2012) 30–61, arXiv:1207.7235 [hep-ex].
[3] J. C. Romao and J. W. F. Valle, *Neutrino masses in supersymmetry with spontaneously broken R parity*, Nucl. Phys. **B381** (1992) 87–108.
[4] M. Hirsch and J. W. F. Valle, *Supersymmetric origin of neutrino mass*, New J. Phys. **6** (2004) 76, arXiv:hep-ph/0405015.
[5] H. Murayama, *Origin of neutrino mass*, Prog. Part. Nucl. Phys. **57** (2006) 3–21.
[6] F. Feruglio, *Pieces of the Flavour Puzzle*, Eur. Phys. J. **C75** (2015) 8 373, arXiv:1503.04071 [hep-ph].

[7] G. Abbas, R. Adhikari, E. J. Chun and N. Singh, *The problem of flavour*, Eur. Phys. J. Plus **140** (2025) 1 73, arXiv:2308.14811 [hep-ph].

[8] H. P. Nilles and S. Ramos-Sanchez, *The flavor puzzle: Textures and symmetries*, Int. J. Mod. Phys. A **39** (2024) 09n10 2441003, arXiv:2308.14810 [hep-ph].

[9] S. Profumo, L. Giani and O. F. Piattella, *An Introduction to Particle Dark Matter*, Universe **5** (2019) 10 213, arXiv:1910.05610 [hep-ph].

[10] J. C. Pati and A. Salam, *Lepton Number as the Fourth Color*, Phys. Rev. **D10** (1974) 275–289, [Erratum: Phys. Rev.D11,703(1975)].

[11] R. N. Mohapatra and J. C. Pati, *A Natural Left-Right Symmetry*, Phys. Rev. **D11** (1975) 2558.

[12] G. Senjanovic and R. N. Mohapatra, *Exact Left-Right Symmetry and Spontaneous Violation of Parity*, Phys. Rev. **D12** (1975) 1502.

[13] G. Senjanovic, *Spontaneous Breakdown of Parity in a Class of Gauge Theories*, Nucl. Phys. **B153** (1979) 334–364.

[14] R. N. Mohapatra and G. Senjanovic, *Neutrino Mass and Spontaneous Parity Violation*, Phys.Rev.Lett. **44** (1980) 912.

[15] G. Senjanovic and V. Tello, *Parity and the origin of neutrino mass*, Int. J. Mod. Phys. A **35** (2020) 09 2050053, arXiv:1912.13060 [hep-ph].

[16] M. Gell-Mann, P. Ramond and R. Slansky, *Complex Spinors and Unified Theories*, Conf.Proc. **C790927** (1979) 315–321, arXiv:1306.4669 [hep-th].

[17] T. Yanagida, *Horizontal gauge symmetry and masses of neutrinos*, Conf. Proc. C **7902131** (1979) 95–99.

[18] R. N. Mohapatra and G. Senjanovic, *Neutrino Masses and Mixings in Gauge Models with Spontaneous Parity Violation*, Phys. Rev. **D23** (1981) 165.

[19] P. Minkowski, $\mu \to e\gamma$ *at a Rate of One Out of 1-Billion Muon Decays?*, Phys. Lett. **B67** (1977) 421.

[20] J. Schechter and J. W. F. Valle, *Neutrino Masses in SU(2) x U(1) Theories*, Phys. Rev. **D22** (1980) 2227.

[21] J. Schechter and J. W. F. Valle, *Neutrino Decay and Spontaneous Violation of Lepton Number*, Phys. Rev. **D25** (1982) 774.

[22] M. Nemevsek, F. Nesti, G. Senjanovic and Y. Zhang, *First Limits on Left-Right Symmetry Scale from LHC Data*, Phys. Rev. D **83** (2011) 115014, arXiv:1103.1627 [hep-ph].

[23] C.-Y. Chen, P. S. B. Dev and R. N. Mohapatra, *Probing Heavy-Light Neutrino Mixing in Left-Right Seesaw Models at the LHC*, Phys. Rev. **D88** (2013) 033014, arXiv:1306.2342 [hep-ph].

[24] P. S. B. Dev, D. Kim and R. N. Mohapatra, *Disambiguating Seesaw Models using Invariant Mass Variables at Hadron Colliders*, JHEP **01** (2016) 118, arXiv:1510.04328 [hep-ph].

[25] S. Patra, F. S. Queiroz and W. Rodejohann, *Stringent Dilepton Bounds on Left-Right Models using LHC data*, Phys. Lett. **B752** (2016) 186–190, arXiv:1506.03456 [hep-ph].

[26] M. Lindner, F. S. Queiroz and W. Rodejohann, *Dilepton bounds on left?right symmetry at the LHC run II and neutrinoless double beta decay*, Phys. Lett. **B762** (2016) 190–195, arXiv:1604.07419 [hep-ph].

[27] M. Mitra, R. Ruiz, D. J. Scott and M. Spannowsky, *Neutrino Jets from High-Mass W_R Gauge Bosons in TeV-Scale Left-Right Symmetric Models*, Phys. Rev. D **94** (2016) 9 095016, arXiv:1607.03504 [hep-ph].

[28] P. S. B. Dev, R. N. Mohapatra and Y. Zhang, *Probing the Higgs Sector of the Minimal Left-Right Symmetric Model at Future Hadron Colliders*, JHEP **05** (2016) 174, arXiv:1602.05947 [hep-ph].

[29] J. Chakrabortty, J. Gluza, T. Jelinski and T. Srivastava, *Theoretical constraints on masses of heavy particles in Left-Right Symmetric Models*, Phys. Lett. **B759** (2016) 361–368, arXiv:1604.06987 [hep-ph].

[30] G. Cottin, J. C. Helo, M. Hirsch and D. Silva, *Revisiting the LHC reach in the displaced region of the minimal left- right symmetric model*, Phys. Rev. D **99** (2019) 11 115013, arXiv:1902.05673 [hep-ph].

[31] S. Bertolini, A. Maiezza and F. Nesti, *Kaon CP violation and neutron EDM in the minimal left-right symmetric model*, Phys. Rev. D **101** (2020) 3 035036, arXiv:1911.09472 [hep-ph].

[32] A. E. C. Hernández and I. Schmidt, *A renormalizable left-right symmetric model with low scale seesaw mechanisms*, Nucl. Phys. B **976** (2022) 115696, arXiv:2101.02718 [hep-ph].

[33] N. Cabibbo, *Unitary Symmetry and Leptonic Decays*, Phys.Rev.Lett. **10** (1963) 531–533.

[34] M. Kobayashi and T. Maskawa, *CP Violation in the Renormalizable Theory of Weak Interaction*, Prog. Theor. Phys. **49** (1973) 652–657.

[35] J. D. Vergados, *The Neutrinoless double beta decay from a modern perspective*, Phys. Rept. **361** (2002) 1–56, arXiv:hep-ph/0209347.

[36] W. Rodejohann, *Neutrino-less Double Beta Decay and Particle Physics*, Int. J. Mod. Phys. E **20** (2011) 1833–1930, arXiv:1106.1334 [hep-ph].

[37] J. D. Vergados, H. Ejiri and F. Simkovic, *Theory of Neutrinoless Double Beta Decay*, Rept. Prog. Phys. **75** (2012) 106301, arXiv:1205.0649 [hep-ph].

[38] H. Päs and W. Rodejohann, *Neutrinoless Double Beta Decay*, New J. Phys. **17** (2015) 11 115010, arXiv:1507.00170 [hep-ph].

[39] G. Senjanovi? and V. Tello, *Right Handed Quark Mixing in Left-Right Symmetric Theory*, Phys. Rev. Lett. **114** (2015) 7 071801, arXiv:1408.3835 [hep-ph].

[40] G. Senjanovi? and V. Tello, *Restoration of Parity and the Right-Handed Analog of the CKM Matrix*, Phys. Rev. **D94** (2016) 9 095023, arXiv:1502.05704 [hep-ph].

[41] M. Lindner, M. Platscher and F. S. Queiroz, *A Call for New Physics : The Muon Anomalous Magnetic Moment and Lepton Flavor Violation*, Phys. Rept. **731** (2018) 1–82, arXiv:1610.06587 [hep-ph].

[42] H. Ishimori et al., *Non-Abelian Discrete Symmetries in Particle Physics*, Prog. Theor. Phys. Suppl. **183** (2010) 1–163, arXiv:1003.3552 [hep-th].

[43] W. Grimus and P. O. Ludl, *Finite flavour groups of fermions*, J. Phys. **A45** (2012) 233001, arXiv:1110.6376 [hep-ph].

[44] S. F. King and C. Luhn, *Neutrino Mass and Mixing with Discrete Symmetry*, Rept. Prog. Phys. **76** (2013) 056201, arXiv:1301.1340 [hep-ph].

[45] S. F. King, *Models of Neutrino Mass, Mixing and CP Violation*, J. Phys. **G42** (2015) 12 123001, arXiv:1510.02091 [hep-ph].

[46] F. Feruglio and A. Romanino, *Lepton flavor symmetries*, Rev. Mod. Phys. **93** (2021) 1 015007, arXiv:1912.06028 [hep-ph].

[47] G. Chauhan et al., *Discrete flavor symmetries and lepton masses and mixings*, in *2022 Snowmass Summer Study* (2022) pages –, arXiv:2203.08105 [hep-ph].

[48] A. Kakoti, B. B. Boruah and M. K. Das, *Minimal left–right symmetric model with A4 modular symmetry*, Int. J. Mod. Phys. A **38** (2023) 28 2350150, arXiv:2301.13552 [hep-ph].

[49] R. Kalita and M. Patgiri, *Neutrino model in left-right symmetric linear seesaw augmented with A_4 modular group*, Eur. Phys. J. C **85** (2025) 4 453, arXiv:2409.10195 [hep-ph].

[50] A. Kakoti and M. K. Das, *keV Sterile Neutrino as Dark Matter in Doublet Left-Right Symmetric Model with A4 Modular Symmetry*, PTEP **2025** (2025) 12 123B12, arXiv:2502.18869 [hep-ph].

[51] B. Kumar and M. K. Das, *Neutrino phenomenology and dark matter in a left-right asymmetric model with non-holomorphic modular A4 group*, Phys. Lett. B **872** (2026) 140064, arXiv:2509.01205 [hep-ph].

[52] W. Rodejohann and X.-J. Xu, *A left?right symmetric flavor symmetry model*, Eur. Phys. J. **C76** (2016) 3 138, arXiv:1509.03265 [hep-ph].

[53] J. C. Gomez-Izquierdo and A. Perez-Lorenzana, *A left-right symmetric model with $\mu \leftrightarrow \tau$ symmetry*, Phys. Rev. **D82** (2010) 033008, arXiv:0912.5210 [hep-ph].

[54] J. C. Gómez-Izquierdo, *Non-minimal flavored $S_3 \otimes Z_2$ left-right symmetric model*, Eur. Phys. J. **C77** (2017) 8 551, arXiv:1701.01747 [hep-ph].

[55] D. Das and P. B. Pal, *S_3 flavored left-right symmetric model of quarks*, Phys. Rev. D **98** (2018) 11 115001, arXiv:1808.02297 [hep-ph].

[56] E. A. Garcés, J. C. Gómez-Izquierdo and F. Gonzalez-Canales, *Flavored non-minimal left–right symmetric model fermion masses and mixings*, Eur. Phys. J. C **78** (2018) 10 812, arXiv:1807.02727 [hep-ph].

[57] H. Borgohain and M. K. Das, *Phenomenology of two texture zero neutrino mass in left-right symmetric model with Z_8 \times Z_2*, JHEP **02** (2019) 129, arXiv:1810.04889 [hep-ph].

[58] A. E. Cárcamo Hernández, S. Kovalenko, J. W. F. Valle and C. A. Vaquera-Araujo, *Neutrino predictions from a left-right symmetric flavored extension of the standard model*, JHEP **02** (2019) 065, arXiv:1811.03018 [hep-ph].

[59] C. Bonilla et al., *Neutrino phenomenology in a left-right D_4 symmetric model*, Phys. Rev. D **102** (2020) 3 036006, arXiv:2003.06444 [hep-ph].

[60] Z. Maki, M. Nakagawa and S. Sakata, *Remarks on the unified model of elementary particles*, Prog.Theor.Phys. **28** (1962) 870–880.

[61] B. Pontecorvo, *Neutrino Experiments and the Problem of Conservation of Leptonic Charge*, Sov. Phys. JETP **26** (1968) 984–988, [Zh. Eksp. Teor. Fiz.53,1717(1967)].

[62] J. Kubo, A. Mondragon, M. Mondragon and E. Rodriguez-Jauregui, *The Flavor symmetry*, Prog. Theor. Phys. **109** (2003) 795–807, [Erratum: Prog. Theor. Phys.114,287(2005)], arXiv:hep-ph/0302196 [hep-ph].

[63] J. Kubo, *Majorana phase in minimal S(3) invariant extension of the standard model*, Phys. Lett. **B578** (2004) 156–164, [Erratum: Phys. Lett.B619,387(2005)], arXiv:hep-ph/0309167 [hep-ph].

[64] J. Kubo et al., *A minimal S(3)-invariant extension of the standard model*, J. Phys. Conf. Ser. **18** (2005) 380–384.

[65] O. Felix, A. Mondragon, M. Mondragon and E. Peinado, *Neutrino masses and mixings in a minimal S(3)-invariant extension of the standard model*, AIP Conf. Proc. **917** (2007) 383–389, arXiv:hep-ph/0610061.

[66] A. Mondragon, M. Mondragon and E. Peinado, *Lepton masses, mixings and FCNC in a minimal S_3-invariant extension of the Standard Model*, Phys. Rev. **D76** (2007) 076003, arXiv:0706.0354 [hep-ph].

[67] A. Mondragon, M. Mondragon and E. Peinado, *S(3)-flavour symmetry as realized in lepton flavour violating processes*, J. Phys. **A41** (2008) 304035, arXiv:0712.1799 [hep-ph].

[68] A. Mondragon, M. Mondragon and E. Peinado, *Nearly tri-bimaximal mixing in the S(3) flavour symmetry*, AIP Conf. Proc. **1026** (2008) 164–169, arXiv:0712.2488 [hep-ph].

[69] F. Gonzalez Canales and A. Mondragon, *The S_3 symmetry: Flavour and texture zeroes*, J. Phys. Conf. Ser. **287** (2011) 012015, arXiv:1101.3807 [hep-ph].

[70] F. G. Canales, A. Mondragon, U. S. Salazar and L. Velasco-Sevilla, *S_3 as a unified family theory for quarks and leptons*, arXiv:1210.0288 (2012), arXiv:1210.0288 [hep-ph].

[71] F. Gonzalez Canales, A. Mondragon and M. Mondragon, *The S_3 Flavour Symmetry: Neutrino Masses and Mixings*, Fortsch.Phys. **61** (2013) 546–570, arXiv:1205.4755 [hep-ph].

[72] F. Gonzalez Canales and A. Mondragon, *The neutrino mixing angle theta(13) in an S(3) flavour symmetric model*, J.Phys.Conf.Ser. **387** (2012) 012008.

[73] F. Gonzalez Canales and A. Mondragon, *The flavour symmetry S(3) and the neutrino mass matrix with two texture zeroes*, J.Phys.Conf.Ser. **378** (2012) 012014.

[74] F. G. Canales et al., *Fermion mixing in an S_3 model with three Higgs doublets*, J.Phys.Conf.Ser. **447** (2013) 012053.

[75] F. González Canales et al., *Quark sector of S3 models: classification and comparison with experimental data*, Phys.Rev. **D88** (2013) 096004, arXiv:1304.6644 [hep-ph].

[76] P. Langacker and S. U. Sankar, *Bounds on the Mass of W(R) and the W(L)-W(R) Mixing Angle xi in General SU(2)-L x SU(2)-R x U(1) Models*, Phys. Rev. **D40** (1989) 1569–1585.

[77] H. Harari and M. Leurer, *Left-Right Symmetry and the Mass Scale of a Possible Right-Handed Weak Boson*, Nucl. Phys. **B233** (1984) 221–231.

[78] M. A. B. Beg, R. V. Budny, R. N. Mohapatra and A. Sirlin, *Manifest Left-Right Symmetry and Its Experimental Consequences*, Phys. Rev. Lett. **38** (1977) 1252, [Erratum: Phys. Rev. Lett.39,54(1977)].

[79] E. Barradas-Guevara et al., *Systematic analysis of fermionic masses and flavor mixings: a model-independent approach*, Revista Mexicana de Fisica **72** (2026) 5 1–14, ISSN 0035-001X, URL http://dx.doi.org/10.31349/RevMexFis.72.050801.

[80] P. Zyla et al. (Particle Data Group), *Review of Particle Physics*, PTEP **2020** (2020) 8 083C01.

[81] J. Barranco, F. Gonzalez Canales and A. Mondragon, *Universal Mass Texture, CP violation and Quark-Lepton Complementarity*, Phys. Rev. **D82** (2010) 073010, arXiv:1004.3781 [hep-ph].

[82] S. Navas et al. (Particle Data Group), *Review of particle physics*, Phys. Rev. D **110** (2024) 3 030001.

[83] G. yuan Huang and S. Zhou, *Precise values of running quark and lepton masses in the standard model*, Phys. Rev. D **103** (2021) 016010.

[84] H. Fusaoka and Y. Koide, *Updated estimate of running quark masses*, Phys. Rev. D **57** (1998) 3986–4001.

[85] R. Workman et al. (Particle Data Group), *Review of particle physics*, Theor. Exp. Phys. **083C01** (2022), to be published (2022).

[86] K. G. Chetyrkin, J. H. Kuhn and M. Steinhauser, *RunDec: A Mathematica package for running and decoupling of the strong coupling and quark masses*, Comput. Phys. Commun. **133** (2000) 43–65, arXiv:hep-ph/0004189 [hep-ph].

[87] I. Esteban et al., *NuFIT 6.1 (2025)*, https://www.nu-fit.org (2025), three-neutrino fit based on data available in November 2025.

[88] I. Esteban et al., *Nufit-6.0: updated global analysis of three-flavor neutrino oscillations*, JHEP **12** (2024) 216.

[89] W. Elbers et al. (DESI Collaboration), *Constraints on neutrino physics from desi dr2 bao and dr1 full shape*, Phys. Rev. D **112** (2025) 8 083513, arXiv:2503.14744 [astro-ph.CO].

[90] G. Li, M. Ramsey-Musolf and J. C. Vasquez, *Left-Right Symmetry and Leading Contributions to Neutrinoless Double Beta Decay*, Phys. Rev. Lett. **126** (2021) 15 151801, arXiv:2009.01257 [hep-ph].

[91] E. Fernandez-Martinez, J. Hernandez-Garcia and J. Lopez-Pavon, *Global constraints on heavy neutrino mixing*, JHEP **08** (2016) 033, arXiv:1605.08774 [hep-ph].

[92] W.-C. Huang and J. Lopez-Pavon, *On neutrinoless double beta decay in the minimal left-right symmetric model*, Eur. Phys. J. C **74** (2014) 2853, arXiv:1310.0265 [hep-ph].

[93] P. S. Bhupal Dev, S. Goswami and M. Mitra, *TeV Scale Left-Right Symmetry and Large Mixing Effects in Neutrinoless Double Beta Decay*, Phys. Rev. D **91** (2015) 11 113004, arXiv:1405.1399 [hep-ph].

[94] D. Borah and A. Dasgupta, *Neutrinoless Double Beta Decay in Type I+II Seesaw Models*, JHEP **11** (2015) 208, arXiv:1509.01800 [hep-ph].

[95] M. Agostini et al., *Toward the discovery of matter creation with neutrinoless double-beta decay*, Rev. Mod. Phys. **95** (2023) 2 025002, arXiv:2202.01787 [hep-ex].

[96] S. Abe et al. (KamLAND-Zen Collaboration), *Search for majorana neutrinos with the complete kamland-zen dataset*, Phys. Rev. Lett. **135** (2025) 262501.

[97] LEGEND Collaboration (LEGEND Collaboration), *First results on the search for lepton number violating neutrinoless double-beta decay with the legend-200 experiment*, Phys. Rev. Lett. **136** (2026) 022701.

[98] N. Abgrall et al. (LEGEND Collaboration), *Legend-1000 preconceptual design report*, arXiv (2021), arXiv:2107.11462 [physics.ins-det].

[99] R. Aliberti et al., *The anomalous magnetic moment of the muon in the Standard Model: an update*, Phys. Rept. **1143** (2025) 1–158, arXiv:2505.21476 [hep-ph].

[100] B. Abi et al. (Muon g-2), *Measurement of the Positive Muon Anomalous Magnetic Moment to 0.46 ppm*, Phys. Rev. Lett. **126** (2021) 14 141801, arXiv:2104.03281 [hep-ex].

[101] G. W. Bennett et al. (Muon g-2), *Final Report of the Muon E821 Anomalous Magnetic Moment Measurement at BNL*, Phys. Rev. D **73** (2006) 072003, arXiv:hep-ex/0602035.

[102] D. P. Aguillard et al. (Muon g-2), *Measurement of the Positive Muon Anomalous Magnetic Moment to 127 ppb*, Phys. Rev. Lett. **135** (2025) 10 101802, arXiv:2506.03069 [hep-ex].

[103] MEG II Collaboration, *New limit on the $\mu^+ \to e^+\gamma$ decay with the meg ii experiment*, Eur. Phys. J. C **85** (2025) 1177, arXiv:2504.15711 [hep-ex].